# THE BENEFICIAL EFFECTS OF INHIBITION OF HEPATIC APPL2 ON METABOLIC HOMEOSTASIS

**CHEN XI**

**PhD**

The Hong Kong Polytechnic University

2024

The Hong Kong Polytechnic University

Department of Health Technology & Informatics

# The Beneficial Effects of Inhibition of Hepatic APPL2 on Metabolic Homeostasis

**CHEN XI**

A thesis submitted in partial fulfilment of the

requirements for the degree of Doctor of Philosophy

August 2022

# CERTIFICATE OF ORIGINALITY

I hereby declare that this thesis is my own work and that, to the best of my knowledge and belief, it reproduces no material previously published or written, nor material that has been accepted for the award of any other degree or diploma, except where due acknowledgement has been made in the text.

_____ (Signed)

Chen Xi (Name of student)

# Abstract

APPL2 (Adaptor Protein, Phosphotyrosine Interacting with PH Domain and Leucine Zipper 2) can interact with adiponectin receptors and negatively regulate adiponectin signaling. Human genome studies displayed correlation between single nucleotide polymorphisms (SNPs) of APPL2 gene and obesity or type 2 diabetes mellitus (T2DM). In animal studies, APPL2 was proved to interact with TBC1D1 and then regulate insulin-stimulated glucose transporter type 4 (Glut4) translocation in muscle cells, thereby fine-tuning glucose homeostasis. In other tissues, APPL2 was shown to regulate insulin exocytosis from β-cell and enhance subcutaneous white adipose tissue beiging. In the liver, hepatocyte-specific APPL2 deficiency enhanced adiponectin signaling and protected mice against diet-induced insulin resistance.

As a novel therapy, antisense oligonucleotides (ASOs) for the treatment of genetic disorders have been approved for years. The primary purpose of this study is to examine whether and how selectively hepatic APPL2 knockdown by GalNAc-*APPL2*-ASO contributes to glucose, lipid, and energy metabolism.

***Key findings:***

1. Subcutaneous injection of N-Acetylgalactosamine GalNAc-*APPL2*-ASO was able to selectively silence hepatic APPL2 on mRNA and protein levels of mice, with acceptable safety and not obvious off-target effect.
2. An animal model with high-fat-diet (HFD) induced obesity and insulin

resistance was used to investigate the effect of GalNAc-APPL2-ASO treatment on glucose metabolism. The results showed that the treatment can improve glucose tolerance and increase insulin sensitivity, as well as suppressing gluconeogenesis. *In vitro* study suggested that the inactivation of hepatic APPL2 by both two sequences of GalNAc-*APPL2*-ASO substantially reduced glucagon-induced glucose production in primary hepatocytes.

3. RNA-Sequencing (RNA-Seq) analysis results with various approaches, including Gene Ontology, Kyoto Encyclopedia of Genes and Genome, and Gene Set Enrichment Analysis, indicated that liver-specifically knockdown APPL2 regulated several pathways associated with glucose and lipid metabolism. Some of the most remarkable ones included fatty acids metabolism and amino acid metabolism.
4. GalNAc-*APPL2*-ASO treatment alleviated diet-induced hypercholesterolemia, via decreasing total cholesterol and low-density-lipoprotein cholesterol.
5. GalNAc-*APPL2*-ASO treatment improved energy expenditure. With the trigger of cold exposure, the treatment also protected against hepatic steatosis and adipocyte hypertrophy induced by high-fat-diet.

Taken together, this study presented here revealed that, for the first time, hepatic APPL2 knockdown by GalNAc-*APPL2*-ASOs improved glucose metabolism (insulin sensitivity and gluconeogenesis). The suppression of gluconeogenesis was due to the inhibitory action of APPL2 on glucose production from pyruvate as a precursor. In addition, GalNAc-*APPL2*-ASO treatment also alleviated lipid metabolism (hypercholesterolemia), and enhanced energy expenditure in HFD-induced mice.

# Acknowledgements

First of all, I would like to express my gratitude to my supervisor, Dr. Kenneth Cheng. I learned a lot from his professional knowledge, experimental planning, and research mind on my research project. His continuous and valuable guidance has always kept me going ahead during my PhD study. I would not have the ability to accomplish my project and study without all this support during my study.

Great thanks to my teammates, Dr. Lin huige, Dr. Kekao Long, Dr. Kalok Wu for their kind assistance and technical support in my daily study and thesis revision. During my work and life, I am very grateful to my colleagues at the Department of Health Technology and Informatics for being there when the help was needed. They are Shama, Thashma, Mengjie, Xiaofan, Pujie, Martin, Chujun, Ka Ying, Mengyao, Arka. I also would like to thank Dr. LI, Hoi Yee Gloria for the RNA-Seq data analyzing. I am deeply thankful to the staff in the Centralised Animal Facilities and the University Research Facility in Life Science for their assistance in facilitating my animal experiment needs.

Last but not least, my inestimable measure of gratitude goes to my parents and friends for their kindness and thoughtfulness support.

# Publications arising from the thesis

1. Huige Lin,Lin Wang,Zhuohao Liu,Kekao Long,Mengjie Kong,Dewei Ye,Xi Chen,Kai Wang,Kelvin KL Wu,Mengqi Fan,Erfei Song,Cunchuan Wang,Ruby LC Hoo,Xiaoyan Hui,Philip Hallenborg,Hailong Piao,Aimin Xu,Kenneth KY Cheng; Hepatic MDM2 Causes Metabolic Associated Fatty Liver Disease by Blocking Triglyceride-VLDL Secretion via ApoB. *Advanced Science*.

# Conference

1. **Chen Xi**, Kenneth KY Cheng. The Beneficial Effects of Inhibition of Hepatic APPL2 on Metabolic Homeostasis. 30th International Conference on Diabetes and Endocrinology. Barcelona, Spain (online). 30 Aug 2022

# Table of Contents

# List of Tables and Figures

# List of Abbreviations

| | |
|---|---|
| Ome | 2'-O-Methylation |
| DAB | 3,3' Diaminobenzidine |
| DiI-LDL | 3,3'-Dioctadecylindocarbocyanine-Low Density Lipoproteins |
| APPL2 | Adaptor Protein, Phosphotyrosine Interacting With PH Domain And Leucine Zipper 2 |
| ALT | Alanine Aminotransferase |
| ASESC | Animal Subjects Ethics Sub-Committee |
| ASO | Antisense Oligonucleotides |
| ApoB | Apolipoprotein B |
| ASGPR | Asialoglycoprotein Receptor |
| AST | Aspartate Aminotransferase |
| BAR | Bin/Amphiphysin/Rvs |
| BP | Biological Process |
| BAT | Brown Adipose Tissue |
| CREB | Camp-Response Element Binding Protein |
| VCO2 | Carbon Oxide Production Volume |
| CC | Cellular Component. |
| CVD | Cardiovascular Disease |
| CM | Chylomicron |
| cAMP | Cyclic Adenosine 3′,5′-Monophosphate |
| Cyp7b1 | Cytochrome P450 Family 7 Subfamily B Member 1 |
| DNL | De Novo Lipogenesis |
| DCC | Deleted In Colorectal Cancer |
| DIO | Diet-Induced-Obese |
| DEGs | Differential Expression Genes |
| EMA | European Medicines Agency |
| FRET | Fluorescence Resonance Energy Transfer |
| FDA | Food And Drug Administration |
| FOXO1 | Forkhead Box O1 |
| FFA | Free Fatty Acids |
| GIPC1 | GAIP-Interacting Protein, COOH Terminus |
| GO | Gene Ontology |
| GSEA | Gene Set Enrichment Analysis |
| GSIS | Glucose-Stimulated Insulin Secretion |
| GTT | Glucose Tolerance Test |
| GLUT1 | Glucose Transporter Type 1 |

| | |
|---|---|
| GLUT2 | Glucose Transporter Type 2 |
| GLUT4 | Glucose Transporter Type 4 |
| G6PC | Glucose-6-Phosphatase |
| GAP | GTPase Activating Protein |
| HBSS | Hanks' Balanced Salt Solution |
| H&E | Hematoxylin And Eosin |
| HGP | Hepatic Glucose Production |
| HDL | High-Density Lipoprotein |
| HFD | High-Fat-Diet |
| HoFH | Homozygous Familial Hypercholesterolemia |
| INSR | Insulin Receptor |
| IR | Insulin Resistance |
| ITT | Insulin Tolerance Test |
| IGFBP-2 | Insulin-Like Growth Factor-1 Binding Protein 2 |
| IGFs | Insulin-Like Growth Factors |
| IV | Intravenously |
| KO | Knockout |
| KEGG | Kyoto Encyclopedia ff Genes And Genomes |
| LPL | Lipoprotein Lipase |
| LDL | Low-Density Lipoprotein |
| LDL-C | Low-Density Lipoprotein Cholesterol |
| mRNA | Messenger RNA |
| MCP-1 | Monocyte Chemoattractant Protein-1 |
| MF | Molecular Function |
| GalNAc | N-Acetylgalactosamine |
| NAFLD | Non-Alcoholic-Fatty-Liver-Disease |
| non-HDL-C | Non-High-Density Lipoprotein Cholesterol |
| NES | Normalized Enrichment Scores |
| VO2 | Oxygen Consumption Volume |
| PGC1α | Peroxisome Proliferator-Activated Receptor-Co-Activator 1α |
| PBS | Phosphate Buffered Saline |
| PBST | Phosphate-Buffered Saline, 0.1% Tween 20 |
| PI3K | Phosphatidylinositol 3-Kinase |
| PCK1 | Phosphoenolpyruvate Carboxykinase |
| PTB | Phosphotyrosine Binding |
| PH | Pleckstrin Homology |
| PCA | Principal Component Analysis |
| PKA | Protein Kinase A |

| | |
|---|---|
| PC | Pyruvate Carboxylase |
| PTT | Pyruvate Tolerance Test |
| QC | Quality Control |
| RIPA | Radioimmunoprecipitation |
| RER | Respiratory Exchange Rate |
| RIN | RNA Integrity |
| SIM | Selected Ion Monitoring |
| SNPs | Single Nucleotide Polymorphisms |
| SDS-PAGE | Sodium Dodecyl Sulphate-Polyacrylamide Gel Electrophoresis |
| STC | Standard Chow |
| Scd1 | Stearoyl-CoA Desaturase Enzyme 1 |
| SC | Subcutaneous |
| DAVID | The Database for Annotation, Visualization and Integrated Discovery |
| TNP | Thermoneutral Point |
| TC | Total Cholesterol |
| Tri-GalNAc | Triantennary N-Acetylgalactosamine |
| TG | Triglycerides |
| TAE | Tris-Acetate EDTA |
| TBS | Tris-Buffered Saline |
| TBST | Tris-Buffered Saline, 0.1% Tween 20 |
| T2DM | Type 2 Diabetes Mellitus |
| VLDL | Very Low-Density Lipoprotein Cholesterol |
| WAT | White Adipose Tissue |
| QPCR | Quantitative Polymerase Chain Reaction |

# Chapter 1 Introduction

## 1.1 Metabolism and disease

### 1.1.1 Prevalence of Type 2 diabetes mellitus (T2DM)

Over the past decades, the prevalence of T2DM has continued to increase over the world. T2DM is a chronic metabolic disorder with abnormally high blood glucose levels, characterized as the progressive worsening of impaired insulin sensitivity (also called insulin resistance, IR), compensatory insulin secretion increase, and β-cell dysfunction, culminating in morbidity and mortality[1].

The disease can lead to many serious complications over time such as kidney failure, heart attack, and stroke. According to IDF (International Diabetes Federation) data[2], the global number of adults with diabetes will reach 537 million in 2021. The predicted prevalence of diabetes will further increase to 12.2% by 2025. About 6.7 million people will die from diabetes or its complications in 2021. Diabetes accounts for 9% of total healthcare expenditure worldwide. The situation of diabetes prevention and control in China is not optimistic. The number of diabetic patients in our country has increased from 90 to 140 million over the past 10 years. It is predicted that the number of diabetic patients in China will reach 174.4 million by 2045, since more adults have impaired glucose tolerance and impaired fasting glucose statistically. Because of the heavy burden and risk of these complications, future public health and clinical strategies will meet great challenges[3].

### 1.1.2 Insulin resistance, T2DM and obesity

Under physiological conditions, insulin and glucagon secrete from the pancreas maintain glucose homeostasis in the whole body. The pancreas secretes insulin into the

blood, as a response to elevated blood glucose levels[4]. Insulin promotes translocation of the insulin-sensitive and -dependent GLUT4 to the cell surface, stimulating glucose uptake into the adipose tissues and muscle[5]. Under overeating, β-cells in islets increase insulin release to get over the reduced performance of insulin action and maintain normal glucose balance. However, chronic nutritional excess enhances insulin secretion but reduces glucose uptake by insulin in tissues, such as the liver, skeletal muscle, and adipose tissue[6]. For instance, a high-fat diet and/or overeating deregulate hepatocyte gluconeogenesis and increase hepatic glucose production. In muscle, the imbalanced nutrition status brings down GLUT4 response to insulin and decreased glucose uptake. Moreover, a decreased responsiveness of periapical tissues to insulin cause hyperglycemia, which stimulates insulin secretion. The above routes lead to hyperinsulinemia and then accelerate hepatic lipogenesis and secretion of hepatic lipid[6] (**Figure** 1.1).

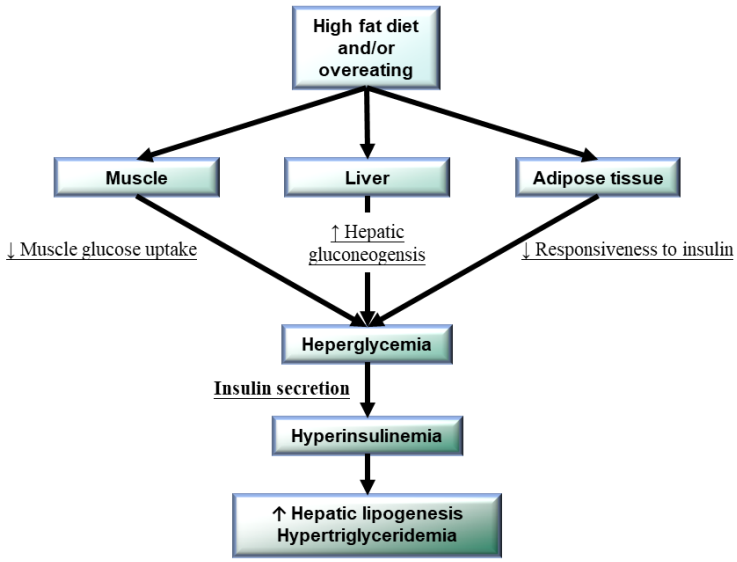


**Figure 1.1.1 Overnutrition induces metabolic unbalance.**

When β-cells are unable to compensate for impaired insulin sensitivity,

hyperinsulinemia occurs. The high levels of blood glucose (chronic hyperglycemia) lead to the formation of systemic IR, which is a major characteristic of prediabetes. IR or β-cell dysfunction induced by excess insulin can lead to exceptional insulin secretion and result in the development of T2DM through different pathways[7]. Obesity is major risk factor for IR and T2DM. Excess visceral fat pad raises circulating free fatty acids (FFA) concentration. FFA and metabolites in turn induce IR, interfere with insulin signaling, and impair β-cell function[8], further causing glucose and lipid toxicity[9].

### 1.1.3 Hepatic carbohydrate metabolism and disease

In this section, I will give background knowledge of glucose and lipid metabolism. Due to the essential role of the liver in regulating the levels of lipid, glucose, and energy metabolism, here I focus on hepatic metabolism, as well as briefly describe its relationship with systematic metabolism. It is difficult to separate multitudinous metabolic pathways of glucose and lipid in the liver because they have intermediate metabolites and regulating factors[10]. Understanding these basic mechanisms can reorganize glucose-associated metabolic disorders more clearly. For example, the effect of insulin signaling on regulating fatty acid metabolism bears out the close relationship between lipid and glucose metabolism[11].

In healthy people, the liver is a major place of glucose utilization after meals. It has been found that the liver contributes to glucose consumption from 30% to 50–60% of the total glucose ingested[12] and produces approximately 85% of endogenous glucose[13]. The liver performs important functions in maintaining blood glucose levels under different nutrition statuses through glycolysis, glycogenesis, glycogenolysis, and gluconeogenesis. Generally, glycolysis and glycogenesis are for storing and utilizing

glucose, while gluconeogenesis and glycogenolysis are for generating glucose, respectively[14] (**Figure** 1.2).

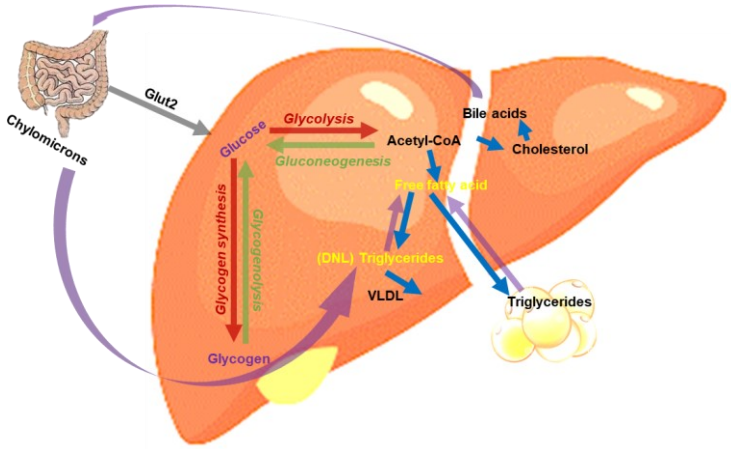


**Figure 1.1.2 Glucose Input and Output in the Liver**

In health conditions, dietary carbohydrates are broken down into soluble monosaccharides during digestion. Glucose can pass across the intestinal wall into the circulatory system to elevated blood sugar[15], then be transported throughout the body. Circulating glucose can entry into hepatocytes via glucose transporters (mainly GLUT2)[16], stored as glycogen in hepatocytes (glycogenesis)[12]. During the period, 1/3 glycogen is synthesized endogenously by glucose derived from gluconeogenesis[17]. Excess dietary glucose produces fat by de novo lipogenesis in the liver[18]. Glucose is poorly stored as glycogen in patients with glucose intolerance[19], which becomes a major contributor to elevated blood sugar. As another pathway to utilize glucose, glycolysis converts glucose into pyruvate[20], providing substrates for anabolic processes and transferring energy to ATP[21]. In T2DM, hyperinsulinemia brings about a slightly compensatory increase in glycolysis rate[22].

Under a fasting state, the liver maintains a constant blood sugar level by activating glycogenolysis (releasing glucose from the glycogen), suppressing glycogen synthesis, and enhancing gluconeogenesis[23]. In type 2 diabetic patients, insulin suppresses glucagon secretion, which diminishes glycogenolysis inhibition by insulin[24], leading to excessive hepatic glucose output[25-26].

Gluconeogenesis is a metabolic pathway that generates glucose from noncarbohydrate precursors, such as amino acids, pyruvate, glycerol, fatty acids, and lactate.

In healthy individuals, physiological insulin secretion suppresses 20% of gluconeogenesis[27]. Half of the hepatic glucose production (HGP) generates from gluconeogenesis overnight fast and primarily contributes to the increase in fasting HGP in patients with T2DM. Hepatic gluconeogenesis is regulated by various transcriptional factors. For example, FFA and glycerol produced from the lipolysis of white adipose tissue stimulate gluconeogenesis. Mitochondrial acetyl-CoA, made from β-oxidation of FFA, promotes gluconeogenesis by activating PC[28]. Besides, glucagon and insulin control gluconeogenesis through transcriptional regulation of gluconeogenic genes *Pck1* and *G6pc*. The insulin can bind to INSR and activates AKT, which phosphorylates and releases FOXO1 from the nucleus. When lack of insulin, FOXO1 promotes transcription of gluconeogenic gene with co-activator PGC1α[29]. Glucagon stimulates the PKA activation, phosphorylates CREB and initiates G6Pc and Pck1, thereby up-regulating gluconeogenesis[30-31].

Abbreviation: pyruvate carboxylase (PC); glucose-6-phosphatase (G6PC); phosphoenolpyruvate carboxykinase (PCK1); insulin receptor (INSR); Forkhead box O1 (FOXO1); peroxisome proliferator-activated receptor-γ co-activator 1α (PGC1α); Cyclic adenosine 3′,5′-monophosphate(cAMP); protein kinase A (PKA); (cAMP-

response element binding protein, CREB)

### 1.1.4 Hepatic lipid metabolism

Recently, it is well-known that lipid changes may not only be a consequence of glucose imbalance but also a reason for it. Elevated triglyceride levels result in high levels of FFA. Elevated circulating FFA disrupts the functions of insulin receptors and glucose transporters, eventually causing insulin resistance and β-cell dysfunction[32-33]. Therefore, hypertriglyceridemia deteriorates glucose metabolism[10].

In the conditions of overnutrition and insulin resistance, circulating and hepatic FFA levels are increased due to elevated lipolysis from adipocytes, which leads to induced hepatic De novo lipogenesis (DNL)[34]. Excess FFA cannot be consumed by oxidation therefor is utilized to directly synthesize TG, leading to excessive hepatic TG storage and VLDL overproduction[35].In health conditions, the fat is decomposed into glycerol and FFA in the small intestine, then synthesized into triglyceride by the intestinal mucosal cells and then assembled with the cholesterol absorbed in the food and ApoB48 protein into chylomicron CM, which enters the blood circulation. In blood circulation, lipoprotein lipase (LPL) hydrolyzes triglycerides (TG) in CM to release FFA. Various tissues (muscles, heart, and adipose tissue) can uptake FFA, using them for energy or substrate. The remaining CM will be carried to the liver by ApoB48. Liver cells will decompose some cholesterol and triglycerides from the residual CM. Cholesterol and triglycerides form particle VLDL with ApoB100.VLDL can be transported from the hepatocyte to blood circulation[36] (**Figure** 1.3).

During blood circulation, the triglyceride (releasing FFA) and cholesterol on VLDL will be utilized by tissues. Unloading triglyceride gradually increases the particles'

density. VLDL will become LDL. LDL-Cholesterol deposit in the artery wall and develop into atherosclerosis, which has been the major cause of cardiovascular disease (CVD). That is the reason LDL-C is also called bad cholesterol. The receptor LDLR on the surface of the hepatocyte recognizes ApoB100. The Uptake of LDL into the hepatocyte is the main path that decreases LDL in the blood[37]. The liver and small intestinal cells will synthesize HDL transported by ApoA1 protein. The HDL collects free cholesterol in the blood circulation and transports it back to the liver. HDL is also called a blood vessel scavenger, which removes cholesterol in blood vessels and reduces cholesterol deposition. A high concentration of HDL is beneficial to the human body[38].

Among the current cholesterol-lowering drugs, such as statins, are the rate-limiting enzymes that inhibit cholesterol synthesis, allowing cells to reduce cholesterol synthesis, plus increase LDLR receptors on the cell surface. The PCSK9 inhibitor inhibits the competitive binding between the PCSK9 protein and the LDLR receptor, allowing the LDLR receptor to bind to LDL, reducing bad cholesterol in the blood.

Besides of glucocentric perspective, insulin resistance can be defined as center theory of fatty acids metabolism. In state of insulin resistance, esterification is reduced and lipolysis is enhanced in adipose tissue. In non-adipose tissues, fatty acid oxidation is blocked and lipid synthesis is enhanced. When whole fatty acid levels increase, overaccumulated fatty acids saturate the storage capacity of adipose tissue, then enter peripheral organs. Ectopic deposition of generated triglycerides in non-adipose tissue (such as liver steatosis) will be very quick. When this buffer capacity is saturated, excess lipids enter non-oxidative pathways, the producted toxic reactive lipids induce specific toxic responses promote metabolically relevant cellular dysfunction (such as

hepatic lipotoxicity) and apoptosis(such as hepatic lipoapoptosis)[39-45].

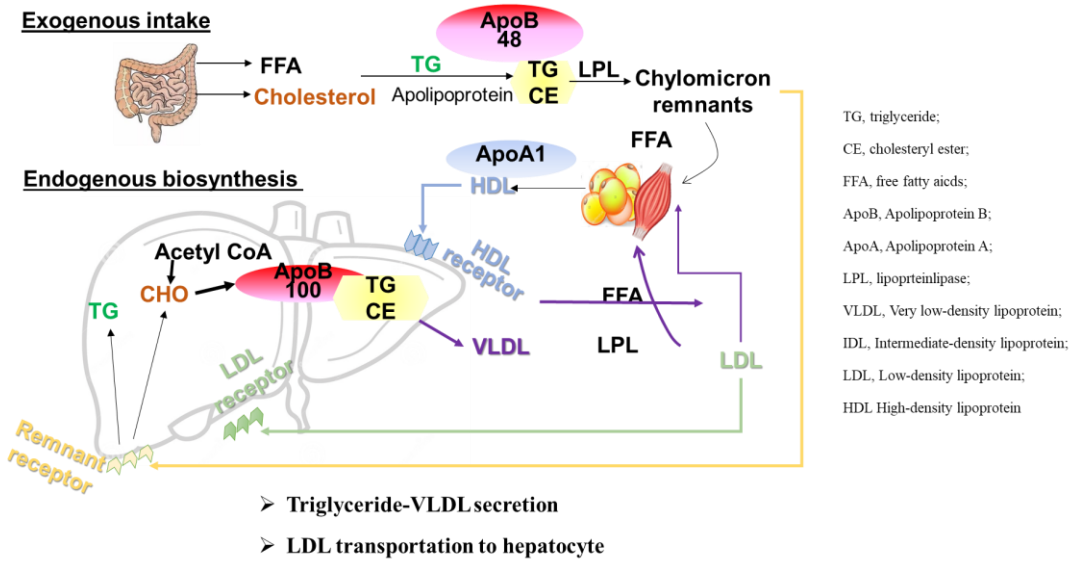


**Figure 1.1.3 Triglyceride and cholesterol transportation**

## 1.2 Adaptor Protein, Phosphotyrosine Interacting with PH Domain And Leucine Zipper (APPL2)

### 1.2.1 Identification and structure

When external stimuli are received by receptors of cell surface, intracellular signals are activated. The signals are manipulated by the recruitment of protein-binding partners to specific substructures (generally the membrane). Adaptor proteins can bind and interact with the protein-binding partners and generate larger signaling complexes[46]. For example, as one of adaptor proteins, APPL1 promotes [insulin receptor substrate proteins 1 and 2]-[insulin receptor] interaction, which is essential for the regulation of insulin sensitivity[47].

APPL protein was first screened as a novel AKT2-interactor in a yeast two-hybrid

experiment to investigate AKT2 function[48]. AKT2 is a serine/threonine kinase, which can be activated by insulin via phosphatidylinositol 3-kinase (PI3K). Another two-hybrid experiment demonstrated APPL1 can interact with the tumor suppressor protein DCC (deleted in colorectal cancer) and was called DCC-interacting protein 13α[49]. DIP-13β, an isoform of DIP- 13α, was subsequently named APPL2.

The crystal structures of APPL protein contain N-terminal Bin/Amphiphysin/Rvs (BAR) domain, pleckstrin homology (PH) domain, and a phosphotyrosine binding (PTB). BAR-PH domain may function as a unit[50-51].

The proteins containing the BAR domain can participate in membrane bending and vesicle formation, or act as small GTPases effectors. Rely on the BAR domain function, those proteins involved in intracellular transportation of endocytosis[52]. PH domain targets proteins to specific membrane units by promoting the lipid specificity of the BAR domain[53] and GTPase binding[54]. The PH domain of APPLs shows similarity to GTPase activating protein (GAP), as a negative regulator of GTPase proteins. PTB domain has homology with CED-6, an adaptor protein that promotes cell apoptosis, and IB1, an activator of the GLUT2[48]. Proteins with PTB domains primarily function as adaptors to organize the signaling pathways involved in biological processe[55]. The PTB domain can interact with Akt2[48].

Genes encoded by APPL2 are in human chromosome 12. The protein has 664 amino acids. Homologous with APPL1, APPL2 shares 52% identity and 72% similarity in amino acid sequence. 45 amino acids in the COOH of APPL2 are absent in APPL1[56], beyond that, both of APPLs have the same domain.

*APPL1* and *APPL2* mRNAs are present in various human and mouse tissues[57]. Unlike APPL1, APPL2 is more concentrated in the nucleus with marginal distribution in the

cytoplasm[56].

### 1.2.2 Biofunctions

APPLs have many binding partners, including signaling proteins, transmembrane receptors, and phosphoinositides. They dynamically link to membranes in endosomes and function in endosome-mediated pathways. Not only all of the APPLs domains can target membranes and bind to phospholipids, but the full-length proteins also bind phosphoinositides, even sufficient for *in vitro* binding[57]. This feature mediates APPL–APPL interactions. As an adaptor, the interacting ability meets an important role in cell signaling[50]. Like APPL1, PH and PTB in APPL2 domains also mediate phosphoinositide binding[57] and interact with Rab5, and follicle-stimulating hormone receptors but not with Akt2[58]. APPLs bind to Rab5 to nuclear signal transduction via an endosomal compartment[56]. In response of external stimuli, APPLs can be translocated from the endosome to the nucleus by small GTPase Rab5, then regulate endocytosis. GAIP-interacting protein, COOH terminus (GIPC1), is involved in the protein's recruitment associated with endocytosis and trafficking events[59]. APPL2 also plays a role in cell proliferation. APPL2 knockdown reduces the number of cells entering the S-phase[56]. APPL1 and APPL2 bind to each other via the N-terminus which contains the BAR domain[52, 57]. APPL BAR domains mediate homotypic and heterotypic interactions. Fluorescence resonance energy transfer (FRET) experiments revealed that APPL minimal BAR domain interacts directly in a homotypic and heterotypic manner on curved cell membranes[60](**Figure** 2.1).

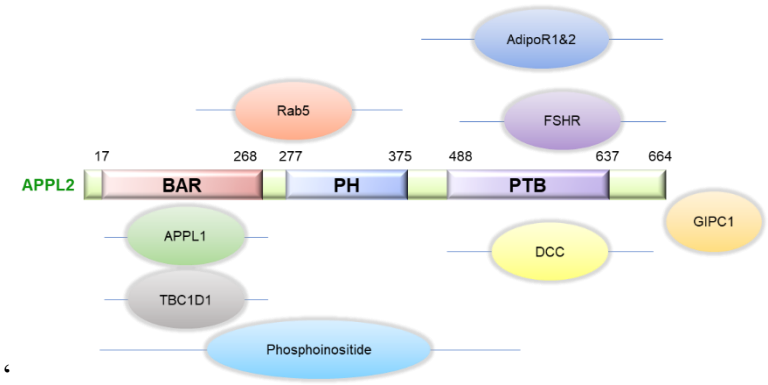


**Figure 1.2.1 APPL2 structure and the regions that interact with binding partners.**

Abbreviations: BAR, Bin/amphiphysin/Rvs domain; PH, central pleckstrin homology; PTB, COOH-terminal phosphotyrosine binding domain; AdipoR, adiponectin receptor; GIPC1, GAIP-interacting protein, COOH terminus; DCC, deleted in colorectal cancer; FSHR, FSH receptor; TBC1D1, TBC domain family member 1

APPL1 is involved in regulating adiponectin and insulin signaling in targeted tissues[61-62]. Adiponectin was an adipokine with anti-atherogenic, anti-diabetic, and insulin-sensitizing properties. It binds to AdipoR 1&2 to mediate adiponectin signaling. This process elicits downstream events, such as glucose uptake and glucose transport 4 (GLUT4) translocation to membrane[61]. Since the PTB domain interacts with the adiponectin receptors AdipoR1 and AdipoR2[62], APPL1 acts as a yin-yang regulator of adiponectin and insulin signaling[63] and promotes metabolic and cardiovascular actions of adiponectin[64]. Besides APPL1 promotes insulin actions by promoting Akt activity in early endosomes and cytomembrane[65]. Hepatic APPL1 enhances the inhibiting effect of insulin on gluconeogenesis via upregulating Akt activity[65]. The effect on the metabolism of APPL2 was also studied based on the well-known functions of APPL1. APPL2 already has been shown to have a similar role to APPL1 in mediating cell proliferation [56] and β-catenin/TCF-dependent transcription[66].

Study showed that hepatic APPL2 showed similar expression between HFD- and chow-

fed mice. However, compared with STC fed mice, higher levels of APPL2 were detected on membrane fraction of hepatocytes from HFD-fed mice. This suggested that theose extra APPL2 proteins on the membrane can seperate APPL1 from interacting with adiponectin receptors. Hepatocyte-specific knockout of APPL2 enhances adiponectin signaling and adiponectin sensitivity in the liver and inhibits monocyte chemoattractant protein-1(MCP-1) expression. MCP-1 recruits and activates inflammatory cells. The process eventually prevented mice from developing HFD-induced inflammation, insulin resistance, and glucose intolerance[67].

APPL1 can enhance insulin and adiponectin-associated glucose uptake in skeletal muscle[68]. In muscle cells, APPL2 competes with APPL1 for binding to AdipoR1 and blocks adiponectin and insulin signaling as a negative regulating effect[63]. Insulin stimulation induces phosphorylation of TBC1D1, leading to membrane translocation of GLUT4 and glucose uptake. TBC1D1 phosphorylation brings its interaction with APPL2, which in turn inhibits further phosphorylation required for GLUT4 targeting in the membrane. Therefore, APPL2 negatively regulates insulin-stimulated GLUT4 translocation by regulating the phosphorylation of TBC1D1[69].

Our lab reported that APPL1 upregulates glucose-stimulated insulin secretion (GSIS), dependent on the Akt pathway, which protects mice against β-cell dysfunction and glucose intolerance[70]. Inhibition or overexpression of APPL1 suppresses or stimulates adiponectin-potentiated GSIS in beta cells, respectively[71]. In response to glucose, APPL2 improves F-actin remodeling by antagonizing the inhibiting effect of RacGAP1 on Rac1 activation, allowing the trafficking of insulin to the plasma membrane for exocytosis, which eventually enhances GSIS[72].

APPL2 has also been reported to function in other tissues and associate with metabolic

symptoms. For example, genetic ablation of APPL2 in mice neurons diminishes beiging (the opposite of browning) of sWAT, increases adiposity, and impairment of adaptive thermogenesis, leading to cold intolerance and obesity in mice scilicet[73]. Reduction of the APPL2 in the gastrocnemius muscle contributes to the decline of glucose intolerance when exercise therapeutic intervention was effective[74](**Figure** 2.2).

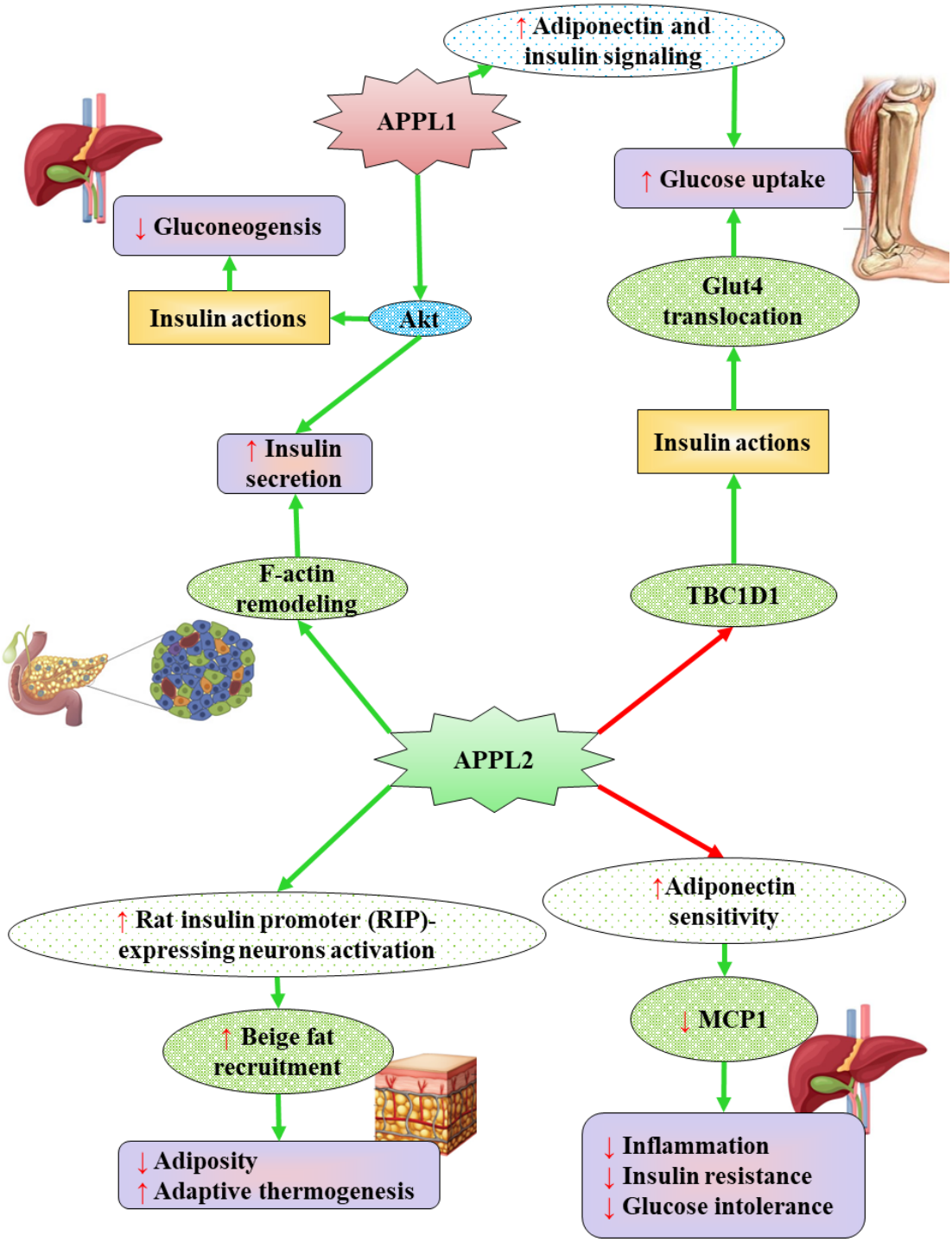


**Figure 1.2.2 APPL proteins regulate metabolism**

Abbreviations: MCP1, monocyte chemoattractant protein-1; TBC1D1, TBC domain family member 1

### 1.2.3 Association with metabolism disease

There is some more evidence showing that APPL2 is associated with metabolic disease according to genetic variance analysis. Human genetic studies displayed associations of single nucleotide polymorphisms (SNPs) in APPL2 gene with higher cardiovascular disease risk[75], overweight and obesity[76], NAFLD[77], and T2DM[78].

## 1.3 Antisense oligonucleotides

### 1.3.1 Concept

Antisense therapy is an approach to cure diseases using oligonucleotides. Antisense-mediated RNA regulation was observed in nature at first[79]. Quickly followed, synthetic antisense oligonucleotides (ASOs) were generated and identified to selectively reduce mRNA levels in the cell system[80]. The oligonucleotides are usually designed to be less than 20 nucleotides, with very high selectivity to target a specific complementary RNA. The feature allows ASOs accurately keep the target genes silenced, thereby preventing the expression of many diseased-causing proteins[81]. ASOs regulate mRNA through a variety of different mechanisms, some of the most commonly ones are:

- **RNA knockdown.** ASOs bind anywhere in pre-mRNA and recruit RNAse H1 to cleave ASO, hence degrade the RNA.
- **Splice modulation.** ASOs bind in or near an interested exon of pre-mRNA to occlude a splice enhancer or repressor binding site.
- **Inhibiting translation.** ASOs bind near the start codon, and sterically block translation machinery or ribosome.

### 1.3.2 Pharmacokinetics

Most ASOs were administered by subcutaneous (SC) or intravenous (IV) infusion[82]. There were a few reports showed that nucleic acid drugs were administered orally, of which bioavailability was low[83]. The bioavailability of ASOs administered subcutaneously was generally high[84], which has been reported to reach 80% to 100% in monkeys, with rapid absorption, and reached peak concentration (Cmax) after 3-4 hours[85].

Either intravenous or subcutaneous administration, plasma concentrations of ASOs decreased rapidly from peak value, then rapidly distributed from circulation to organ within minutes to hours. ASOs finally can be disposed of with a half-life from 4 weeks to 2 months[84].

ASOs circulated throughout the body and more than 80% of the drugs distributed in liver and kidney[84]. The distributed ASOs were mainly metabolized by exonuclease and endonuclease in blood and tissues. The nuclease metabolites were mainly excreted in urine[86].

### 1.3.3 Advantages

Each cell in the human body contains unique genetic information: DNA. DNA can be copied into cells. The copy contains a specific command for generating the protein, called messenger RNA (mRNA). mRNA carries the command to the location where proteins are made. Usually, over, lack, or mistake of protein translation causes many human genetic diseases.

In the last decades, traditional medicines like small molecule inhibitors[87] or antibodies[88] have worked to target those proteins once they are produced to damage body functions. However, antisense therapies block the production before it starts. Compared to conventional small-molecule protein inhibitors, ASOs are a high potential for targeted therapy.

Antisense therapies are designed to target mRNA, binding or degrading with high specificity so that the amount of disease-causing protein is dramatically decreased or dysfunctional. Sometimes, antisense is used to increase protein production, thereby recovering the deficient protein to normal amounts.

Usually, peptides or monoclonal antibodies are hard to deliver to cells and appear in immunoreaction when used for therapies. ASOs are more appropriate for therapeutic applications as high stability, lower immunogenicity, and ease of delivery. Another advantage is that due to their easier and more effective design and production, the duration between conceptualization and clinical use is abridged[89].

### 1.3.4 Delivery

Monoclonal antibody drugs usually bind to extracellular soluble targets or targets on the cell surface to function, whereas oligonucleotide drugs must enter cells to have pharmacological activities. Typical oligonucleotides are large and hydrophilic, which makes them hard to pass through the plasma membrane[90]. Therefore, effective delivery of oligonucleotide to targeted tissues is a big challenge. Several key approaches were studied to address the delivery challenges, such as chemical modification, bioconjugation, and the use of nanocarriers.

Chemical modification is one of the most effective ways to enhance oligonucleotide drug delivery. With the wide usage of modification on the nucleic acid backbone, sugar part of ribose, and nuclear base, chemical modification was identified to protect ASOs from degradation and improve bioavailability and binding affinity to their target[91]. For example, 2′-O-methyl substitutions increased oligonucleotide nuclease resistance, improved stability, and prolonged drug effects.

Direct covalent binding can promote the intracellular uptake of ASOs. This approach can target the drug to specific cells/tissues, reduce drug clearance from circulation, and lower administrated dosage. The covalent binding constituents included lipids[92] (e.g., cholesterol that facilitates interaction with circulating lipoprotein particles), peptides[93] (for cell targeting and/or cell penetration), and sugars (e.g., N-acetylgalactosamine, GalNAc).

Bioconjugates are homogeneous single molecules, that can be administrated precisely with well-defined pharmacokinetic properties. N-acetylgalactosamine (GalNAc) can link to ASO and be recognized by the asialoglycoprotein receptor (ASGPR) on the surface of hepatocytes and uptaken into targeted hepatocytes[94]. ASGPR is a class C lectin that is highly specific on the surface of liver cells and less than 5% in tissues other than the liver and kidney[95]. Each hepatocyte expresses 0.5 to 1 million copies of ASGPR[96], which is highly conserved among species[97]. ASGPR can be internalized rapidly and recycled to the surface of hepatocytes within about 15 minutes and finally disposed of in hepatocytes. These advantages make it an ideal receptor for targeting the liver. The best ligands of ASGPR are triantennary N-acetylgalactosamine (tri-GalNAc)[98], which can achieve targeted delivery of ASO to hepatocytes (**Figure** 3.1). When GalNAC-ASO enters the hepatocyte inclusions (e.g., endosome), its low pH

dissociates ASGPR from GalNAC-ASO, ASGPR is recycled to the hepatocyte surface, and GalNAC-ASO escapes to the cytoplasm or is transported to lysosomes[94].

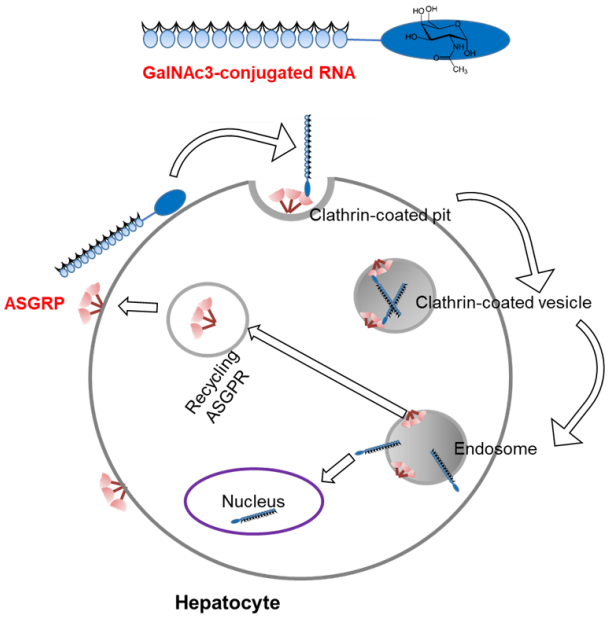


**Figure 1.3.1 Delivery of GalNAc-ASO to hepatocyte**

### 1.3.5 Safety and Potential side effects

ASO toxicities and off-target effects are associated with their sequence and chemical structures. Therefore, each ASO molecular must be considered independently with a complete toxicology evaluation[99].

Off-target effects have two results. ASO can bind to unintended RNA with a similar sequence to the target RNA, which can cause adverse effects by affecting the expression of unintended genes[100]. Secondly, ASO might be delivered to other tissues instead of the target tissue. When selecting a technology to inhibit the expression of a target gene, it is necessary to consider whether nonspecific inhibition or off-target effect, will occur. Studies have found that the ASOs activation RNase H can cut the target RNA

sequences. It is because the ASOs and target RNA with 6 or 7 consecutive bases complementary can activate the RNase H[101]. In addition, the translation initiation site design ASOs may also occur near nonspecific suppression, because the site may contain conserved sequence[102].

There are currently 10 ASOs approved by the US Food and Drug Administration (FDA, USA) and/or the European Medicines Agency (EMA), and/or the Ministry of Health, Labour and Welfare of Japan, most of which have received marketing authorizations in the past 4 years. For example, Mipomersen is an antisense oligonucleotide targeting human apolipoprotein B 100 (ApoB100) mRNA, the major apolipoprotein of human LDL. It has been verified in patients with homozygous familial hypercholesterolemia (HoFH) to lower LDL-C, ApoB, TC, and non-HDL-C. Clinical trials have shown that Mipomersen reduced the content of atherogenic lipoproteins in statistically significant ways. The most common adverse effects that led to discontinuation of treatment in patients treated with Mipomersen and occurred more frequently than in the placebo group were injection-site reactions, elevated alanine aminotransferase, and aspartate aminotransferase levels.

Ionis provided their development strategies (**Figure** 3.2): first, the metabolism of different ASO in various organs and tissues was studied in detail, and a large amount of data was accumulated; Second, although ASO can be administered through a variety of routes, Ionis focuses on local administration, mainly to lower the dose and reduce adverse reactions.

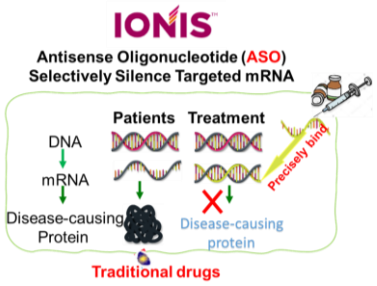


**Figure 1.3.2 Principle of ASO for silencing mRNA**

## 1.4 Aim of the study

As discussed above, numerous pieces of evidence have pointed out the critical roles of APPL1 in glucose metabolism by mediating adiponectin and insulin signaling. APPL2 shares high sequence and structural similarity with APPL1. Since previous studies demonstrated that the APPL2 knockdown enhanced insulin-stimulated glucose uptake by regulating the membrane recruitment of GLUT4 in skeletal muscle, and hepatocyte-specific knockout of APPL2 enhanced adiponectin signaling and adiponectin sensitivity, prevented mice from developing high-fat diet-induced insulin resistance and glucose intolerance. As a novel kind of therapy, antisense oligonucleotides manipulate protein expression from transcriptional levels instead of gene modification, for which have the potential to participate in human chronic disease treatment.

In this study, we aim to explore the effect of GalNAc-*APPL2*-ASOs (*APPL2*-ASOs) on metabolism improvement. To achieve this, we obtained *APPL2*-ASOs from the IONIS company. Unexpectedly, this ASO treatment not only alleviated glucose intolerance and insulin resistance in diet-induced obese mice but also shows ameliorated dyslipidemia and enhanced energy expenditure. In this thesis, I provided several

underlying speculations of the *APPL2*-ASOs on regulating metabolism. In Chapter 3 the efficiency of liver-specific inactivation and of *APPL2*-ASOs were evaluated with safety assessment. Glucose metabolic characterization by hepatic APPL2 silencing was extensively carried out. In Chapter 4, I utilized RNA-Seq, a deep-sequencing technology, to investigate novel features of glucose metabolism alteration regulated by APPL2-ASO. These features, including differentially expressed genes nd enriched pathways, are also expectedly helpful to explore more APPL2 regulating functions. Based on the changes in glucose metabolic phenotype with RNA-Seq analysis, several possibilities about how *APPL2*-ASOs regulate glucose metabolism were suggested and verified. The main aims of Chapters 5 and 6 were to explore the advanced potential of *APPL2*-ASOs on lipid and energy expenditure since the three important aspects of hepatic metabolism are connective by multitudinous metabolic pathways. The leading aim of this study is to investigate the beneficial effects of inhibition of hepatic APPL2 by antisense on metabolic homeostasis and the underlying mechanism.

# Chapter 2 Materials and Methods

## 2.1. Materials, Equipment and Buffer Recipe

### 2.1.1 Chemical and reagents

| Reagents | Provider | Catalog number |
|---|---|---|
| D-(+)-Glucose | Sigma-Aldrich | 346351 |
| Insulin, Recombinant Human | Sigma-Aldrich | 91077C |
| Sodium pyruvate | Sigma-Aldrich | P5280 |
| L-Alanine | Sigma-Aldrich | A7627 |
| Tyloxapol | Sigma-Aldrich | T8761 |
| AdipoRon | ApexBio | B1879 |
| Ketamine, 10% | Alfasan International B.V. | 0904088-05 |
| Xylazine, 2% | Alfasan International B.V. | 1205117-05 |
| Sodium chloride | Sigma-Aldrich, USA | S9888 |
| Direct PCR lysis reagent (Tail) | Viagen, USA | 102-T |
| 2×Es Taq MasterMix | CoWin Biosciences, China | CW0690 |
| Proteinase K | Sangon Biotech, China | |
| SYBR™ Safe DNA Gel Stain | Thermofisher, USA | S33102 |
| TRIzol™ Reagent | Thermofisher, USA | 15596018 |
| QuantiNova SYBR Green PCR Kit | Qiagen, Germany | 208057 |
| GoScript™ Reverse Transcription Mix, Random primers | Promega Corporation, USA | A2801 |
| PageRuler™ Plus Prestained Protein Ladder, 10 to 250kDa | Thermofisher, USA | 26620 |
| TEMED | Thermofisher, USA | 17919 |
| Acryl/Bis 30% Solution (37.5:1) | Sangon Biotech, China | B546018 |
| Immun-Blot PVDF Membrane | Bio-Rad, USA | 1620177 |
| Protease Inhibitor Cocktail | MedChemExpress, USA | HY-K0010 |
| 2-Mercaptoethanol | Bio-Rad, USA | 1610710 |

| | | |
|---|---|---|
| Clarity Western ECL Substrate | Bio-Rad, USA | 1705061 |
| Clarity Max Western ECL Substrate | Bio-Rad, USA | 1705062 |
| WesternBright ECL HRP substrate | Advansta | K-12045-D20 |
| Tween-20 | Sigma-Aldrich | WXBC9582V |
| Richard-Allan Scientific™ Neutral Buffered Formalin (10%) | Thermofisher, USA | 5705 |
| Richard-Allan Scientific™ Histoplast Paraffin | Thermofisher, USA | 8330 |
| 10% neutral buffered formalin | Thermo Fisher Scientific | 6764240 |
| Xylene | Sigma-Aldrich | 185566 |
| Absolute ethanol | Sigma-Aldrich | 459844 |
| DPX Mountant for histology | Sigma-Aldrich | 6522 |
| Hematoxyline | Sigma-Aldrich | HHS32 |
| Eosin | Sigma-Aldrich | 318906 |
| Sodium citrate dihydrate | Sigma-Aldrich | W302600 |
| 3,3’ diaminobenzidine (DAB) **Table**ts | Sigma-Aldrich | SLBM4338V |
| Anhydrous citric acid | Sigma-Aldrich | C0759 |
| Superfrost™ ultra plus adhesion slides | Thermo Fisher Scientific | J3800AMNT |
| Super PAP Pen | Thermo Fisher Scientific | 8899 |
| Collagenase from Clostridium histolyticum Type IV | Sigma-Aldrich | C5138 |
| Low Density Lipoprotein from Human Plasma, DiI complex (DiI LDL) | Invitrogen | L3482 |
| Glucagon | Sigma-Aldrich | G2044 |
| Penicillin-Streptomycin (10,000 U/mL) | Thermofisher, USA | 15140163 |
| Glucagon | Sigma-Aldrich | G2044 |

### 2.1.2 Biochemical assay

| Assay | Provider | Catalog number |
|---|---|---|
| Pierce™ BCA Protein Assay Kit | Thermofisher, USA | 23225 |
| Mouse Insulin ELISA | Mercodia, USA | 10-1247-01 |
| Mouse Adiponectin ELISA Kit | ImmunoDiagnostics Limited, Hong Kong | 32010 |
| RNeasy Mini Kit | Qiagen, Germany | 74004 |
| Picro Sirius Red Stain Kit | Abcam, USA | ab150681 |
| ALT/SGPT Liqui-UV® Test | Stanbio, USA | 2930-500 |
| AST/SGOT Liqui-UV Test | Stanbio, USA | 2920-500 |
| Triglyeride LiquiColor® Reagent Set (enzymatic) | Stanbio, USA | 2100-430 |
| Cholesterol LiquiColor® test (enzymatic) | Stanbio, USA | 1010-430 |
| Low-density lipoprotein cholesterol assay kit | Nanjing Jiancheng, China | A113-1-1 |
| High-density lipoprotein cholesterol assay kit | Nanjing Jiancheng, China | A112-2-1 |
| Kairos Amino Acid Kit | Waters, USA | 50-203-8910 |
| Agilent RNA 6000 Nano Kit | Agilent, USA | 5067-1513 |
| Pyruvate Assay Kit | Abcam, USA | ab65342 |
| Glucose Content Assay Kit | Solarbio Life Sciences | BC2505 |

### 2.1.3 Medium and Buffers

| Medium and buffer | Recipe |
|---|---|
| William's E medium | William's E medium (Catalog #12 551 032, Gibco, MA) supplemented with 10% FBS, 1% penicillin-streptomycin and 2 mM glutamine (Catalog #25 030 081, Gibco) |

| | |
|---|---|
| Dulbecco's modified eagle medium, powder, high glucose, pyruvate | DMEM (Catalog #12800082, Gibco, MA) supplemented with 10% fetal bovine serum (FBS) and 1% penicillin and streptomycin (PS) |
| 1 X Phosphate buffered saline (PBS) | 137 mM NaCl, 2.7 mM KCl, 4.3 mM $Na_2HPO_4$, 1.4 $KH_2PO_4$, 0.1 %Tween 20 (pH 7.4) |
| Phosphate-buffered saline, 0.1% Tween 20 (PBST) | PBS with 0.1% Tween 20 |
| 1 X Tris-buffered saline (TBS) | 50 mM Tris-HCl, 150 mM NaCl, 0.1 %Tween 20 (pH 7.4) |
| Tris-buffered saline, 0.1% Tween 20 (TBST) | TBS with 0.1% Tween 20 |
| Radioimmunoprecipitation (RIPA) buffer | 150 mM NaCl, 50 mM Tris HCl, 2 mM EDTA, 0.5% sodium deoxycholate 0.1% SDS, 1% NP-40 (pH 7.4) |
| Sodium citrate buffer | 0.1 mol/L sodium citrate, 0.1% Tween 20, pH 6.0 |
| Tris-Acetate EDTA (TAE) | 40 mM Tris-acetate, 2 mM EDTA, pH 8.0 |
| SDS-PAGE running buffer | 25 mM Tris, 192 mM glycine, 0.1% SDS |
| Transfer buffer | 25 mM Tris, 192 mM glycine, 20% Methanol (pH 8.3) |
| Tris-buffered saline, 0.1% Tween 20 (TBST) | 20 mM Tris, 150 mM NaCl, (pH 7.6) |
| 5X SDS sample loading dye | 250 mM Tris-Cl (pH 6.8), 0.05% Bromophenol blue, 50% Glycerol, 10% SDS, 5% 2-Mercaptoethanol |
| 2X Modified sample loading dye | 62.5 mM Tris-HCl, 40% Glycerol, 0.01% Bromophenol Blue, (pH 6.8) |
| Liver perfusion buffer | 119.78 mM NaCl, 23.8 mM $NaHCO_3$, 5 mM HEPES, 4.8 mM KCl, 1.2 mM $MgSO_4$, 1.2 mM $KH_2PO_4$, and 5.55 mM glucose, 1 mM EGTA, 1% penicillin-streptomycin, (pH 7.4) |
| Complete William s E medium | William's E medium (Catalog #12 551 032, Gibco, MA) supplemented with 10% FBS, 1% penicillin-streptomycin and 2mM glutamine (Catalog #25 030 081, Gibco) |
| Glucose-free HBSS | (GF-HBSS) 127 mM NaCl, 3.5 mM KCl, 0.44 mM $KH_2PO_4$, 4.2 mM $NaHCO_3$, 0.33 mM $Na_2HPO_4$, 1 mM $CaCl_2$, 20 mM HEPES, pH 7.4. |
| FPLC buffer | (0.15 M NaCl, 3 mM EDTA, 0.04% $NaN_3$, pH7.4) |

### 2.1.4 Antibodies

| Antibodies | Provider and catalog number |
|---|---|
| APPL2 | 11140, ImmunoDiagnostics |
| β-actin | #sc-47778, SANTA CRUZ |
| HSP90 | #4874, Cell Signaling Technology |
| Rab5 | #3547, Cell Signaling Technology |
| PCSK9 | 55206-1-AP, Proteintech Group |
| LDLR | sc-18823, SANTA CRUZ |
| ApoB | sc-393636, SANTA CRUZ |
| Adiponectin | 12010, ImmunoDiagnostics |
| APPL1 | 11130, ImmunoDiagnostics |
| Lamp1 | #3243, Cell Signaling Technology |
| IGFBP2 | 11065-3-AP, Proteintech |
| IGFBP2 | sc-25285, SANTA CRUZ |
| UCP1 | 23673-1-AP, Proteintech |
| | |
| Anti-mouse IgG, HRP-linked Antibody | #7076, Cell Signaling Technology |
| Anti-rabbit IgG, HRP-linked Antibody | #7074, Cell Signaling Technology |

### 2.1.5 Primer sequence

| Primer name | Forward (5'-3') | Reverse (5'-3') |
|---|---|---|
| *Mus Gapdh* | CACATTGGGGGTAGGAACAC | CTCATGACCACAGTCCATGC |
| *Mus β-actin* | GCAAATGCTTCTAGGCGGAC | AAGAAAGGGTGTAAAACGCAGC |

| | | |
|---|---|---|
| *Mus 36b4* | CATTCGAACGTCTGCCCTAT | GTTTCTCAGGCTCCCTCTCC |
| *Mus 18s* | AGTCCCTGCCCTTTGTACACA | CGATCCGAGGGCCTCACTA |
| *Mus Ldlr* | TGACTCAGACGAACAAGGCTG | ATCTAGGCAATCTCGGTCTCC |
| *Mus Pcsk9* | TTGCAGCAGCTGGGAACTT | CCGACTGTGATGACCTCTGGA |
| *Mus Acly* | ACCCTTTCACTGGGGATCACA | GACAGGGATCAGGATTTCCTTG |
| *Mus Appl1* | GAGGACAGCCCGCAGACA | TCCGATGCATAGCTTGATAC |
| *Mus Appl2* | CTTTGAAGGATCTCTTTGGAC | GGGAGCCTGCTATACTTTGC |
| *Mus Bad* | AAGTCCGATCCCGGAATCC | GCTCACTCGGCTCAAACTCT |
| *Mus Cyp2c23* | CAGCAAGATCGAGGAGGAGAAA | GCTCCTTCTTCACTCGGGGTA |
| *Mus Cyp7b1* | AGCCGATTATCAGCGAAAGCC | GCATCCAAAGGTTTGCCTTGT |
| *Mus Fasn* | GGCTCTATGGATTACCCAAGC | CCAGTGTTCGTTCCTCGGA |
| *Mus Fgf21* | ACGACCAAGACACTGAAGC | ACCCAGGATTTGAATGACCC |
| *Mus Fgfr4* | TTGGCCCTGTTGAGCATCTTT | GCCCTCTTTGTACCAGTGACG |
| *Mus G6pc* | ACTGTGGGCATCAATCTCCTC | CGGGACAGACAGACGTTCAGC |
| *Mus Gas6* | TGCTGGCTTCCGAGTCTTC | CGGGGTCGTTCTCGAACAC |
| *Mus GLUT4* | GTGACTGGAACACTGGTCCTA | CCAGCCACGTTGCATTGTAG |
| *Mus Hmgcr* | AGCTTGCCCGAATTGTATGTG | TCTGTTGTGAACCATGTGACTTC |
| *Mus Marco* | ACAGAGCCGATTTTGACCAAG | CAGCAGTGCAGTACCTGCC |
| *Mus Mcp1* | TTAAAAACCTGGATCGGAACCAA | GCATTAGCTTCAGATTTACGGGT |
| *Mus Notch1* | GATGGCCTCAATGGGTACAAG | TCGTTGTTGTTGATGTCACAGT |
| *Mus Pck1* | CTGCATAACGGTCTGGACTTC | CAGCAACTGCCCGTACTCC |
| *Mus Prkn* | TCTTCCAGTGTAACCACCGTC | GGCAGGGAGTAGCCAAGTT |
| *Mus Scd1* | TTCTTGCGATACACTCTGGTGC | CGGGATTGAATGTTCTTGTCGT |
| *Mus Sm* | ATAAGAAATGCGGGGATGTCAC | ATATCCGAGAAGGCAGCGAAC |
| *Mus Srebp2* | GTGGAGCAGTCTCAACGTCA | TGGTAGGTCTCACCCAGGAG |

| | | |
|---|---|---|
| *Mus Trem2* | CTGGAACCGTCACCATCACTC | CGAAACTCGATGACTCCTCGG |
| *Mus APPL2-flox* | CAC ACA GGA GCG TCT GTG GTG GTC | CCT CCC TCT GTT GAA CCA GGA ACG |
| *Mus Cre* | CCTGGAAAATGCTTCTGTCCG | CAGGGTGTTATAAGCAATCCC |

### 2.1.6 Diets

| Diets | Provider | Catalog number |
|---|---|---|
| PicoLab® Rodent Diet 20 | LabDiet | 5053 |
| Rodent Diet With 60 kcal% Fat | Research Diets | D12492 |

### 2.1.7 Equipment and Software

| Equipment | Company |
|---|---|
| Agilent 6460 Liquid Chromatography – Electrospray Ionisation Triple Quadrupole Mass Spectrometer | Agilent Technologies |
| Refrigerated CentriVap Centrifugal Concentrator and CentriVap Cold Traps | Labconco |
| Varioskan LUX Multimode Microplate Reader | Thermo Fisher Scientific |
| 96 Microplate Reader | Bio-Rad Laboratories |
| NanoDrop 2000 Spectrophotometer | Thermo Fisher Scientific |
| 2100 Bioanalyzer | Agilent Technologies |
| Accu-Check Performa Glucose Meter | Roche (USA) |
| TCS SPE Confocal Microscope | Leica Microsystems |
| Nikon Eclipse Ni-U Fluorescent Microscope | Nikon Instruments Inc. |
| Nikon Y-THPL Microscope | Nikon Instruments Inc. |
| ViiA7 Realtime PCR | Applied Biosystems |
| Excelsior AS Tissue Processor | Thermo Fisher Scientific |
| Paraffin Embedding Station | Thermolyne™ |
| Veriti™ Thermal Cycler | Applied Biosystems |
| Promethion Metabolic Cage System | Sable Systems International |
| ER4000 Energizer/Receiver | Starr Life Sciences |
| Rodent thermometer | Bioseblab |
| NGC Discover 10 Pro Chromatography | Bio-Rad Laboratories |
| Superdex 200 Increase 10/300 GL | Cytiva |
| Gene Set Enrichment Analysis (GSEA) 4.2.3 | Broad Institute, Inc. |
| Fiji/ImageJ | NIH |
| Ingenuity Pathway Analysis tool (IPA) | Qiagen |
| SPSS 25.0 | SPSS Inc., Chicago, IL |

| | |
|---|---|
| GraphPad Prism 9 | GraphPad Software Inc. |
| MacroInterpreter | Sable Systems International |
| MassHunter Quantitative Analysis | Agilent Technologies |

## 2.2. General protocols

### 2.2.1 Animal experiments

All animal experiments were approved by Department of Health HKSAR Government (Ordinance Cap. 340), and the Animal Subjects Ethics Sub-Committee (ASESC) of the Hong Kong Polytechnic University. C57BL/6J wild-type mice were housed in the Centralized Animal Facilities of the Hong Kong Polytechnic University at 23℃±1℃ on standard 12 h light/12 h dark cycle with ad libitum access to drinking water and diet of standard-chow (STC), high-fat-diet (HFD) or high-surcose-high-cholesterol-diet (HSHC).

#### 2.2.1.1 Glucose tolerance test (GTT), insulin tolerance test (ITT) and pyruvate tolerance test (PTT).

For GTT, mice were fasted for 6 hours on settled duration each time. The fasted mice were intraperitoneally injected with glucose dissolved in sterile PBS as indicated dosage. Blood glucose levels were measured from the tail vein at 0, 15, 30, 60, 90 and 120 min accordingly by glucose strips (Accu-Chek glucose meter (Roche Diagnostics).

For ITT, mice were fasted for 4-6 hours on settled duration each time. Insulin powder was dissolved then progressively diluted in sterile PBS for delivery. The fasted mice

were intraperitoneally injected with insulin as indicated dosage. Blood glucose levels were measured from the tail vein every 20 min accordingly by glucose strips.

For PTT, mice were fasted for 16 hours. Sodium pyruvate was dissolved in sterile PBS for delivery. The fasted mice were intraperitoneally injected with pyruvate solution as indicated dosage. Blood glucose levels were measured from the tail vein at 15, 30, 60, 90 and 120 min accordingly by glucose strips.

#### 2.2.1.2 Glucose and arginine-stimulated insulin secretion (GSIS)

For GSIS, mice were fasted for 6 hours. The fasted mice were intraperitoneally injected with glucose dissolved in sterile PBS as indicated dosage. Blood was collected from tail vein at 0, 10 and 30 min after glucose injection. The serum was separated for measurement of insulin using a mouse insulin ELISA.

#### 2.2.1.3 TG-VLDL secretion and lipid clearance test

For TG-VLDL secretion test, mice were fasted overnight then intravenously injected via lateral tail veins with tyloxapol at dosage of 500 mg/kg b.w. Blood were collected from tail vein at 0, 1, 2 and 3 hours after tyloxapol administration. For lipid clearance test, mice were fasted overnight then orally garaged with corn oil at dosage of 10 μL/g b.w. Blood were collected from tail vein at 0, 1, 2 and 3 hours after oil gavage. The serum was separated for triglyceride or cholesterol measurement, and Apolipoprotein B (ApoB) protein expression test.

#### 2.2.1.4 Assessment of Indirect Calorimetry Using the Promethion Metabolic System

Promethion metabolic cage system (8 cages, Sable Systems) was used to monitor indirect calorimetry of mice. The mice were housed individually in metabolic cage and fed for 24 hours with free food and water. Oxygen consumption rate ($VO_2$), carbon oxide production rate ($VCO_2$), respiratory exchange rate (RER), and energy expenditure (kcal) were recorded at different tenperature. The food, water consumption and mice body weight were also recorded by the system. The horizontal and vertical movement (XYZ-axis) in the metabolic cage were monitored using ER4000 Energizer/Receiver for the quantitative measurement of physical activity of mice. The metabolic and behavioral data was integrated by the MacroInterpreter analysis software. $VO_2$ and $VCO_2$ were normalized by mouse body weight. Housing in the environment-controlled cabinets, the environmental conditions of the system can be changed and monitored during experiment.

#### 2.2.1.5 Rectal (or colonic) thermometry

Rodent thermometer (BIO-TK8851, [+/-0.1% reading + 0.7ºC]) was used to determine mice core body temperature. Mice were in 4℃ for 6 hours with food and water, but without embedding. To obtain highest temperatures in the body of endotherms, the probe was inserted to depth of >2 cm to reach colon as deep (core) body temperature.

### 2.2.2 Real-time PCR

Total RNA was extracted from mice tissues with TRIzol and 2.5ug of total RNA was

used for cDNA synthesis by reverse transcription reaction. Expression level of target genes were detected using QuantiNova SYBR® Green using with the primers specific primers listed in section 2.1.5 on Real-Time PCR System. Housekeeping genes GAPDH, β-actin, 18s and 36b4 were used for normalization.

### 2.2.3 Immunoblotting

#### 2.2.3.1 General SDS-PAGE

Tissues were homogenized in RIPA lysis buffer and protein concentration was determined by BCA protein quantification assay kit. Extracted proteins were denatured by sample loading buffer under 95℃ for 5 min. Equal proteins were loaded into and separated by sodium dodecyl sulphate-polyacrylamide gel electrophoresis (SDS-PAGE), and then transferred to PVDF membrane with constant 100 voltage for 90 min. After blocking with 5 % non-fat milk in 1 X TBST for 1 hour at room temperature, the membrane was probed with different primary antibodies in 5 % BSA in 1 X TBST at 4℃ for overnight. The membrane was washed with 1 X TBST for three times (5min each) and subsequently incubated with HRP-conjugated secondary antibody prepared in 5 % non-fat milk in 1 X TBST for 1 hour at room temperature. Afterwards, the membrane was washed with 1 X TBST for four times (10 min each). The specific signal of protein was visualized by ECL western blot detection kit and developed. The intensity of protein bands was quantified by the Image J software, relative target proteins expression levels were normalized by indicated internal control.

#### 2.2.3.2 Native PAGE

2 µL mouse serum were diluted with mixed 48 µL MilliQ water and 50 µL 2X modified sample loading dye. The samples were ready for loading without any heating. The following protocol was similar as SDS-PAGE, but with no SDS in gel and running buffer. Separated proteins were transferred to PVDF membrane by using transfer buffer without methanol, using constant 500mA currency for 3 hours.

### 2.2.4 Histology

After mice sacrifice, small pieces of tissue were placed into tissue embedding cassettes and fixed in 10% neutral formalin for 24 hours. Tissues were then processed with Excelsior™ AS Tissue Processor using the following protocol: 30 min in 75% ethanol; 75 min in 95% ethanol x 2 times; 75 min in 95% ethanol x 3 times; 60 min in xylene x 2 times; Overnight paraffin infiltration at 60°C. Tissues were subsequently embedded in freshly melted paraffin and stored until further analysis.

The paraffin-embedded blocks were cut into 5-µm-thick sections, which were deparaffinized and rehydrated by 15 min xylene x 2 times, 5 min 100 % ethanol x 2 times, 1 min 95 % ethanol x 2 times, 1 min 70 % ethanol x once and then rinsed in tap water, then the slides were ready for following staining.

#### 2.2.4.1 Hematoxylin and eosin (H&E) staining

For H&E staining, the sections were stained with hematoxylin 30 seconds for liver or brown adipose tissue and 3mins for white adipose tissue. Then the sections were stained with eosin for 45 seconds for liver or browning adipose tissue and 10 mins for white

adipose tissue, followed by rinse in tap water and dehydration (1 min 70 % ethanol x once, 1 min 95 % ethanol x 2 times, 5 min 100 % ethanol x 2 times). Finally, the stained sections were immersed in xylene and then mounted with DPX mounting medium.

#### 2.2.4.2 Sirius Red staining

Collagen I and III fibers was stained by Sirius red to evaluate fibrosis stage in tissue. Sections were immersed in Picro Sirius red solution and stain for 60 min at room temperature, then rinsed quickly in acetic acid solution, following in absolute alcohol, followed by rinse in tap water and dehydration. Finally, the stained sections were mounted with DPX mounting medium.

#### 2.2.4.3 Immunohistochemistry

For immunohistochemistry staining, sections were deparaffinised, followed by boiling in antigen retrieval buffer (citrate) for 30 minutes using the microwave oven. Next, the sections were treated with 3% $H_2O_2$ in methanol solution and blocked with 3% of FBS in PBS solution to inactivate endogenous peroxidase and block non-specific binding, respectively. 0.2 % Triton X-100 in PBS was added if the samples needed to be permeabilized. After washing with PBS, the sections were incubated with primary antibody overnight at 4 ℃, followed by incubation with secondary antibodies, biotinylated anti-mouse Ig, or anti-rabbit Ig. Sections were washed three times after each incubation. Finally, DAB peroxide substrate (Cat#D4418, Sigma) was used for diaminobenzidine staining according to manufacturer's instructions.

### 2.2.5 Hepatic lipid and glycogen content

Approximately 25 mg liver tissues were homogenized with 200 μL PBS, followed by mixing with 5 mL chloroform-methanol mixture (chloroform: methanol, 2:1, v/v) at 4 °C overnight. An aliquot of 1 mL of the mixture was washed with 200 μL of saline, followed by centrifugation at 5000 g for 15 min. the washing procedure was repeated. The chloroform layer was collected and air-dried, and then resuspended in 100% ethanol. The TG levels were measured using kit and normalized with protein concentration of tissue lysates. The hepatic glycogen contents in harvested livers were measured by a glycogen assay kit (Solarbio Science and Technology) according to the manual.

### 2.2.6 Serum chemicals test

Mice blood were collected from heart after sacrificed. The blood was stayed in room temperature at least for 30min then centrifuged with 3000rpm for 15min at room temperature, the supernatant serum was separated and centrifuged with 8000rpm for 15min at 4℃. Serum was stored at -80℃ until further analysis. Blood chemicals or enzymes, such as total triglyceride (TG), total cholesterol (TC), alanine aminotransferase (ALT), aspartate aminotransferase (AST), low-density-lipoprotein-cholesterol (LDL-C), high-density-lipoprotein-cholesterol (HDL-C), and pyruvate content was measured using assay kits (section 2.1.2).

### 2.2.7 Circulating amino acids.

Mice serum was pretreated by using Kairos Amino Acid Kit. Internal standards (**Table**

2.3) were added, and protein was precipitated, then 50 µL of calibrator or quality control (QC) or sample was added with vortex for 5 seconds. 50 µL of water was add with vortex for 5 seconds. The mixture was centrifuged for 15 min at 9000 x g. Supernatant was mixed with 70 µL of borate buffer, then added 20 µL of AccQ•Tag reagent. The mixture was vortex for 5 seconds and stayed at room temperature for 1min, followed by heating for 10 minutes at 55 °C.

The LC/MS/MS (Section 2.1.7) was used to determine circulating amino acids analysis. CORTECS UPLC C18 (1.6 µm, 2.1 x 150 mm) was used to separate compounds. Mobile phase A was water + 0.1 % formic acid, while mobile phase B was acetonitrile + 0.1% formic acid. The flow rate was set at 0.5 mL/min and gradient program was listed in **Table** 2.1. MS/MS data was acquired by Selected Ion Monitoring (SIM) in a positive ion mode. The mass spectrometer was operated with the voltage set to 0.8 kV and source temperature held at 120°C. The recommended retention time and ion transitions are listed in **Table** 2.2., each amino acid has specific isotope internal standard. MassHunter Quantitative Analysis software was used to quantify amino acid in serum.

**Table 2.1 Mobile Phase of liquid chromatogram**

| Time (min) | Mobile Phase A (%) | Mobile Phase B (%) |
|---|---|---|
| 0.0 | 99% | 1% |
| 1.0 | 99% | 1% |
| 2.0 | 87% | 13% |
| 5.5 | 85% | 15% |
| 6.5 | 5% | 95% |

| | | |
|---|---|---|
| 7.5 | 5% | 95% |
| 7.6 | 99% | 1% |
| 9.0 | 99% | 1% |

**Table 2.2 The retention time and ion transitions of compounds**

| Target | SIM Transition | Internal standard | SIM Transition | Retention time |
|---|---|---|---|---|
| Alanine | 260.20 > 171.10 | Alanine $_{13}C_3$,$_{15}N$ | 264.20 > 171.10 | 4.9 |
| Arginine | 345.20 > 171.10 | Arginine $_{13}C_6$, $_{15}N_4$ | 355.20 > 171.10 | 3 |
| Asparagine | 303.20 > 171.10 | Asparagine $_{13}C_4$, $_{15}N_2$ | 309.20 > 171.10 | 2.8 |
| Aspartic Acid | 304.20 > 171.10 | Aspartic Acid $_{13}C_4$, $_{15}N$ | 309.20 > 171.10 | 4 |
| Cystine | 291.10 > 171.10 | Cystine $_{13}C_6$, $_{15}N_2$ | 295.10 > 171.10 | 6.5 |
| Glutamic Acid | 318.20 > 171.10 | Glutamic Acid $_{13}C_5$,$_{15}N$ | 324.20 > 171.10 | 4.4 |
| Glutamine | 317.20 > 171.10 | Glutamine $_{13}C_5$,$_{15}N_2$ | 324.20 > 171.10 | 3.5 |
| Glycine | 246.20 > 171.10 | Glycine $_{13}C_2$, $_{15}N$ | 249.20 > 171.10 | 3.8 |
| Histidine | 326.20 > 171.10 | Histidine $_{13}C_6$,$_{15}N_3$ | 335.20 > 171.10 | 1.9 |
| Isoleucine | 302.20 > 171.10 | Isoleucine $_{13}C_6$,$_{15}N$ | 309.20 > 171.10 | 12.9 |
| Leucine | 302.20 > 171.10 | Leucine $_{13}C_6$,$_{15}N$ | 309.20 > 171.10 | 13.5 |
| Lysine | 244.10 > 171.10 | Lysine $_{13}C_6$, $_{15}N_2$ | 248.10 > 171.10 | 6.4 |
| Methionine | 320.20 > 171.10 | Methionine $_{13}C_5$,$_{15}N$ | 326.20 > 171.10 | 7.6 |

| | | | | |
|---|---|---|---|---|
| Phenylalanine | 336.20 > 171.10 | Phenylalanine $_{13}C_9$, $_{15}N$ | 346.20 > 171.10 | 15.1 |
| Proline | 286.20 > 171.10 | Proline $_{13}C_5$,$_{15}N$ | 292.20 > 171.10 | 5.5 |
| Serine | 276.20 > 171.10 | Serine $_{13}C_3$,$_{15}N$ | 280.20 > 171.10 | 3.5 |
| Threonine | 290.20 > 171.10 | Threonine $_{13}C_4$,$_{15}N$ | 295.20 > 171.10 | 4.6 |
| Tryptophan | 375.20 > 171.10 | Tryptophan $_{13}C_{11}$, $_{15}N_2$ | 388.20 > 171.10 | 17.5 |
| Tyrosine | 352.20 > 171.10 | Tyrosine $_{13}C_9$, $_{15}N$ | 362.20 > 171.10 | 7.3 |
| Valine | 288.20 > 171.10 | Valine $_{13}C_5$,$_{15}N$ | 294.20 > 171.10 | 8 |

### 2.2.8 Fractionation of lipoproteins and albumin from serum

Mouse serum was fractionated by size-exclusion chromatography (SEC) using NGC Discover 10 Pro Chromatography fast protein liquid chromatography (FPLC) system (Bio-Rad Laboratories) equipped with a Superdex 200 Increase 10/300 GL (Cytiva). Elution was performed with FPLC buffer (Table 2.1.3). The serum sample of each group was a mixture of 11 mice. The mixed serum was centrifuged at 15000 g for 15 min to remove debris then filtered the supernatant with 0.22 μm filter. After loading 100 μL of serum, the SEC system was run with a constant flow of 250 μL/min with 300 μL of fractions. Fractions 1~26 containing serum lipoproteins and fractions 27~35 containing serum albumin were used for further analyses.

### 2.2.9 Primary hepatocyte isolation and *in vitro* experiment

To isolate primary hepatocytes from mice with HFD feeding and ASOs injection, liver was cannulated via inferior vena cava and perfused with a pre-warmed buffer, followed by digestion with buffer containing collagenase Type IV (0.5 mg/mL, Catalog #17104019, Thermo Fisher Scientific). The digested liver was gently dissociated in cold complete William's E medium to stop digestion. The cell suspension was filtered by a 100 μm Falcon strainer and washed with cold PBS by centrifugation at 50 g for 2 min at 4℃, followed by resuspension with complete William's E medium.

Hepatocytes with 2*10^5/well density were seeded in 12 well plates, cultured at 37℃ for 4 h, then changed with fresh complete William's E medium and incubated for 20 h. Cells were then washed by Hanks' Balanced Salt Solution (HBSS, 127 mM NaCl, 3.5 mM KCl, 0.44 mM $KH_2PO_4$, 4.2 mM $NaHCO_3$, 0.33 mM $Na_2HPO_4$, 1 mM $CaCl_2$, 20 mM HEPES, pH 7.4.) for 3 times and starvation in HBSS for 2 hours, then washed again. Primary hepatocytes were incubated for 3 h in HBSS buffer, divided to 3 groups, respectively added with 100nM glucagon, 100nM glucagon+20 mM sodium pyruvate, or 100nM glucagon+20 mM sodium pyruvate+100nM insulin in each group. After 3 hours of incubation, the culture medium was collected and centrifuged. The concentration of glucose in the supernatant was measured with the Glucose content assay kit (Catalog #BC2505, Solarbio Science and Technology) according to the manufacturer's instructions.

### 2.2.10 RNA-Seq analysis

Total RNA in fresh mice liver was extracted using Trizol reagent and cleaned up by RNeasy Mini Kit. The RNA quality was determined using RNA 6000 Pico kit by

Agilent 2100 Bioanalyze or Fragment Analyzer. The qualified samples were subjected to RNA-Sequencing in BGI Group (Shenzhen).

The sequencing of all RNA samples was performed using DNBSEQ platform via 100 bp reads from the paired ends. With raw sequencing data, simple quality control metrics were generated using fastQC. The reads were aligned to the mouse genome (Genome assembly: GRCm39) using STAR. Raw reads counts were quantified using the featureCounts function of the Rsubread package. Differential expression genes (DEGs) analysis was performed using DESeq2, which internally corrected for the library size. For further DEGs analysis, DAVID (http://david.ncifcrf.gov), EnrichR (http://amp.pharm.mssm.edu/Enrichr/), and GSEA (www.gsea-msigdb.org/gsea/downloads.jsp) were used to enrich the pathways with regulated genes.

### 2.2.11 Statistical analysis

Figures were generated by GraphPad Prism 9.5.1. All results were presented as Mean ± SEM. Significance was determined using two-sided Student's t-test with Bonferroni correction or Repeated-measures One-way ANOVA with Bonferroni correction except specific mention. A p-value of less than 0.05 represented a statistical significance.

# Chapter 3 GalNAc-*APPL2*-ASO treatment improves glucose metabolism

## 3.1 Introduction

Overnutrition is chronically excessive nutrient supply over the normal metabolism, leading to insulin resistance and obesity. In obesity, insulin resistance manifests in target tissues, including the liver, adipose tissues, and muscle. As the underlying cause of T2DM, insulin resistance in muscle and adipose tissues leads to impaired glucose uptake. Therefore, multiple insulin-sensitizing drugs, like metformin and thiazolidinediones, can increase glucose disposal in peripheral tissues. In the liver, selective insulin resistance occurs, which augments gluconeogenesis. This insulin resistance is mainly due to defective signaling transduction from the insulin receptor to the downstream effectors such as GLUT4 in adipose tissue and skeletal muscle and PEPCK and G6Pase in the liver.

Besides, insulin resistance impairs the ability to utilize glucose as fuel and amplifies the effect of insulin on lipogenesis, leading to hepatic steatosis. These manifestations can also alter systemic lipid metabolism and contribute to atherosclerotic plaque formation, resulting in cardiovascular disease (CVD)[103]. CVD is the number one cause of death in people living with T2D. CVD causes over 60% of deaths in people with T2D[104]. Hypercholesterolemia is one of the major risk factors causing CVD. LDL-C level are positively associated with cardiovascular risk. Although several drugs, such as statin and PCSK9 inhibitors, are available to treat hypercholesterolemia, they exert detrimental effects on glucose metabolism and increase the risk of T2D[105]. Therefore, there is an urgent need to develop new treatments that can simultaneously improve

glucose and lipid homeostasis.

Adaptor protein, phosphotyrosine interacting with PH domain and leucine zipper 2 (APPL2) causes insulin resistance in liver and skeletal muscle via inhibiting insulin and adiponectin actions in animal models[67, 69]. Single nucleotide polymorphisms in the APPL2 gene are associated with LDL-C, non-alcoholic fatty liver disease, and coronary artery disease in humans[75, 77].

Our research team and others previously demonstrated that APPL2 is a negative regulator of insulin signaling. APPL2 binds to TBC1D1 in response to insulin, which hinders the translocation of GLUT4 to the plasma and thereby inhibits glucose uptake in the muscle cells[69]. This APPL2 action is independent of Akt signaling. APPL2 has been found to block adiponectin-induced AMPK activation and subsequent glucose uptake and fatty acids oxidation in the muscle cells[63]. While hepatic APPL2 expression was similar between mice fed with HFD or STC, higher levels of APPL2 were measured on the plasma membrane of hepatocyte from HFD-fed mice compared with STC-fed mice, suggesting that accumulation of APPL2 on the plasma membrane under HFD conditions might separate and thereby prevent APPL1 from interacting with adiponectin receptors. Hepatocyte-specific knockout of APPL2 ($APPL2^{HepKO}$) prevented mice from HFD-induced inflammation, insulin resistance, and glucose intolerance via enhancing adiponectin sensitivity[67].

Besides, our research team found that genetic deletion of APPL2 in pancreatic beta cells causes defective glucose-stimulated insulin secretion because of aberrant F-actin

remodeling[72]. Inactivating APPL2 in the hypothalamus causes impairment of adipose tissue thermogenesis and increases adiposity[73]. Although genetic inhibition of APPL2 in the liver and muscle improves glucose homeostasis in obese conditions, its inhibition in beta cells and the central nervous system exerts detrimental effects on glucose and energy metabolism. Therefore, we aim to develop a hepatocyte-specific gene silencing approach to inactivate APPL2 and improve insulin resistance and hyperglycemia in T2D.

Antisense oligonucleotide (ASO) is a novel therapeutic approach to knock down specific proteins by targeting its corresponding mRNA conjugating with N-Acetylgalactosamine (GalNAc). The ASO can selectively silence the gene in the hepatocytes without a significant off-target effect in other peripheral metabolic tissues. Our collaborator, Ionis Pharmaceuticals, Inc., synthesized a series of APPL2 antisense oligonucleotides to liver-specifically inactivate APPL2 expression. My project investigates whether APPL2-ASOs can alleviate diet-induced T2D and hypercholesterolemia in animal models.

In this chapter, I tested the effect of two different APPL2-ASO conjugated with GalNAc on hepatic APPL2 inhibition and their effects on glucose metabolism in animal models under the standard chow (STC) and high-fat diet (HFD) feeding conditions.

## 3.2 Result

### 3.2.1 *APPL2*-ASO-226 and *APPL2*-ASO-228 are the most effective ASOs.

ASO is a novel technology to silence genes by inhibiting mRNA expression. Our collaborator (Ionis Pharmaceuticals, Inc) synthesized a series of *APPL2*-ASOs and subcutaneously injected them into mice to inactivate hepatic APPL2. To improve the hepatocyte-binding affinity and decrease toxicity, ASOs were chemically modified with conjugated with GalNAc. APPL2 knockdown efficiency by synthesized ASOs was evaluated upon APPL2 mRNA level in the liver. Finally, two GalNAc-*APPL2*-ASOs (**#1449226** and **#1449228**), exerted a significant inhibitory effect on hepatic APPL2 and the minimal off-target effect in other tissues. GalNAc-*APPL2*-ASOs **#1449226** and **#1449228** (indicated as *APPL2*-ASO-226 or *APPL2*-ASO-228) were provided from the company.

### 3.2.2 *APPL2*-ASOs have effect on inactivating hepatic APPL2.

The knockdown efficiency was further verified in our laboratory. C57BL/6J male mice (8 weeks old) were fed with STC for two weeks, then were subcutaneously injected with *APPL2*-ASOs (*APPL2*-ASO-226 with 10 mg/kg b.w. dosage, once a week for 14 weeks or *APPL2*-ASO-228 with 5 mg/kg b.w. dosage, once a week for 3 weeks). GalNAc-Control-ASO (indicated as Ctrl-ASO) was injected with corresponding dosage. The dosage was recommended by IONIS company. To a certain extent, the knockdown

efficiency of *APPL2*-ASO-226 with 5 mg/kg b.w. dosage was lower than that with 10 mg/kg b.w. (data not shown). Mice were sacrificed after weeks of treatment, serum, adipose tissue, liver, kidney, and pancreas were collected. APPL2 expression level in liver was determined.

For STC fed mice, QPCR result revealed that an over 90% *APPL2* mRNA knockdown by *APPL2*-ASOs in the liver (**Figure** 3.1. A, C). Immunoblotting analysis confirmed that *APPL2*-ASOs resulted in around 90% reduction on hepatic APPL2 protein level (**Figure** 3.1. B, D). Besides, APPL2 expression levels between *APPL2*-ASOs and Ctrl-ASO were comparable in kidney, fat, muscle, and heart (**Figure** 3.1. A, C).

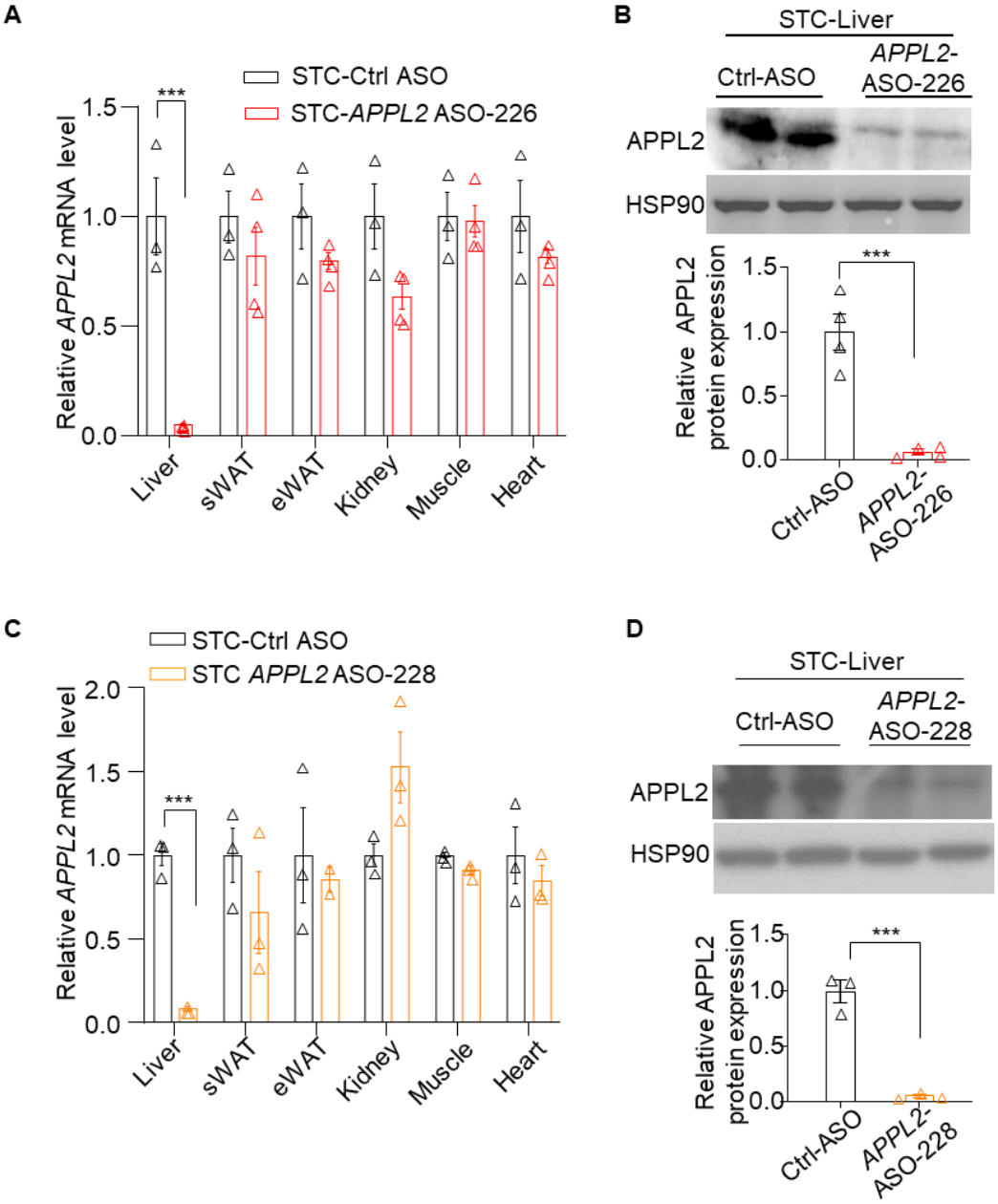


**Figure 3.1. *APPL2*-ASOs selectively reduced hepatic APPL2 in STC fed mice.**

Relative mRNA level of *APPL2* in tissues for *APPL2*-ASO-226 **(A)** or *APPL2*-ASO-228 **(C)** treated mice. Immunoblotting analysis of hepatic APPL2 for *APPL2*-ASO-226 **(B)** or *APPL2*-ASO-228 **(D)** treated mice, relative levels were normalized by internal control HSP90 (heat shock protein 90). Student t-test (***p<0.001). Data are presented as mean ± SEM, n number was 3-4.

Mice body weight and food intake were also monitored during diet feeding and ASO

treatment. Collected tissues were weighted. Under STC diet feeding, mice with *APPL2*-ASOs treatment had comparable body weight, food intake and organ weights (**Table** 3.1.) with those of Ctrl-ASO groups. ALT releases from the liver into the bloodstream once the liver is damaged or inflamed. Elevated hepatic AST level is also attributed to toxic liver injury. Therefore, rising ALT and AST activity levels are clinical diagnoses for liver problem[106]. For C57BL/6J mice, normal range of ALT is 20-40 U/L while AST is 40-60 U/L. AST and ALT circulating levels were respectively comparable in all groups (**Table** 3.1.), although AST levels were exceeded normal range to some extent. These results suggested that silencing hepatic APPL2 can selectively reduce hepatic APPL2 expression with acceptable safety. Results indicated that silencing hepatic APPL2 exerted not obvious toxicity effects.

| | **STC** | |
|---|---|---|
| | **Ctrl-ASO** | ***APPL2*-ASO-226** |
| Body weight (g) | 30.4±1.4 | 30.2±2.1 |
| Food intake (g/day/mouse) | 1.51±0.30 | 2.16±0.34 |
| Liver (g) | 1.41±0.26 | 1.3±0.11 |
| Kidney (g) | 0.40±0.02 | 0.40±0.04 |
| Heart (g) | 0.11±0.01 | 0.10±0.01 |
| sWAT (g) | 0.13±0.01 | 0.22±0.04 |
| eWAT (g) | 0.33±0.08 | 0.42±0.07 |
| BAT (g) | 0.05±0.01 | 0.05±0.00 |
| AST (U/L) | 12.0±4.7 | 9.4±0.7 |
| ALT (U/L) | 36.8±18.3 | 29.1±14.2 |

| | **STC** | |
|---|---|---|
| | **Ctrl-ASO** | ***APPL2*-ASO-228** |
| Body weight (g) | 20.2±0.6 | 21.4±0.5 |

| Food intake (g/day/mouse) | 1.78 | 2.18 |
|---|---|---|
| Liver (g) | 1.01±0.1 | 0.93±0.03 |
| Kidney (g) | 0.28±0.01 | 0.27±0.00 |
| Heart (g) | 0.09±0.01 | 0.10±0.01 |
| sWAT (g) | 0.15±0.01 | 0.16±0.00 |
| eWAT (g) | 0.33±0.02 | 0.34±0.06 |
| AST (U/L) | 83.4±3.9 | 75.8±13.1 |
| ALT (U/L) | 35.1±10.3 | 34.1±21.7 |

**Table 3.1. *APPL2*-ASOs do not change tissue weights in STC fed mice.**

C57BL/6J male mice (8 weeks old) were subcutaneously injected to ASOs with indicated dosage, each injection per week. After 3 (228) or 16 (226) injections, mice were sacrificed, and tissues and serum were collected. Body weight, tissue weights and food intake were monitored. All results are presented as mean or mean ± SEM. n number = 3-4.

The knockdown efficiency was also verified in HFD mice model. C57BL/6J male mice (8 weeks old) were fed with HFD diet for two weeks then subcutaneously injected with *APPL2*-ASO for weeks (*APPL2*-ASO-226 with 10 mg/kg b.w., once a week for 15 weeks or *APPL2*-ASO-228 with 5 mg/kg b.w., once a week for 17.5 weeks). Ctrl-ASOs was injected with corresponding dosage. Mice were sacrificed with collection of serum, and tissues like liver, kidney, muscle, sWAT, eWAT and BAT. For HFD fed mice, *APPL2*-ASOs can inactivate around 90% *APPL2* mRNA and 85% APPL2 protein in liver (**Figure** 3.2). As an isoform of APPL2, mRNA levels of APPL1 in APPL2-ASOs treatment were unaltered, indicated that the hepatic APPL2 inactivation byAPPL2-ASOs did not change the transcriptional levels of hepatic APPL1(**Figure** 3.2. E).

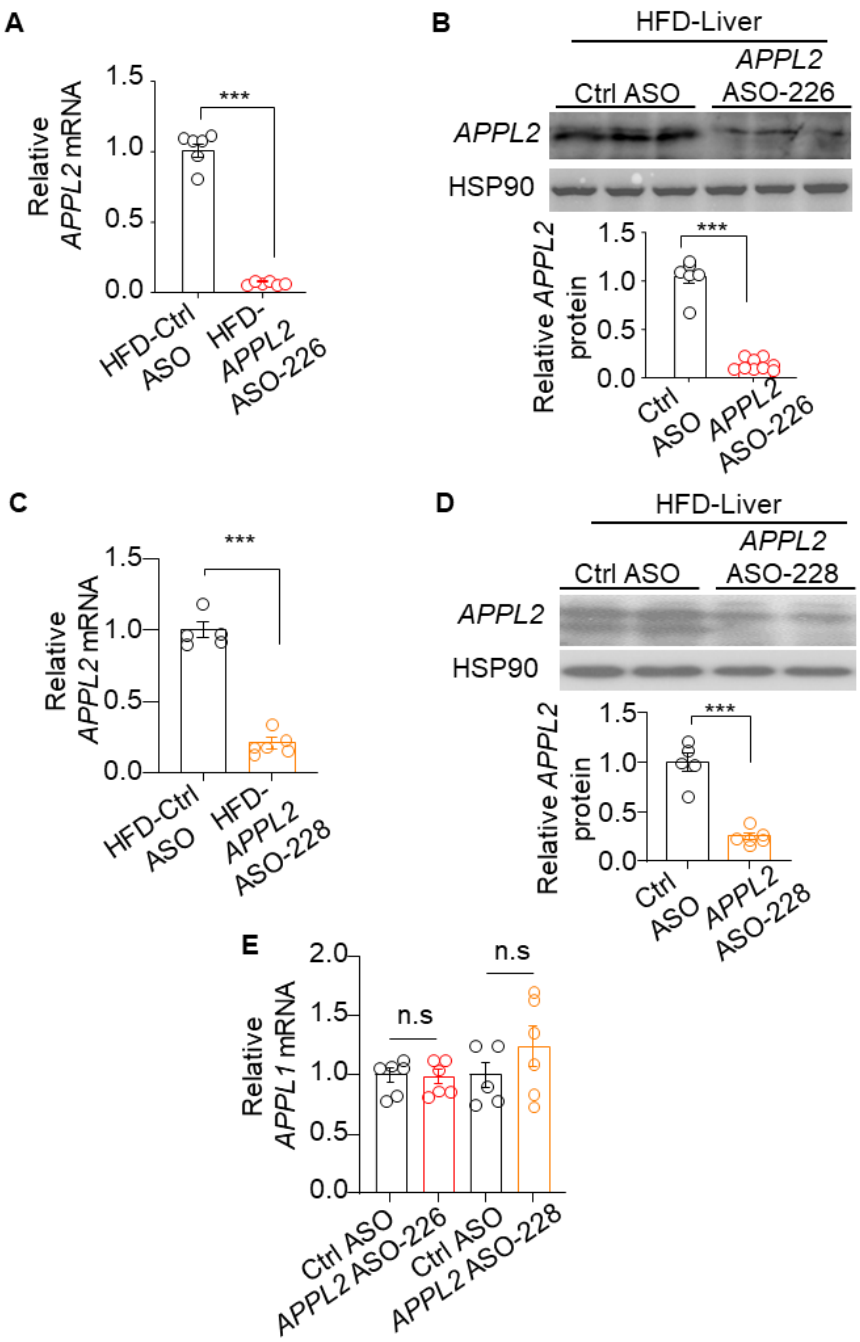


**Figure 3.2. *APPL2*-ASOs selectively reduce hepatic APPL2 in Diet-Induced-Obese (DIO) mice.**

Relative mRNA level of *APPL2* in liver for *APPL2*-ASO-226 **(A)** or *APPL2*-ASO-228 **(C)** treated mice. Relative mRNA level of *APPL1* in liver for *APPL2*-ASOs **(E)** treated mice. Immunoblotting analysis of hepatic APPL2 for *APPL2*-ASO-226 **(B)** or *APPL2*-ASO-228 **(D)** treated mice, relative levels were normalized by internal control HSP90 (heat shock protein 90). Student t-test (***$p<0.001$). Data are presented as mean ± SEM, n number was 5-6.

For evaluated indicators for long-term treatment, such as body weight and food intake were not changed after *APPL2*-ASOs treatment (**Figure** 3.3. A-D). Those treatment also showed no effect on weight of other key tissues, like adipose tissue and kidney (**Figure** 3.3. E,F).

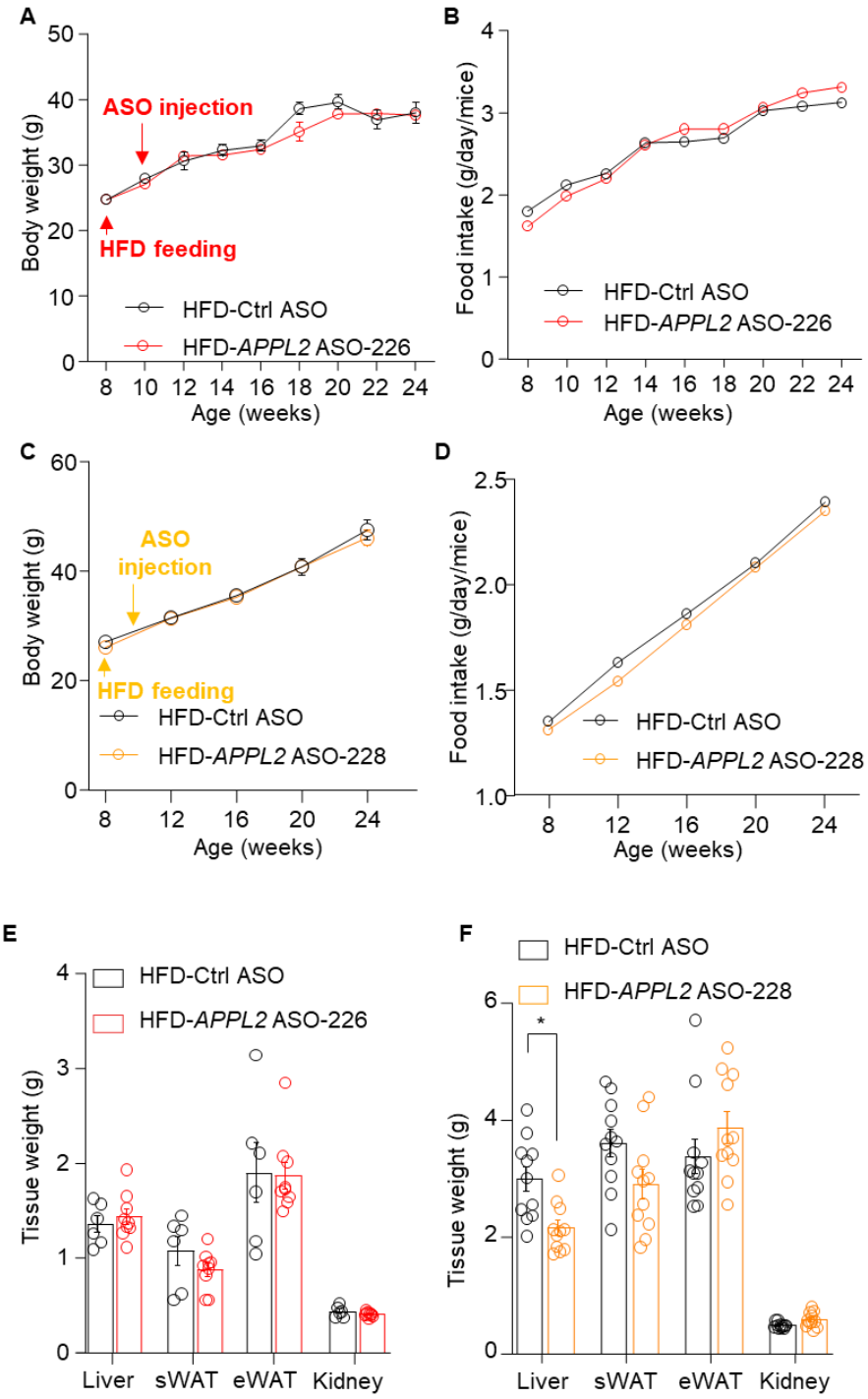


**Figure 3.3. Effect of APPL2 ASOs on body weight, food intake and tissue weight under the HFD feeding conditions.**

Bodyweight, food intake, and tissue weight for mice treated with *APPL2*-ASO-226 **(A,B,E)** or *APPL2*-ASO-228 **(C,D,F)** in HFD fed mice. Results were normalized by weights in control groups. Student t-test. Data are presented as mean ± SEM. Student t-test (*p<0.01).

### 3.2.3 Silencing hepatic APPL2 improves glucose metabolism.

APPL2 deficiency was found to improve insulin sensitivity[67]. To investigate the effect of *APPL2*-ASOs on glucose metabolism, I firstly programmed glucose tolerance test (GTT) and insulin tolerance test (ITT) respectively during treatment duration for STC fed mice. (**Figure** 3.4.)

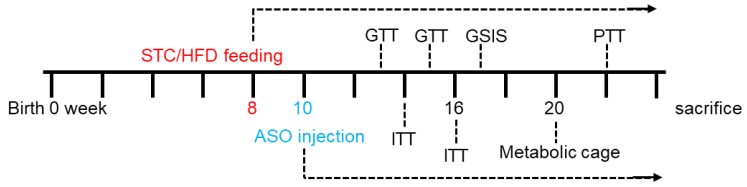


**Figure 3.4. Diagram of the experimental procedures.**

Glucose metabolism in mice can be assessed using a series of autocephalous *in vivo* tests. Glucose and insulin levels in response to stimuli enables a broader metabolic feature. To explore whether knockdown APPL2 affected whole-body glucose homeostasis, I subjected to mice with glucose, insulin, and pyruvate tolerance tests (GTT, ITT, and PTT, respectively).

Fasting glucose levels were first determined in mice fed STC. Mice treated with *APPL2*-ASO-226 or Ctrl-ASO groups have similar fasting blood glucose (FBG, 8.2±1.1 and 8.1±1.4 mmol/L) at the end of experiment. GTT results (including AUC analysis) indicated that *APPL2*-ASO-226 treated and Ctrl-ASO treated groups displayed similar glucose tolerance (**Figure** 3.5. A, B). Besides, *APPL2*-ASO-226 treatment did not change insulin sensitivity obviously (**Figure** 3.5. C, D). GTT and ITT

experiments at different ages were repeated, results showed the similar patterns. Consistent trends between groups were achieved. However, mice treated by *APPL2*-ASO-226 reduced circulating insulin concentration under fasting conditions (**Table** 3.2).

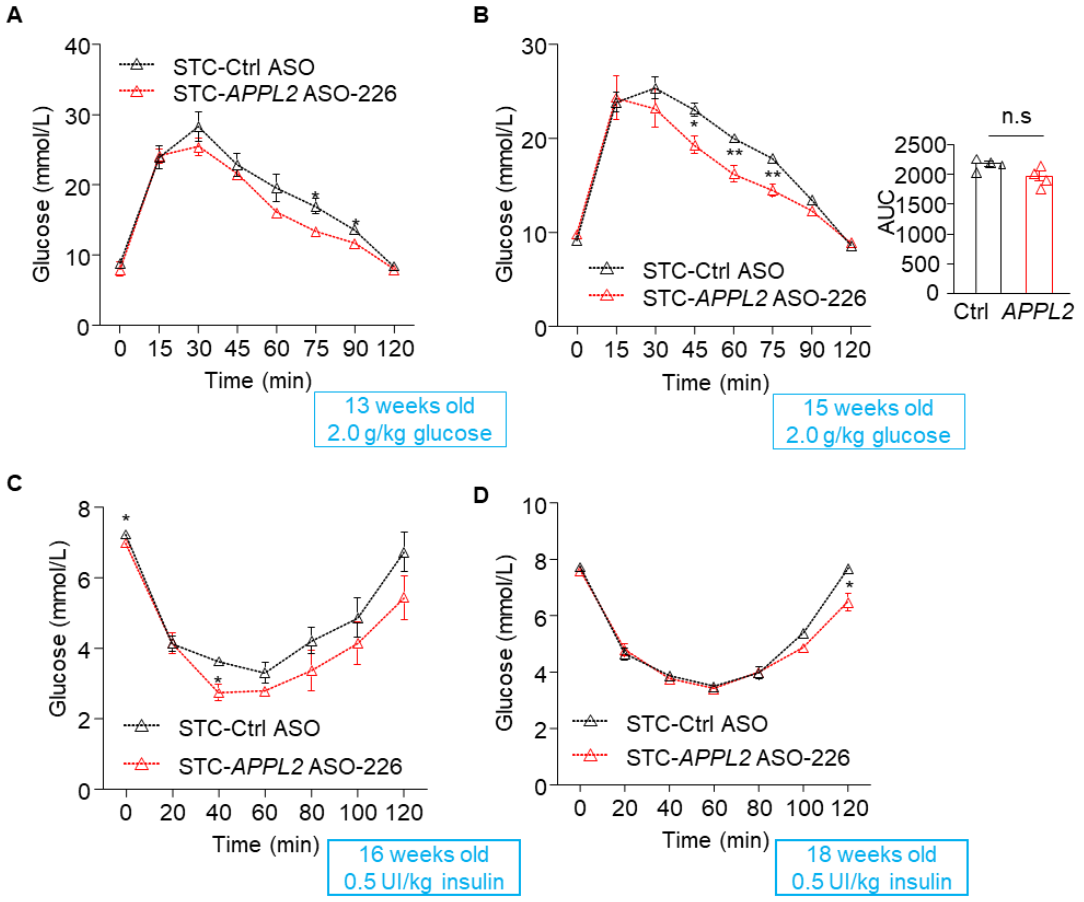


**Figure 3.5. *APPL2*-ASOs unalters glucose tolerance and insulin sensitivity for STC fed mice.**

**(A, B)** At age of 13 weeks and 15 weeks, 6-hour fasted mice were fasted for 6 hours were intraperitoneally injected with glucose (2 g/kg body weight). **(C, D)** At age of 16 and 18 weeks, 6-hour fasted mice were intraperitoneally injected with insulin (0.5 IU/kg). Glucose was tested as indicated timepoints. Two-way repeated measures ANOVA was used in statistics. (*p<0.05, **p<0.01 and ***p<0.001). Data is presented as mean ± SEM.

| | STC | |
|---|---|---|
| | **Ctrl-ASO** | ***APPL2*-ASO-226** |
| **Adiponectin (ug/mL)** | 19.2±2.7 | 22.2±3.9 |
| **MCP1 (ng/mL)** | 81±20 | 57±5 |
| **Glucose (mmol/L)** | 8.2±1.1 | 8.1±1.4 |
| **Insulin (ng/mL)** | 0.34±0.12 | 0.04±0.03* |
| **Triglyceride (mg/dL)** | 22.7±6.3 | 24.6±7.9 |
| **Cholesterol (mg/dL)** | 67.4±4.6 | 60.8±11.5 |

**Table 3.2. Effect of *APPL2*-ASOs on biomarkers levels in mice fed with STC.**

Mice treatment was described in legend of Table 3.1. Student t-test. Data are presented as mean ± SEM. Student t-test (*p<0.01).

A long-term HFD feeding significantly induces obesity and hyperglycemia, accompanied by impaired tolerance to both glucose and insulin[107]. To evaluate the effect of APPL2-ASOs treatment on glucose metabolism under different extent of insulin resistance, we conducted tolerance test on mice with different HFD feeding durations. GTT result presented that, differently from STC mice model, HFD-induced glucose intolerance was significantly alleviated in *APPL2*-ASO-226 treated mice compared to Ctrl (**Figure** 3.6. A, B), together with a reduced insulin level (**Table** 3.2.), suggesting that hepatic APPL2 knockdown protects mice from HFD-induced insulin resistance. This concept was verified by ITT, which displayed an explicit glucose-lowering and improved insulin-sensitive effect from silencing hepatic APPL2 by *APPL2*-ASO-226 (**Figure** 3.6. C, D).

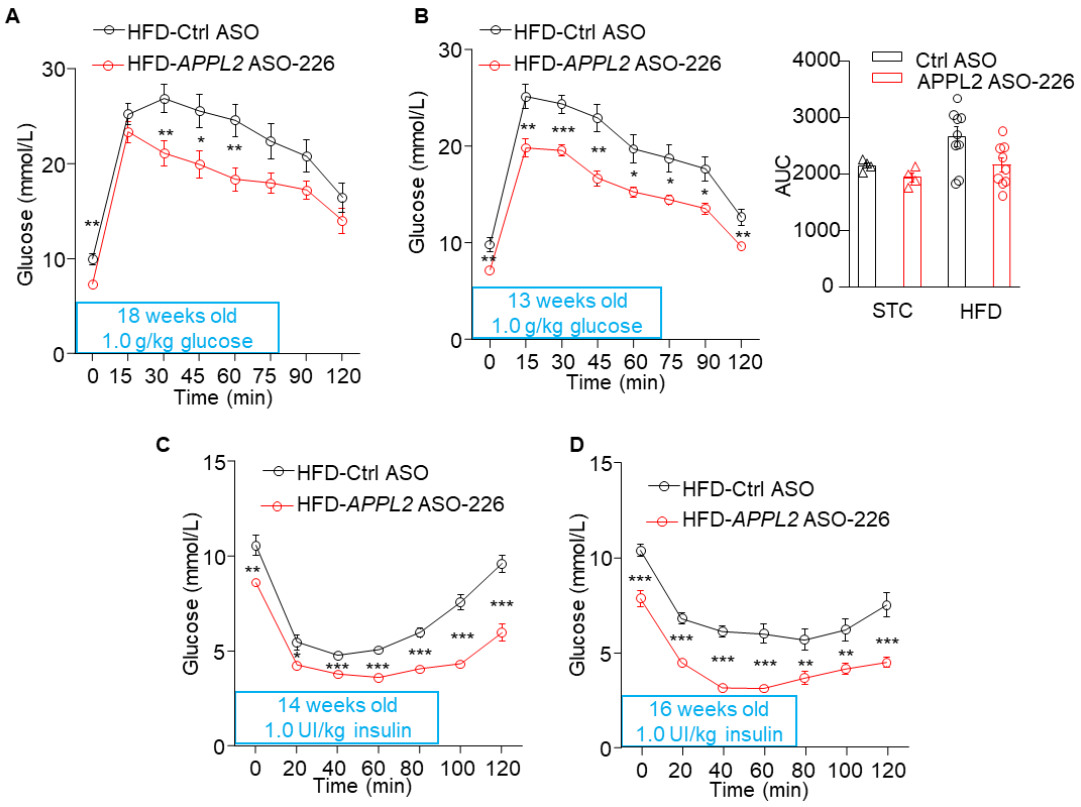


**Figure 3.6. *APPL2*-ASO-226 improves glucose metabolism for HFD fed mice.**

**(A, B)** At age of 13 weeks and 18 weeks, 6-hour fasted mice were fasted for 6 hours were intraperitoneally injected with glucose (1.0 g/kg body weight). **(C, D)** At age of 14 and 16 weeks, 6-hour fasted mice were intraperitoneally injected with insulin (1.0 IU/kg). Glucose was tested as indicated timepoints. Two-way repeated measures ANOVA was used in statistics. (*p<0.05, **p<0.01 and ***p<0.001). Data are presented as mean ± SEM.

| | **HFD + 10 mg/kg ASO** | | **HFD + 5 mg/kg ASO** | |
|---|---|---|---|---|
| | **Ctrl-ASO** | ***APPL2*-ASO-226** | **Ctrl-ASO** | ***APPL2*-ASO-228** |
| **Adiponectin (ug/mL)** | 25.4±1.2 | 23.9±1.8 | 30.1±6 | 51.0±7.6 *** |
| **MCP1 (ng/mL)** | 85.5±10.1 | 111.5±34.9 | 68.7±21.7 | 14.2±5.8 * |
| **Glucose (mmol/L)** | 12 W: 8.8±1<br>18 W: 10.5±1 | 12 W: 6.1±0.6 **<br>18 W: 8.6±0.7 *** | 16.4±0.7 | 15.9±0.6 |
| **Insulin (ng/mL)** | 12 W: 0.62±0.06<br>18 W: 1.13±0.12 | 12 W: 0.40±0.11 **<br>18 W: 0.83±0.11 *** | 0.72±0.36 | 0.75±0.31 |
| **HOMA-IR** | 12 W: 6.1±0.9 | 12 W: 2.7±0.6 *** | 13.0±4.1 | 14.6±4.9 |

| | | | | |
|---|---|---|---|---|
| | 18 W: 13.0±1.7 | 18 W: 7.8±1.5 *** | | |
| **TG (mg/dL)** | 30.9±9.2 | 30.9±6.7 | 39.5±9.8 | 40.7±10.9 |
| **FFA(mM)** | 0.71±0.1 | 0.55±0.1 | 0.42±0.20 | 0.46±0.10 |
| **AST (U/L)** | 14.9±3.2 | 15.1±3.8 | 70.7±23.7 | 68.9±28.0 |
| **ALT (U/L)** | 51.7±30.2 | 44.1±18.3 | 75.3±54.8 | 64.7±36.7 |

**Table 3.3. Serum biomarkers associated to glucose and lipid metabolism and liver injury.**

8 weeks old C57BL/6J male mice were fed with HFD for two weeks, then subcutaneously injected with *APPL2* ASO-226 (10 mg/kg b.w. each injection per week) or *APPL2* ASO-228 (5 mg/kg b.w. each injection per week). Mice were sacrificed at 24 weeks old, and tissues and serum were collected. Student t-test. Data are presented as mean ± SEM. Student t-test (*p<0.05, **p<0.01 and ***p<0.001). W=weeks old

To validate the effect of inactivating hepatic APPL2 on glucose metabolism, sequence of *APPL2*-ASO-228 was also used to treat hyperglycemic mice induced by HFD and high-surocse-high-cholesterol diet (HSHC). GTT and ITT results showed that *APPL2*-ASO-228 also alleviated glucose intolerance and improved insulin sensitivity (**Figure** 3.7). However, fasting insulin level in mice serum was not changed by *APPL2*-ASO-228 (**Table** 3.3.).

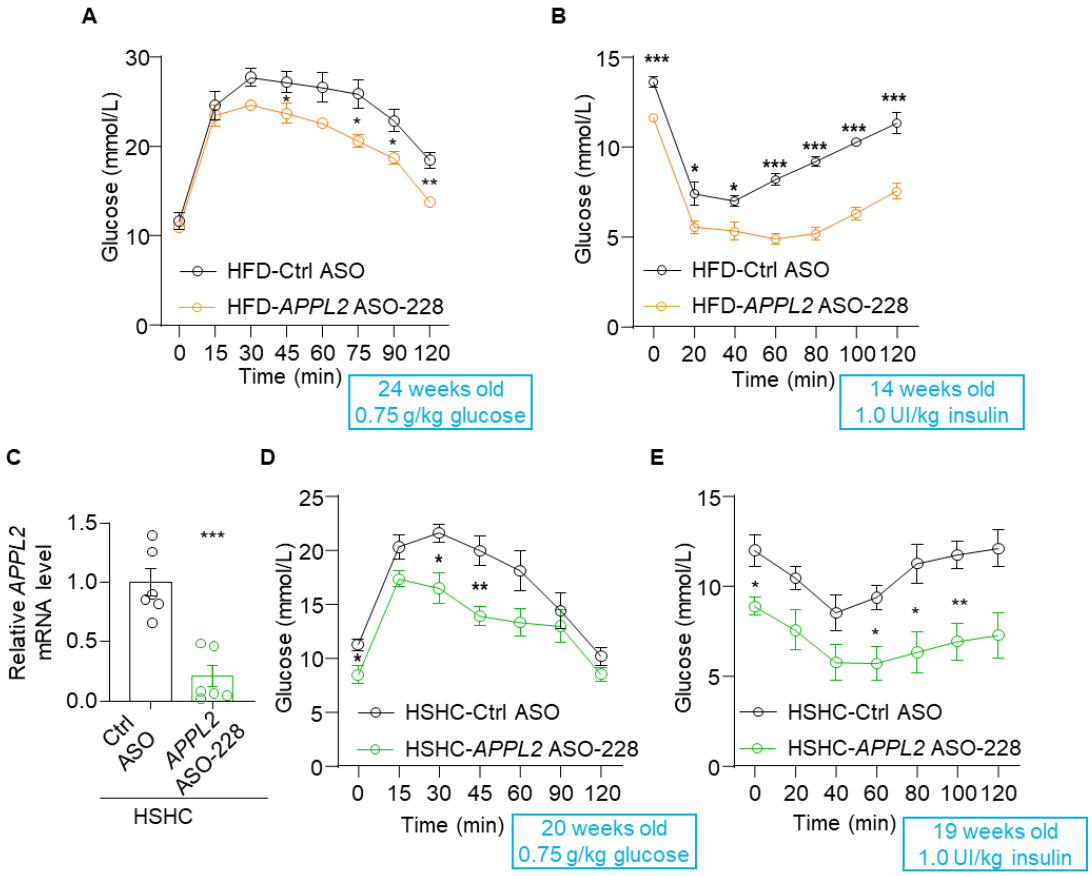


**Figure 3.7. *APPL2* ASO-228 improves glucose metabolism in HFD- or high-sucrose-high-cholesterol-diet fed mice.**

8 weeks old C57BL/6J male mice were fed with HFD or high-sucrose-high-cholesterol-diet (HSHC, 41% kcal fat, Research Diets D20043001) for two weeks, then subcutaneously injected to ASOs per week. After 17 injections (*APPL2* ASO-228, 5mg/kg b.w.), mice were sacrificed, and tissues and serum were collected. Corresponding Ctrl ASO was used as control. GTT **(A, D)** and ITT **(B, E)** were assessed in indicated ages. Two-way repeated measures ANOVA was used to compare glucose level between two groups. (*p<0.05, **p<0.01 and ***p<0.001 ). Relative mRNA levels of Appl2 **(C)** in mice liver were measured. Statistical significance was determined by two-tailed Student's t test.(***p<0.001). Data is presented as mean ± SEM.

De novo glucose generation (gluconeogenesis) and glycogen breakdown (glycogenolysis) play major roles in maintaining whole-body glucose balance. As available precursors, pyruvate maintains glucose homeostasis during prolonged

starvation in animals. Pyruvate tolerance test can be used to evaluate glucose production *in vivo*. The *APPL2*-ASO-226 treated mice displayed markedly reduction on blood glucose excursions in the PTT. The result indicated that hepatic gluconeogenesis was suppressed in mice with *APPL2*-ASO-226 (**Figure** 3.8. A).

Pancreatic β cells are able to perceive extracellular glucose concentration and secrete insulin as required at a given time. Besides higher insulin sensitivity, GSIS (Glucose-stimulated Insulin Secretion) was examined according to insulin levels during the initial 30 min of the glucose administration. Insulin secretion after glucose stimulation were comparable between two groups (**Figure** 3.8. B). This result indicted that hepatic APPL2 knockdown did not alter the insulin action and β cell function.

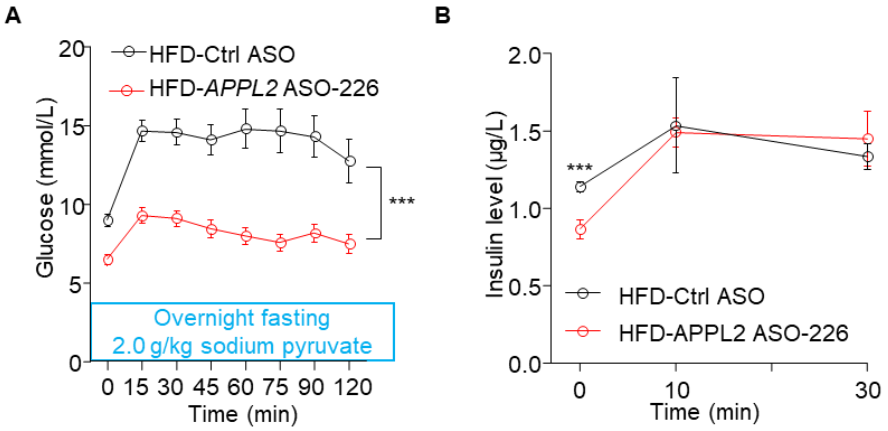


**Figure 3.8. *APPL2*-ASO-226 suppresses enhanced pyruvate tolerance in DIO mice.**

**(A)** After ASOs treatment for 12 weeks, the mice were fasted for overnight, followed by intraperitoneal injection of sodium pyruvate (2.0 g/kg body weight) and measurement of glucose level as indicated. **(B)** After ASOs treatment for 7 weeks, the mice were fasted for 6rs, followed by intraperitoneal injection of glucose (1.2 g/kg body weight) and measurement of insulin levels in 30 min. Two-way repeated measures ANOVA was used to compare glucose level between two groups (***p<0.001). Data is presented as mean ± SEM.

### 3.2.4 *APPL2*-ASOs treatment does not strenght adiponectin signaling.

Adiponectin, a hormone secreted from adipocyte, can improve insulin sensitivity. Hepatocyte-specific APPL2 deficiency enhanced adiponectin signaling in the liver and prevented mice from insulin resistance, and glucose intolerance[67]. Circulating adiponectin concentration significantly increased after *APPL2*-ASO-228 treatment instead of APPL2-ASO-226 (**Table** 3.3.).

Research showed that no significant difference in circulating adiponectin between the $APPL2^{HepKO}$ and Wildtype mice[67], suggested that the effects of hepatic APPL2 on insulin sensitivity appear as cell autonomous. In my result, adiponectin level in serum can be elevated by *APPL2*-ASO-228 but not by *APPL2*-ASO-226, correspondingly, fasting insulin level was decreased by *APPL2*-ASO-226 but not by -226. In this case, I hypothesized that hepatic APPL2 knockdown may promote glucose uptake via an insulin-independent pathway, probably increasing adiponectin signal by activating AdipoR1.

As active synthetic adiponectin receptor agonist, AdipoRon could potentially restore adiponectin signaling and improve insulin sensitivity[108]. Here, I treated mice with AdipoRon (10 mg/kg BW), measured glucose hourly within 6 hours. Result showed that Adiporon can obviously decreased glucose within the monitoring duration (**Figure** 3.9. A). However, the effect cannot be strengthened by both *APPL2*-ASO-228 (**Figure** 3.9. B). The result proves that that silencing APPL2 can improve glucose metabolism but seems not via activating intracellular adiponectin signaling.

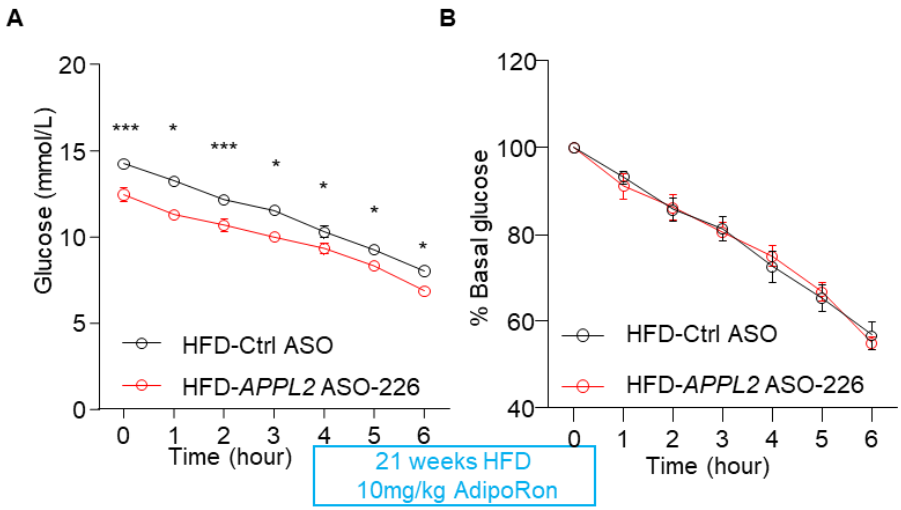


**Figure 3.9. *APPL2*-ASOs do not affect adiponectin signaling in DIO mice.**

After 11 ASOs injections, 3h-fasted mice were intraperitoneally subjected by AdipoRon (#B1879 Apexbio, US, 10 mg/kg body weight). Glucose levels at the indicated times were measured. Two-way repeated-measures ANOVA was used to compare glucose levels between two groups (*p<0.05, and ***p<0.001). Data are presented as mean ± SEM.

Taken together, these data suggested that inactivating hepatic APPL2 resulted in improving glucose homeostasis and insulin sensitivity when mice were metabolically challenged by HFD.

## 3.3 Summary

Unlike genetic modification, GalNAc-ASO is a potential clinical treatment. Protein function can be promoted or inhibited by downregulating target gene expression in specific tissues, thereby achieving a cure for disease. In this chapter, GalNAc-*APPL2*-ASOs of two different sequences were proved to specifically inactivate hepatic APPL2. The treatment was verified to be safe with neither obvious off-target effect nor liver

function damage. HFD was used to induce obesity, insulin resistance and hyperglycemia in mice. Therapeutic approach of GalNAc-*APPL2*-ASO was implemented to reduce hepatic APPL2 expression on gene and protein levels. The treatment regulated glucose metabolism, improved glucose tolerance and insulin sensitivity, and suppressed gluconeogenesis in HFD-induced obese mice.

# Chapter 4 RNA-Seq in mice liver

## 4.1 Introduction

Transcriptomics is a methodology that systematically depicts gene transcriptional profiles and reveals biological pathways and molecular mechanisms in network.

Before the development of sequencing technology, high-throughput gene expression array based on DNA hybridization on cDNA microarrays was the main approach to study gene expression information in animal and plant[109].

RNA-Seq can identify overall changes in gene expression, which reflect responses to specific treatment[110]. Unlike hybridization-based approaches, RNA-Seq can not only detect transcripts corresponding to existing genome sequence, but also discover and quantify novel transcriptional features. In this study, we preformed RNA-seq analysis with liver tissues to investigate transcriptome change by liver-specific knockdown APPL2, focusing on the differentially expressed genes (DEGs) between HFD-Ctrl-ASO and HFD-*APPL2*-ASO-226 groups. Altered transcripts levels of genes are used to enrich regulated pathways. Real-time quantitative polymerase chain reaction (QPCR) was used to verify the results of RNA-Seq.

Many software, such as David (https://david.ncifcrf.gov/); GOEAST (http://omicslab.genetics.ac.cn/GOEAST/ and KEGGArray (http://www.kegg.jp/kegg/download/kegtools.html), can realize annotation, enrichment analysis and functional prediction of differentially expressed genes.

The Gene ontology analysis (GO) aims to identify biological processes, cellular

locations and molecular functions[111]. Generally, genes with similar biological function and regulatory mechanism have similar GO annotation terms. GO term similarity of known genes in database and candidate genes is calculated to evaluate the effect of treatment on biological processes[112].

KEGG (Kyoto Encyclopedia of Genes and Genomes pathway enrichment analysis) is to enrich all differentially expressed genes in each differentially expressed gene pathway by calculating the hypergeometric distribution probability of the differentially expressed gene pathway, and then determine the pathways significantly associated to some differentially expressed genes through statistical test, so as to find the cellular biochemical processes that differentially expressed genes may participate in[113]. The biological hypothesis of pathway enrichment analysis is that changes in the expression of genes upstream will lead to changes in the expression of associated genes downstream, and the changes in the expression amount reach the statistically significant level of enrichment analysis. Among the many differentially expressed genes, many genes do not directly regulate each other in the corresponding pathway but participate in different links of a process together. These genes roughly constitute the overall outline of the pathway. For analysis, differentially expressed gene sets were imported into the pathway analysis software, and the pathways with significantly enriched differentially expressed genes were predicted by probability calculation and significance test of differentially expressed genes[114].

## 4.2 Result

### 4.2.1 Extracted total RNA are qualified.

To better investigate the underlying mechanisms behind hepatic silencing APPL2 associated hyperglycemia progression, RNA-seq analysis was performed to characterize the comprehensive hepatic transcriptome. Firstly, RNA samples were extracted from the liver obtained from mice in STC-Ctrl-ASO, STC-*APPL2*-ASO-226, HFD-Ctrl-ASO and HFD-*APPL2*-ASO-226 groups. The automated parallel capillary electrophoresis and qualification test results showed RNA extracted samples were validated to be qualified with RNA mass, concentration, and integrity. All samples showed RNA integrity (RIN) higher than 7.0, which can be used for subsequent application (**Table** 4.1).

A total of 20 RNA-seq libraries were constructed. The sequencing was on DNBSEQ platform. After sequencing, the raw reads were filtered. The reads were aligned to the mouse genome and quantified. Differential expression analysis was performed using DESeq2. Both featureCounts and DESeq2 were included in the BioConductor package. They were used due to their speed and low computational cost. The brief workflow was shown (**Figure** 4.1).

| No. | Sample name | Concentration ng/μL | RIN | 28S/18S |
|---|---|---|---|---|
| 1 | STC-Ctrl-ASO-226-1 | 873.6 | 10.0 | 2.5 |
| 2 | STC-APPL2-ASO-226-2 | 1993.8 | 8.6 | 1.5 |

| | | | | |
|---|---|---|---|---|
| 3 | STC-Ctrl-ASO-226-3 | 2383.9 | 9.7 | 1.7 |
| 4 | STC-APPL2-ASO-226-4 | 1681.4 | 10.0 | 3.5 |
| 5 | STC-Ctrl-ASO-226-5 | 1087.7 | 8.3 | 4.8 |
| 6 | STC-Ctrl-ASO-226-6 | 1244 | 10.0 | 5.4 |
| 7 | STC-APPL2-ASO-226-7 | 790.4 | 9.8 | 0.1 |
| 8 | STC-APPL2-ASO-226-8 | 1947.7 | 9.0 | 1.6 |
| 9 | HFD-Ctrl-ASO-226-1 | 1066.0 | 8.7 | 2.0 |
| 10 | HFD-Ctrl-ASO-226-2 | 1173.1 | 8.5 | 1.2 |
| 11 | HFD-Ctrl-ASO-226-3 | 1987.1 | 8.9 | 1.1 |
| 12 | HFD-Ctrl-ASO-226-4 | 1124.8 | 8.9 | 2.3 |
| 13 | HFD-Ctrl-ASO-226-5 | 1006.5 | 8.4 | 1.2 |
| 14 | HFD-Ctrl-ASO-226-6 | 2288.7 | 9.6 | 2.7 |
| 15 | HFD-APPL2-ASO-226-8 | 2004.6 | 8.5 | 1.0 |
| 16 | HFD-APPL2-ASO-226-11 | 1438.3 | 8.6 | 1.3 |
| 17 | HFD-APPL2-ASO-226-12 | 1030.4 | 8.6 | 1.4 |
| 18 | HFD-APPL2-ASO-226-13 | 1888.9 | 8.5 | 1.4 |
| 19 | HFD-APPL2-ASO-226-14 | 2748.1 | 8.5 | 1.4 |
| 20 | HFD-APPL2-ASO-226-15 | 2290.4 | 9.6 | 3.3 |

**Table 4.1. Total RNA extracted from the mice liver are qualified.**

After 16 weeks of the experiment, mice livers in four groups were collected for RNA sequencing. Total RNA was extracted from 20 liver samples by Trizol and cleaned up by using RNeasy Mini Kit. Concentration, 28S/18S and RNA integrity (RIN) were determined by Fragment Analyzer.

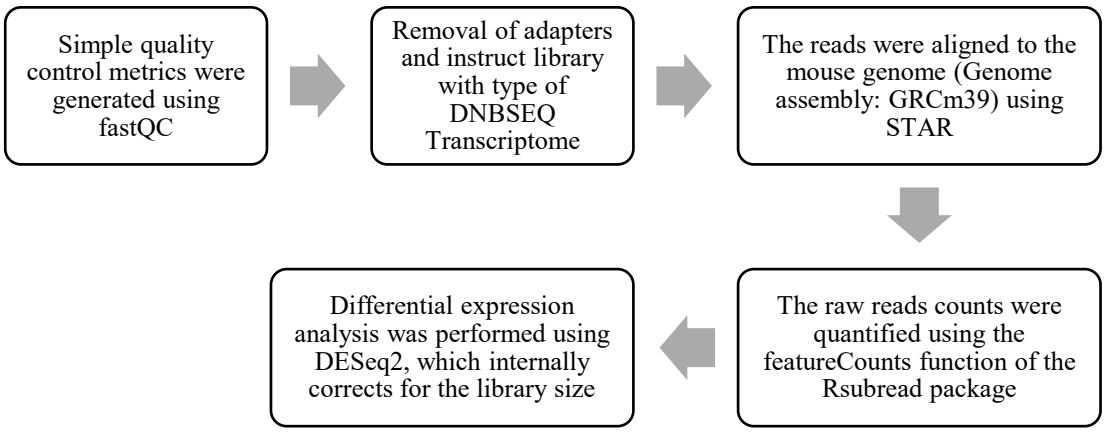


**Figure 4.1. Workflow of RNA-Seq raw data analysis.**

RNA sequencing was performed on an DNBSEQ platform (BGI, the Shenzhen Genomics Institute, https:// www.genomics.org.cn). The differentially expressed genes (DEGs) analysis was performed by using the software of DESeq. The workflow was briefly described.

### 4.2.2 Differentially expressed genes are analyzed.

After filtering low read counts and normalization, over 55000 transcripts remained in each sample. Firstly, principal component analysis (PCA) analysis was preformed to identify subgroups of individual samples. It showed a clear distinction between groups reflecting the pronounced hepatic transcriptome changes in HFD vs. STC, and Ctrl-ASO vs. *APPL2*-ASO (**Figure** 4.2. A).

Of those RNA-transcript expression, only mRNAs showing adjusted p value <0.05 and log2 fold change >1 or <−1 were considered differentially expressed genes (DEGs) for further bioinformatics analyses. The DEGs were further inspected manually and analyzed computationally using normalized read counts. 23781 and 25764 DEGs were indicated in STC or HFD group respectively. In STC group, 2496 genes were significantly regulated with p value<0.05, in which 1138 genes were down regulated, and 1358 genes were upregulated; in HFD group, 3802 genes were significantly regulated with p value<0.05, in which 1903 were down regulated and 1899 genes were upregulated.

The volcano plots showed pairwise ("*APPL2*-ASO-226" Versus "Ctrl-ASO") transcript accumulation differences in HFD (**Figure** 4.2. B) group, which demonstrated substantial differences after APPL2 knockdown.

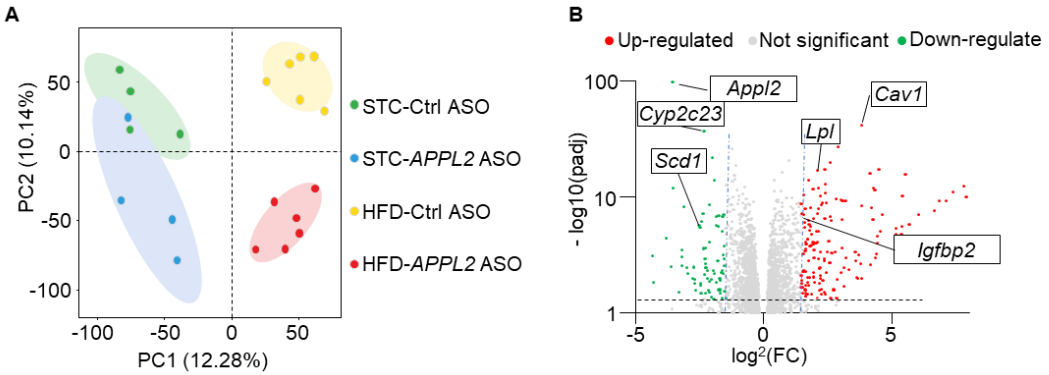


**Figure 4.2. PCA and volcano plot from DEGs of liver**

**(A)** Principal component analysis (PCA) showing the clustering of samples in four groups. **(B)** Enhanced volcano plot showing the statistical significance, with -log10 (adjusted *p*-value (padj)) versus log2 of fold change of gene expression between HFD-Ctrl-ASO and HFD-*APPL2*-ASO-226 livers. Red points: significantly up-regulated; green points: significantly down-regulated.

### 4.2.3 Pathways are enriched using various analysis methods.

The biological hypothesis of pathway enrichment analysis is that changes in the expression of genes upstream of the pathway will lead to changes in the expression of associated genes downstream. Therefore, changing the expression of many genes in the pathway, and the changes in the expression amount reach the statistically significant level of enrichment analysis. To identify the influenced downstream pathway of APPL2 knockdown, the list of differentially expressed genes were used to detect the enrichment of functional gene sets using a variety of computational methods, such as DAVID (http://david.ncifcrf.gov) or EnrichR (http://amp.pharm.mssm.edu/Enrichr/).

Firstly, DAVID analysis was used to enrich pathways. DAVID functional annotation cluster analysis was performed on the list of DEGs with a log2 FC >1 or <−1 with p value<0.05. Only those terms with count number ≥15 genes were selected for analysis.

Functional annotations showing significantly ($p<0.05$) increased or decreased enrichment compared with control groups were classified according to their associated biological processes, cellular components, and molecular functions. The gene ontology (GO) term biological process (BP) in DAVID was used to categorize enriched biological themes. Five terms in each category were listed (**Figure** 4.3. A, B). Pathway mapping was also performed using the KEGG in DAVID (**Figure** 4.3. C, D).

According to the previous result, *APPL2*-ASO-226 treatment led to hepatic APPL2 expression decreased and influenced glucose homeostasis, insulin sensitivity, and energy metabolism. The top enrichment pathways associated to metabolism included fatty acids metabolic process, amino acid degradation, gluconeogenesis, and bile secretion.

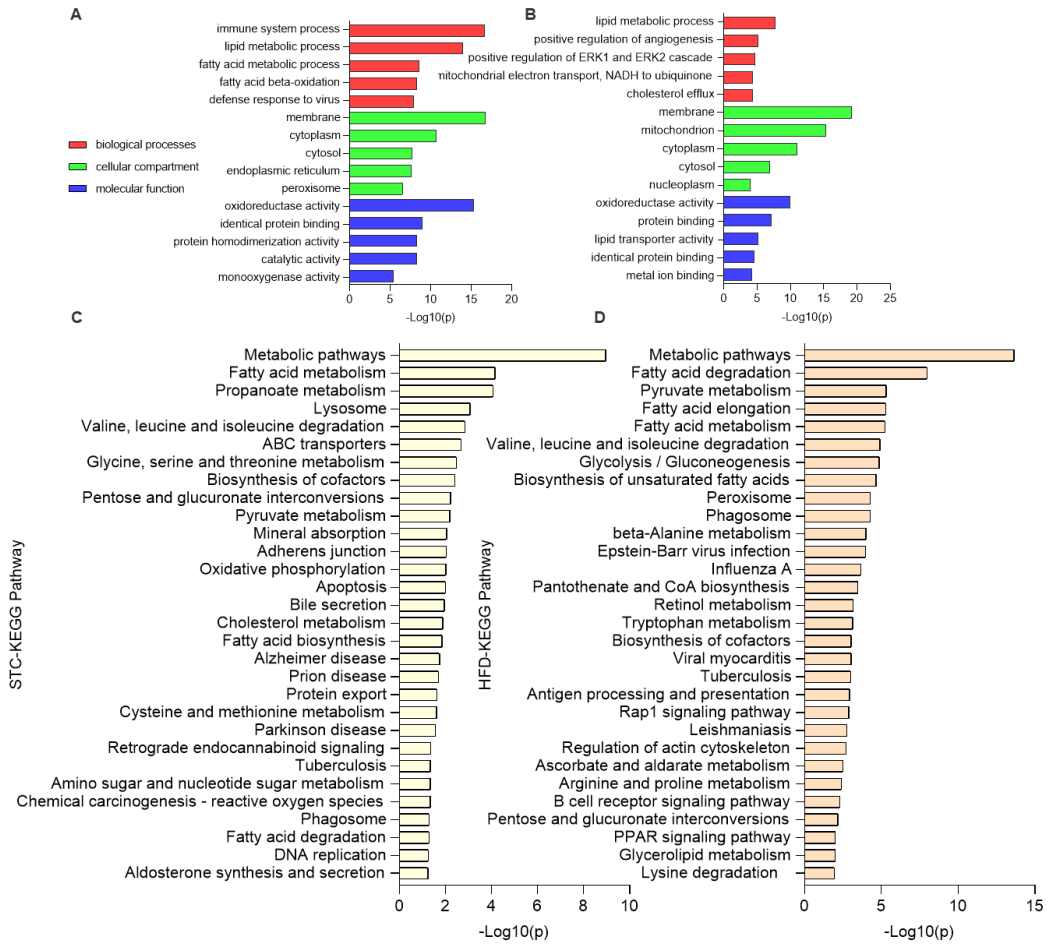


**Figure 4.3. Gene Ontology Enrichment Analysis (GO) analysis using (DAVID).**

The enriched terms in STC **(A)** or HFD **(B)** group were presented as top five biological process (BP) and each top five cellular compartment (CC) or molecular function (MF) category by DAVID. Kyoto Encyclopedia of Genes and Genomes (KEGG) pathways enrichment was analyzed by DAVID. The enriched terms in STC **(C)** or HFD **(D)** group were presented as top thirty pathways. The cutoff of differentially expressed genes was chosen as the p value less than 0.05.

Next, Package EnrichR analysis was used to confirm the DAVID analysis result.

**Figure** 4.4. showed the above four pathways were still top enriched.

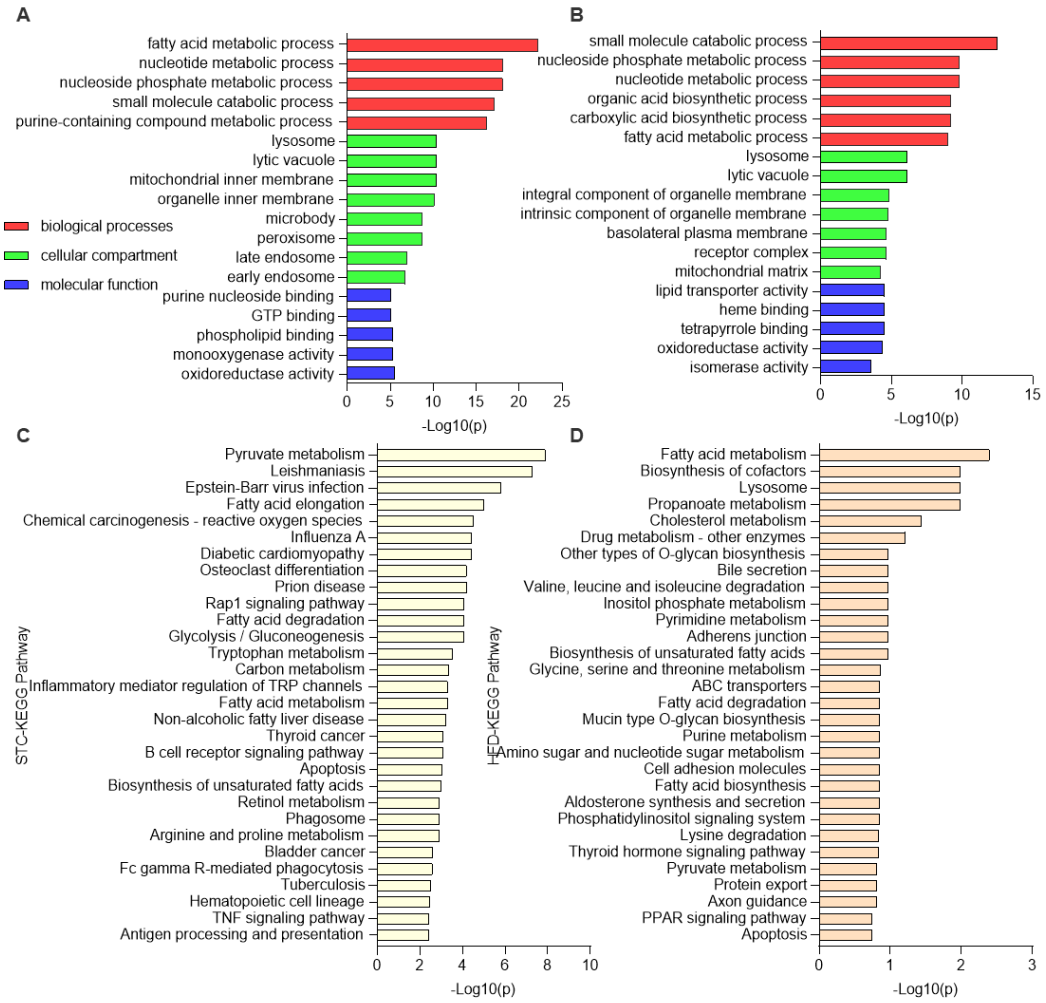


**Figure 4.4. GO and KEGG analysis using R package.**

Go and KEGG were analyzed by using R package integrated with ClusterProfiler and PathView. The enriched terms were presented as the top five for each GO category (**A**, STC; **B**, HFD) and the top thirty for KEGG pathways (**C,** STC; **D**, HFD). The cutoff of differentially expressed genes was chosen as the p-value less than 0.05.

To screen the differentially expressed genes in top enriched pathways and accord with the phenotype of mice after *APPL2*-ASO-226 treatment, GO and KEGG results from R-package and DAVID were integrated (**Figure** 4.5. A, B).

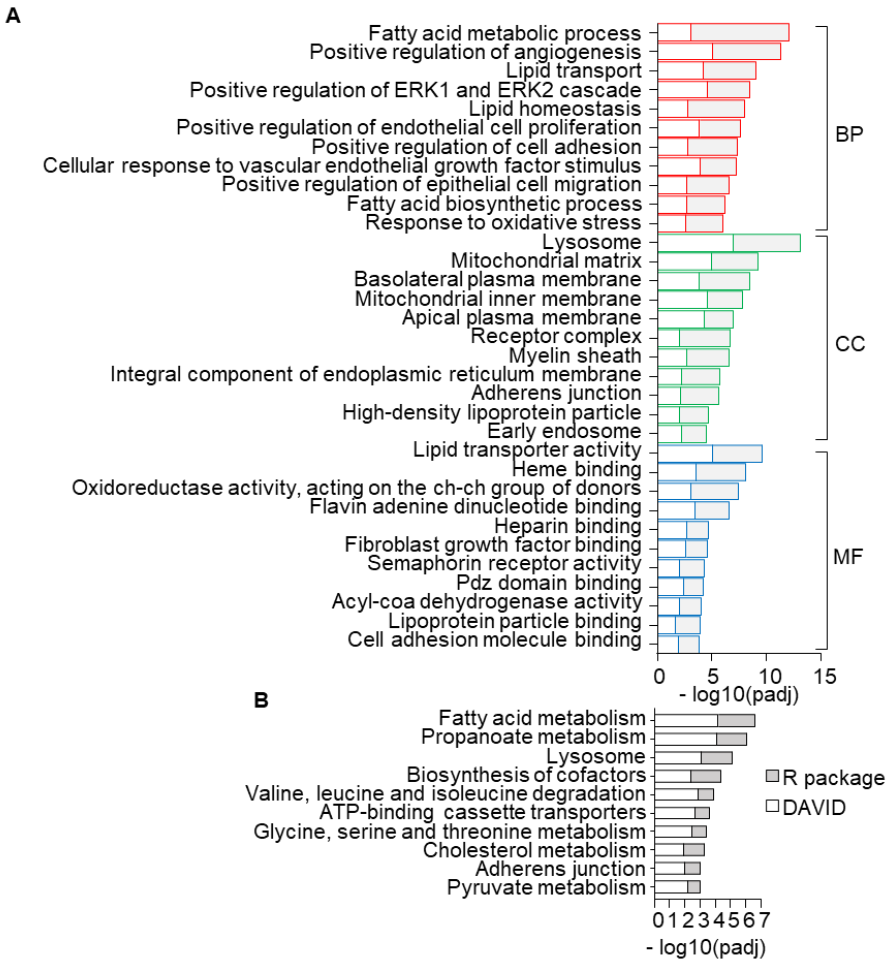


**Figure 4.5. Functional enrichment analysis.**

Analyzed result from HFD groups were integrated from **DAVID and R package**. Chord plot illustrated the 10 remarkably enriched items in the biological processes (BP), cell component (CC) and molecular function (MF) in GO analysis. The top significant 5 GO terms (-log10(padj) < 0.05) **(A)** and the top 10 significant KEGG pathway terms between two compared groups **(B)** were listed.

### 4.2.4 Up- or down-regulation pathways are enriched using GSEA.

In traditional KEGG (pathway enrichment analysis) and GO (functional enrichment analysis) analysis, overall expression pattern of this pathway (inhibited or activated) cannot be indicated, since there are both up-regulated and down-regulated differential genes in the same pathway. This is because the traditional enrichment analysis does not

consider the changing trend of gene expression after treatment, and the core of its algorithm only focuses on whether the distribution of these differential genes is consistent with the distribution obtained by random sampling.

Traditional enrichment analysis separately extracts up-regulated or down-regulated differential genes in advance to avoid the above problem. However, this approach is biased, because Fisher's exact test is intended to prove that the list of differential genes is not randomly sampled and filtering the list of differential genes up or down in advance will interfere with the randomness of the results, and the accuracy of the conclusion will be affected. In addition, when performing biological functions in cells, up-regulated and down-regulated genes play a role together, so it is not practical to analyze up-regulated and down-regulated genes separately when conducting enrichment analysis. I also used Gene Set Enrichment Analysis (GSEA) tool to analyze enrichment of functional gene sets.

Compared to DAVID and R package analysis, GSEA analysis result showed more various pathways. The coincident of top enriched pathways, such as amino acid metabolism, fatty acids metabolism (up-regulated in APPL2-ASO group), and pyruvate metabolism (down-regulated in APPL2-ASO group) were highlighted for further analysis (**Figure** 4.6.).

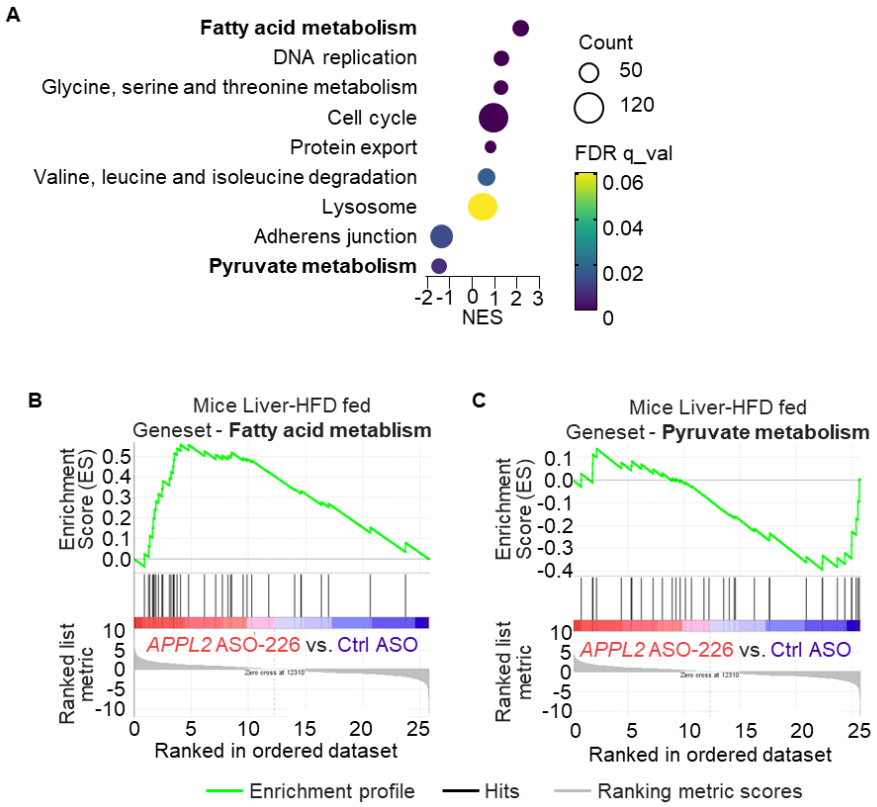


**Figure 4.6. Gene Set Enrichment Analysis (GSEA) highlights several glucose and lipid metabolism associated signatures.**

The reference gene sets were c5.bp.v7.5.1.symbols. gmt, downloaded from the Molecular Signature Database. Genes were ranked using the log2 ratio metric with 1000 permutations centered on gene set. **(A)** Top ten up- or down-regulated biological pathways with the false discovery rate (FDR) value less than 0.25, comparing by the Normalized Enrichment Scores (NES). In the bubble plot, the right bubble represents inhibition determined by negative NES and the left bubble represents activation determined by positive NES. The size of bubble represents gene set size in the enriched pathway and dark blue means small FDR value. Fatty acid metabolism **(B)** and pyruvat metabolism **(C)** pathways was up- or down-regulated in HFD-*APPL2*-ASO group.

To validate the RNA-Seq result, we selected over twenty DEGs from the above enriched pathways (**Figure** 4.7.A) and used QPCR to measure mRNA level of DEGs related to metabolism in mice liver (**Figure** 4.7. B, C).

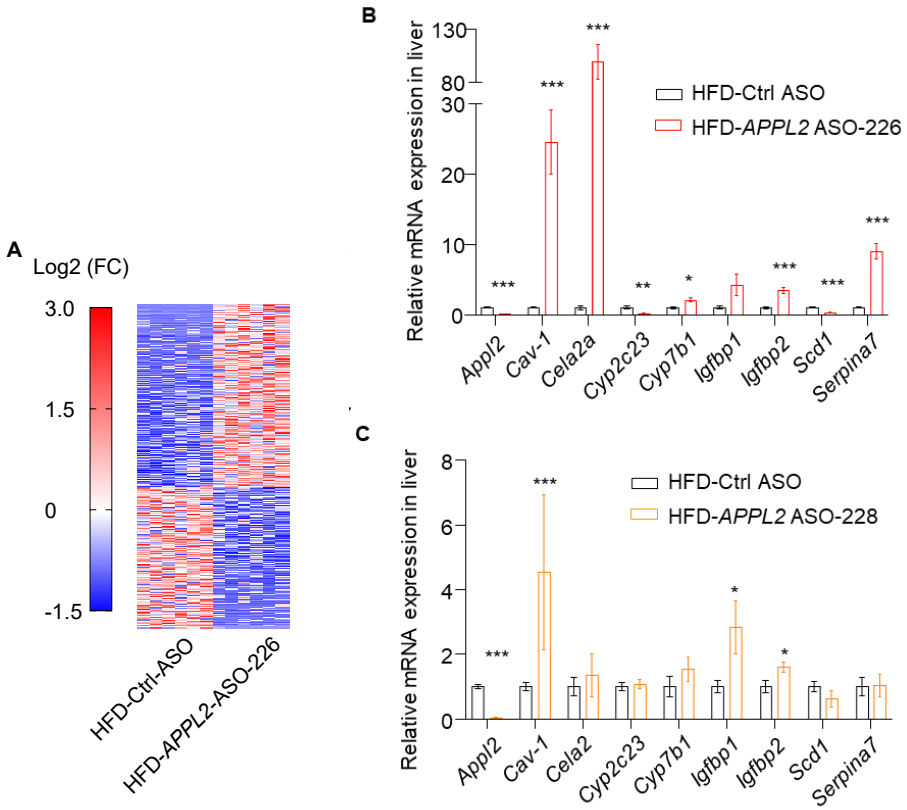


**Figure 4.7. Heatmap and mRNA level validation of RNA-Seq.**

**(A)** Heatmap represented the top 500 significant (sorted based on padj) gene expression in HFD-Ctrl or HFD-*APPL2*-ASO-226 treated livers. RT-qPCR quantification of selected genes in the mice liver treated with HFD-Ctrl, HFD-*APPL2*-ASO-226 **(B)** (n = 6) and HFD-*APPL2*-ASO-228 **(C)** (n = 5). Student's t test (*p<0.05, **p<0.01, ***p<0.001). Data is presented as mean ± SEM.

*Cela2a* and *Igfbp-2* were associated to glucose metabolism. *Cela2a* was reported to trigger insulin secretion and increase insulin sensitivity[115]. Insulin-like growth factor-1 binding protein 2 (IGFBP2) was reported to increase the insulin-stimulated glucose uptake by inducing GLUT4 translocation[116].

Stearoyl-CoA desaturase enzyme 1(*Scd1*), caveolin-1*(Cav-1*) and Cytochrome P450 Family 7 Subfamily B Member 1(*Cyp7b1*) were associated to lipid regulation.

Caveolin-1 was also reported to mediate induction of APPL1 nuclear translocation by adiponectin[117]. As proved in mice model, *Scd1* promotes glucose utilization for fatty acids de novo synthesis[118], Knockout *Cav1* elevated triglyceride and free fatty acids levels[119]. *Cyp7b1* was indicated as a key regulator in fatty acids metabolism[120]. Under cold stress, hepatic *Cyp7b1* induced bile acid synthesis and increased fatty acids uptake in brown adipose tissue (BAT). in addition, adaptive thermogenesis higher glucose needs and insulin sensitivity of BAT[121-122].

Decreased hepatic thyroid binding globulin (*Serpina7*) was responsible for an increased supply of free thyroid hormones to tissues during cold adaptation[123]. Theses QPCR results also proved that RNA-Seq analysis was reliable in our scheme.

### 4.2.5 IGFBP2 mediates anti-hyperglycemia effect of silencing hepatic APPL2.

In RNA-Seq result, some pathways associated to glucose homeostasis were enriched, but none of these pathways were directly associated to insulin sensitivity. We suspected some other possibilities which result the regulation of glucose metabolism in mice. For example, some hepatokines can secrete into the circulation by the liver and acts primarily on peripheral organs, where it gives rise to its insulin-sensitizing effects[124-125]. Considering with the energy metabolism changes, peripheral organs can also consume glucose for energy production. Brown adipose tissue utilizes both glucose as fuel[126]. Glucose metabolism generates energy via the glycolytic and oxidative pathways

in muscle[127]. Thereby, we reasonably suspected the reduction of hepatic APPL2 might affect hepatokines secretion which act on peripheral organs, thereby regulating blood sugar levels.

Based on this, differentially expressed genes with adjusted-p-value < 0.05 and -1.5 < log2 foldchange > 1.5 were screened according to DESeq2 result between two groups with HFD feeding. These DEGs were sorted according to the criteria of p-value from small to large, FC absolute value from large to small, and those with higher expression first. Among the genes with the highest ranking results, several **secretory protein-coding genes** associated with glucose, lipid or energy metabolism were listed, including *Cav-1*[128], *Lpl*[129], *FGF21*[130], *Igfbp1*, *Igfbp2*[131] and *Serpina7* (Figure 4.2. B).

The above mRNA expression differences were validated in liver among mice treated with Ctrl-ASO, *APPL2*-ASO-226 and *APPL2*-ASO-228, respectively. Nevertheless, only Igfbp2 mRNA was simultaneously and significantly upregulated during treatments of both *APPL2*-ASO sequences (**Figure** 4.7. B, C). As reported, IGFBP2 overexpression via adeno-virus reduced blood glucose in wild-type and diabetic mice and potently suppressed hepatic glucose production (HGP)[132]. Thereby, we determined the IGFBP2 protein expression in mouse liver and serum. HSP90 was used as an internal control to calibrate IGFBP2 protein expression in liver samples, and adiponectin or albumin was used in serum samples. Immunoblot result showed that both sequences of *APPL2*-ASOs can significantly increase hepatic IGFBP2 protein levels, in parallel with elevated secretion of IGFBP2 (**Figure** 4.8.). This result was

also consistent with previous animal study[133], the change of gene expression was paralleled by IGFBP2 protein level in liver tissue under different metabolism states, as well as plasma level. In addition, *APPL2*-ASO-226 can increase IGFBP2 expression more markedly than *APPL2*-ASO-228. Correspondingly, the anti-hyperglycemia effect of *APPL2*-ASO-226 was more effective than *APPL2*-ASO-228 (**Figure** 3.8.).

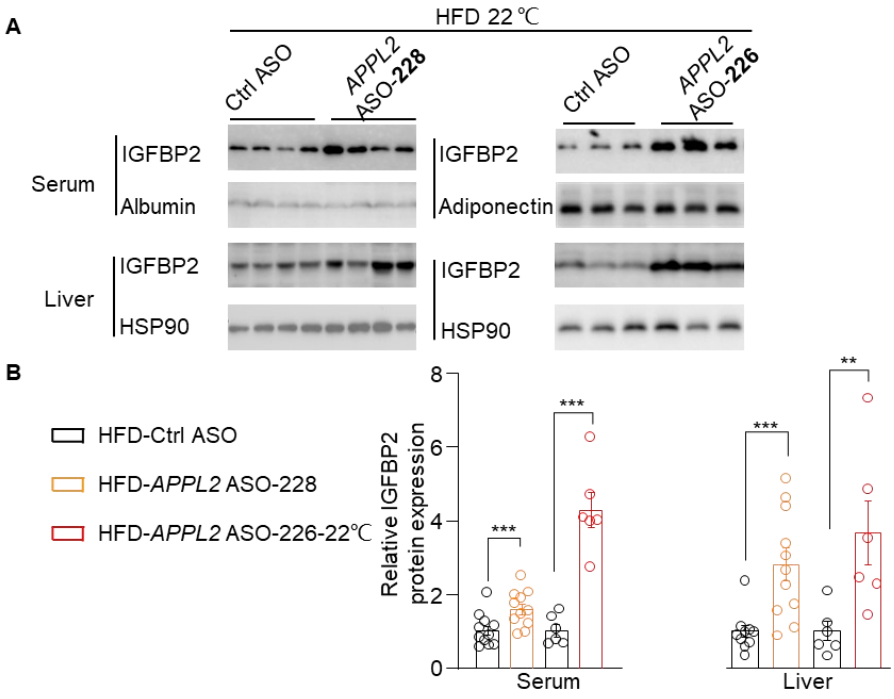


**Figure 4.8. *APPL2*-ASOs up-regulates IGFBP2 expression in liver and serum of DIO mice.**

**(A)** IGFBP2 protein expression in liver and serum of mice with Ctrl-ASO, *APPL2*-ASO-226 and *APPL2*-ASO-228. Hepatic expression was normalized by HSP90, and circulating expression was normalized by adiponectin or albumin. **(B)** Quantification of IGFBP2 expression by ImageJ. Student t test (***p<0.001). Data is presented as mean ± SEM.

To further confirm the *in vivo* findings, we examined the effect of inactivating APPL2 on upregulating IGFBP2 using primary hepatocytes isolated from *APPL2*-ASO-226

treated HFD mice. Conditional medium was concurrently collected to determine IGFBP2 level secreted from primary hepatocyte. Consistent with our observations in the liver, inactive APPL2 primary hepatocytes displayed an increase in IGFBP2 mRNA and protein expression when compared with that in their respective control cells (**Figure**.4.9. A). The secretion of IGFBP2 protein into cell culture supernatant was significantly raised in primary hepatocytes isolated from *APPL2*-ASO-226 treated mice compared to control (**Figure**.4.9. B) and found to be reflected in a significant enhance of circulating IGFBP2 levels in same group (**Figure**.4.8).

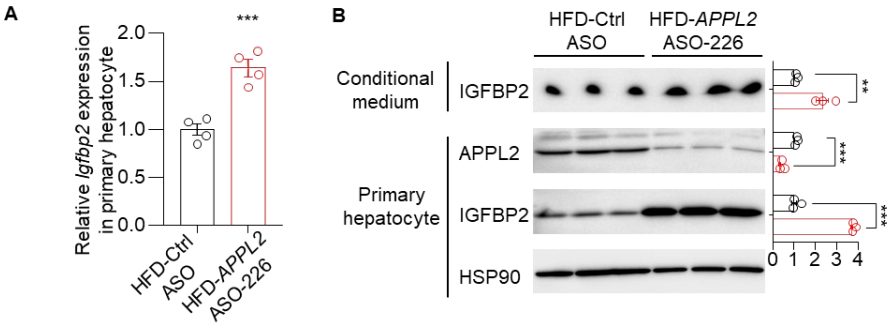


**Figure 4.9. *APPL2*-ASO-226 up-regulates IGFBP2 expression and secretion in primary hepatocyte.**

Primary hepatocyte was isolated from mice fed with HFD and treated by *APPL2*-ASO-226 or Ctrl-ASO, supernatant of culture medium was collected. **(A)** *Igfbp2* mRNA expression of primary hepatocyte. **(B)** IGFBP2 protein expression in cell lysate and conditional medium. Protein expression level was normalized by HSP90. Student t test (***p<0.001). Data is presented as mean ± SEM.

Taken together, these findings indicated IGFBP2, as a hepatokine, might play a role on mediating anti-hyperglycemia effects of silencing hepatic APPL2.

### 4.2.6 Inactivation of hepatic APPL2 lowers pyruvate-driven hepatic glucose production.

The liver is imprtant on maintaining blood glucose, through controling the processes of glycogen breakdown (glycogenolysis), glycogen synthesis (glycogenogenesis) and glucose synthesis (gluconeogenesis). Extra glucose is stored as glycogen after meal. During initial fasting, glucose is produced by glycogenolysis, then by gluconeogenesis. However, hepatic gluconeogenesis happens not only during fasted state but also in common physiologically fed state. Enhanced gluconeogenesis is a signature of T2DM.

In my previous pyruvate tolerance test (**Figure**.3.8. A), pyruvate-induced glucose excursions were decreased, assuming that the anti-hyperglycemic activity of silencing hepatic APPL2 is primarily due to the suppression of hepatic gluconeogenesis. In mammals, gluconeogenic precursors include glycerol, lactate/pyruvate, certain amino acids, and odd-chain length fatty acids[134]. This less utilization of amino acids for de novo glucose synthesis in APPL2-ASO treated mice might be associated with a higher plasma concentration of most amino acids[135].

Therefore, we collected serum of mice with 24h-fasting, measured free animo acid concentration by using LC-MS, and circulating pyruvate content by colorimetric method (Pyruvate Assay Kit, ab65342). The result showed that concentration of Asp reduced, while His, Val, Leu raised (**Table**.4.2).

| Essential amino acid | Concentration (μM) | |
|---|---|---|
| | HFD-Ctrl-ASO | HFD-*APPL2*-ASO-226 |
| Ala | 264±34 | 229±57 |
| Arg | 33±25 | 9±5 |
| Asn | 28±6 | 28±5 |
| Asp | 30±6 | 18±5 ** |
| Gln | 483±130 | 556±176 |
| Gly | 244±43 | 232±41 |
| His | 49±7 | 68±9 ** |
| Met | 34±4 | 39±8 |
| Pro | 58±9 | 48±10 |
| Ser | 93±17 | 128±18 * |
| Val | 144±27 | 191±17 ** |
| Glu | 84±20 | 39±11** |
| Ile | 66±13 | 81±9 |
| Phe | 54±8 | 62±8 |
| Thr | 101±18 | 100±19 |
| Tyr | 47±10 | 57±8 |
| Trp | 65±9 | 70±6 |
| Leu | 110±28 | 148±17 * |
| Lys | 225±20 | 270±76 |

**Table 4.2. *APPL2*-ASO-226 changed circulating amino acid metabolism.**

Circulating amino acids in mice serum was extracted and derivatized, then measured by using liquid chromatography–mass spectrometry (LC–MS). Statistical significance was determined by two-tailed Student's t test. (*$p<0.05$ and **$p<0.01$). Data are presented as mean ± SEM. Ala: Alanine; Arg: Arginine; Asn: Asparagine; Asp: Aspartate; Cys: Cysteine; Glu: Glutamate; Gln: Glutamine; Gly: Glycine; His: Histidine; Ile: Isoleucine; Leu: Leucine; Lys: Lysine; Met: Methionine; Phe: Phenylalanine; Pro: Proline; Ser: Serine; Thr: Threonine; Trp: Tryptophan; Tyr: Tyrosine; Val: Valine

Importantly, silencing hepatic APPL2 reduced pyruvate concentration in mice serum (**Figure**.4.10 A). Alanine is the sole hepatic substrate for gluconeogensis[136], where it is converted to pyruvate by ALT for glucose production through gluconeogenesis[137]. A lot of alanine releases during fasting with much higher level than any other amino acids[135]. To validate that mice with ASO treatment were able to regulate plasma glucose

via hepatic gluconeogenesis, we performed alanine tolerance test, despite the decrease in serum was only slight in *APPL2*-ASO-226 group. After 24h of fasting, the increases of plasma glucose unaltered upon alanine injection in both groups of mice (**Figure**.4.10 B).

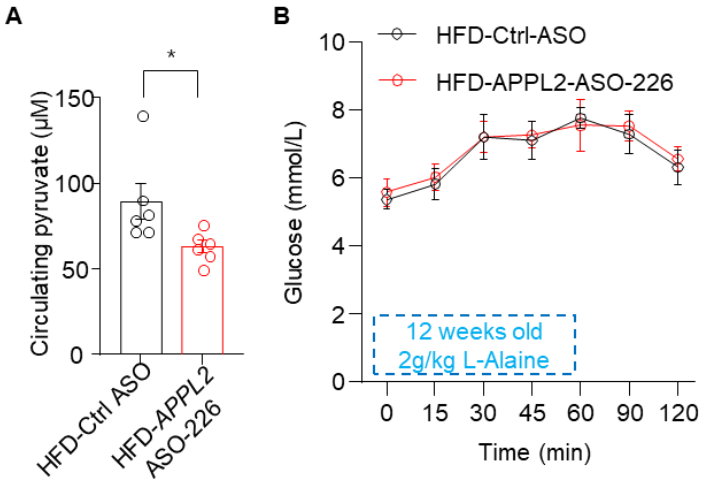


**Figure 4.10. *APPL2*-ASO-226 decreases pyruvate concentration.**

After *APPL2*-ASO-226 treatment for 8 weeks, mice were fasted for 24 hours to collect serum. **(A)** Pyruvate content in serum was measured. **(B)** 24-hour fasted mice were subjected to intraperitoneal injection of L-alanine (2.0 g/kg body weight) and measurement of glucose level as indicated. Two-way repeated measures ANOVA was used to compare glucose level between two groups while Student t test was used in other comparison. Data is presented as mean ± SEM.

Based upon in above results, we suspected that silencing hepatic APPL2 ameliorates hyperglycemia through suppression of pyruvate-driven hepatic glucose production *in vivo*. To validate this, glucose production assay was performed *in vitro*. Mice were fed with HFD and injected wtih *APPL2*-ASO-226, those with Ctrl-ASO was used as control. Primary hepatocyte was isolated from mice treated with ASOs. After starvation, hepatocytes were cultured in HBSS buffer with glucagon to induce gluconeogenesis,

and sodium pyruvate to provide precursor of gluconeogenesis. Insulin was added to suppress gluconeogenesis. After incubation, cell-culture supernatant was collected to measure glucose production. The result was normalized by total protein in cell lysate. Within Ctrl-ASO group, glucagon induced gluconeogenesis to produce more glucose, while insulin decreasing glucose production by suppressed gluconeogenesis, which indicated validity of the experiment. Importantly, the results obtained for *in vitro* experiment further evidenced the inhibition by APPL2-inactivated hepatocytes to produce glucose from pyruvate, compared with control hepatocytes (**Figure**.4.11). The view can also be validated by downrelulation of pyruvate metabolism pathway in APPL2-ASO group according to GSEA analysis (**Figure**.4.6. C).

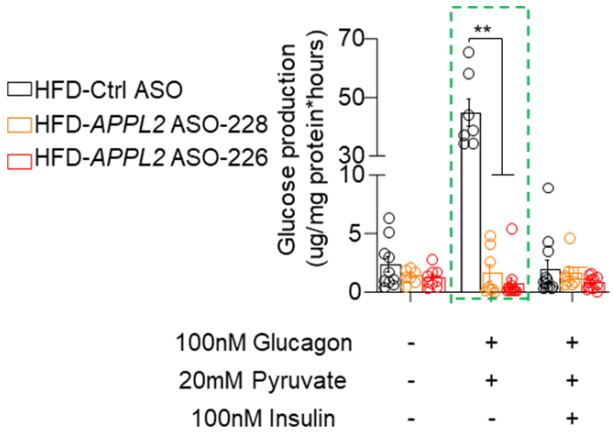


**Figure 4.11. *APPL2*-ASOs decreases hepatic glucose production.**

Primary hepatocyte was isolated from mice fed with HFD and treated by *APPL2*-ASO-226 or Ctrl-ASO. After starvation, 100nM glucagon+20 mM sodium pyruvate, or 100nM glucagon+20 mM sodium pyruvate+100nM insulin were added to the medium. After 3 hours incubation, supernatant was collected to measure glucose content. Hourly glucose production was normalized by total protein concentration in cell lysate. Statistical significance was determined by two-tailed Student's t test. (**p<0.01). Data are presented as mean ± SEM. n=12.

Taken together, liver specific knockdown APPL2 can lower pyruvate-driven hepatic glucose production, contributing to relieve diet-induced hyperglycemia.

## 4.3 Summary

RNA-Seq was used to profile alteration of hepatic transcriptomic levels after APPL2 knockdown in STC and HFD fed mice. The mRNA expression results of a series of genes including APPL2 validated that the RNA-Seq was reliable. Analysis tools of DAVID, EnrichR and GSEA were used and biological process and pathways, such as amino acid metabolism and fatty acids metabolism were enriched. Since amino acids are gluconeogenic precursors, the enrichment of amino acids metabolism might indicate excursion of glucose generation by gluconeogenesis. In addition, several genes involved in glucose metabolism were also found to be the most changed on hepatic relative expression after *APPL2*-ASOs treatment, such as *Igfbp2*. Therefore, according to the effect of *APPL2*-ASOs on glucose metabolism improvement in chapter 3, hypotheses should be verified. Ex vivo experiments revealed that hepatic APPL2 inactivation contributed to decreasing hepatic glucose production by gluconeogenesis, and then govern glucose tolerance and insulin sensitivity.

# Chapter 5 GalNAc-*APPL2*-ASO treatment improves energy metabolism.

## 5.1 Introduction

Glucose is central to energy consumption. Adipose tissue is key regulator of whole-body energy homeostasis. There are two major types of adipose tissues. WAT is primarily an energy storage pad, while the heat-burning BAT is responsible for non-shivering thermogenesis[138]. BAT has a high capacity for increasing glucose uptake[139]. Brown adipocytes can be activated by cold exposure, clear FFA or glucose to increase energy expenditure[122]. Research indicated that BAT activation increased whole-body glucose disposal and insulin sensitivity in humans[140]. Animal experiment also confirmed BAT transplantation significantly increased glucose tolerance and insulin sensitivity[141]. Excessive lipid accumulation resulted in inflammation during obesity[142]. Browning of white adipose tissue resulted in outstanding advancement of glucose uptake by adipose tissue[143]. Cold exposure improved glucose tolerance and enhanced insulin sensitivity[144], and promoted glucose homeostasis associated with adipose tissues in mice.

Energy expenditure increases in response to cold exposure, which is called cold induced adaptive thermogenesis[145]. Mammal can maintain their core temperature only when production and consumption of energy are balanced. The thermoneutral zone is a range of ambient temperatures in which the body can maintain core temperature alone by regulating dry heat loss. Thermoneutral point (TNP) of mice, at which the basal metabolic rate can maintain body temperature, is 29-33°C[146]. Mice at typical housing temperatures (20-22°C) live below thermoneutrality, and about half of their total energy

expenditure is devoted to maintaining core body temperature[146]. Mice energy expenditure increases to keep core body temperature when ambient temperature is below TNP, and body temperature increases when ambient temperature is above TNP[146].

We previously proved that *APPL2*-ASOs remarkably alleviated glucose intolerance induced by HFD. In this chapter, energy expenditure of mice was monitored under room temperature and cold stress to investigate the effect of APPL2 knockdown on glucose homeostasis after thermogenesis.

## 5.2 Result

### 5.2.1 Silencing hepatic APPL2 improves energy expenditure under room temperature.

Association between insulin function and energy expenditure was known[147], APPL2 plays a role of regulating energy homeostasis, oxygen consumption increased in APPL2$^{HepKO}$ mice compared with their controls[67]. Therefore, I used metabolic cages to study the energy expenditure change after APPL2 knockdown. Firstly, in the STC fed mice model, moderately higher energy consumption at the day cycle was observed in the *APPL2*-ASO group compared to the control counterparts. The two treatment groups did not distinguish on other energy metabolic parameters (**Figure** 5.1).

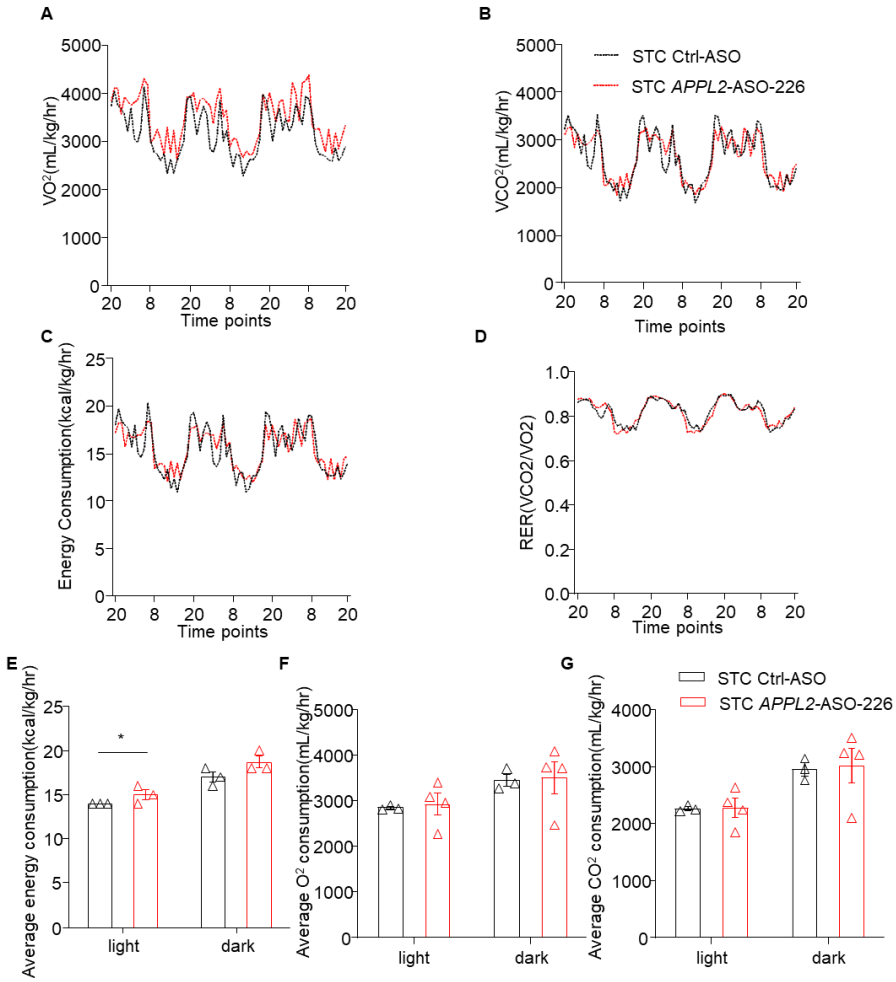


**Figure 5.1. *APPL2*-ASO-226 improves energy expenditure for STC fed mice under room temperature.**

After 14 weeks of *APPL2*-ASO treatment, the energy metabolism of mice was evaluated by monitoring $VO_2$ **(A)**, $VCO_2$ **(B)**, energy expenditure **(C)** and RER **(D)** at 22 °C during 72 hours by using Promethion metabolic cage system. Average values in the light phase and dark phase **(E-G)** were respectively indicated. Student t-test (*p<0.05). Data is presented as mean ± SEM.

Then, in the HFD-fed mice model, *APPL2*-ASO enhanced energy expenditure although not much obviously at room temperature. Concretely, $O_2$ consumption and $CO_2$ release increased, indicates that the energetic balance of mice treated with *APPL2*-ASO is shifted towards energy expenditure increase (**Figure** 5.2).

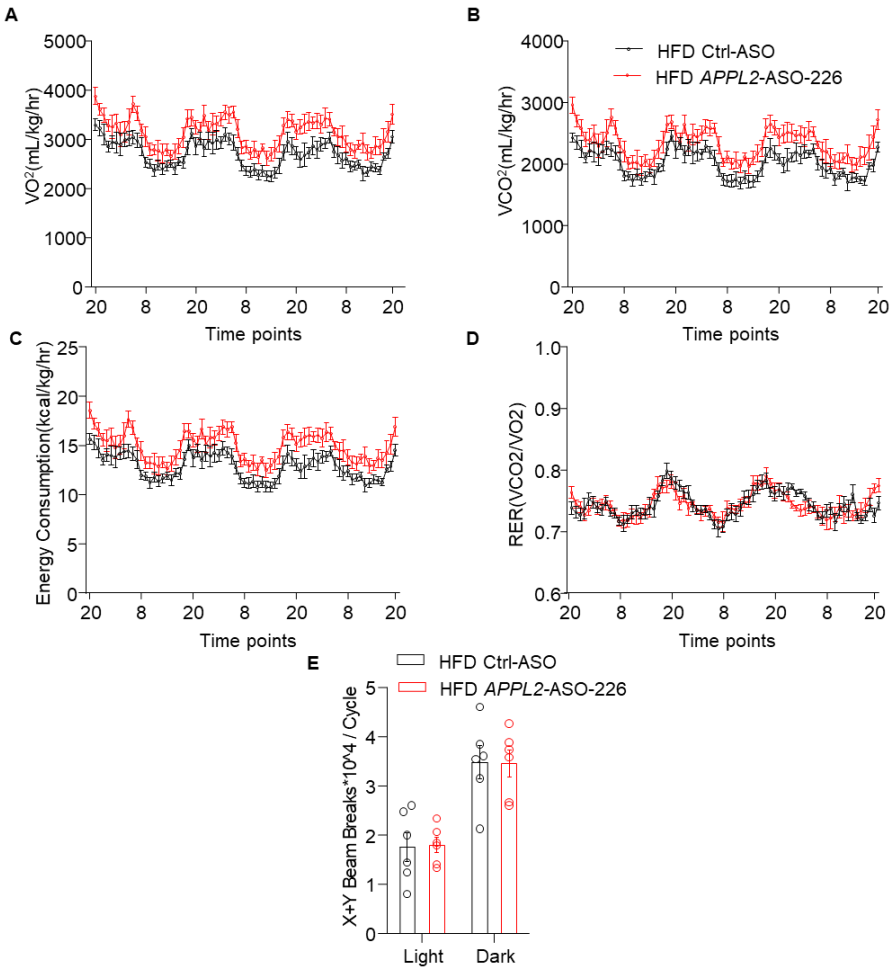


**Figure 5.2. *APPL2*-ASO-226 improves energy expenditure in DIO mice under room temperature.**

After 12 weeks of *APPL2*-ASO treatment, the energy metabolism of mice was evaluated by monitoring $VO_2$ **(A)**, $VCO_2$ **(B)**, energy expenditure **(C)** and RER **(D)** at **22 ℃** during 72 hours by using Promethion metabolic cage system. **(E)** Average activity in the light phase and dark phase were respectively indicated. Student t-test. Data are presented as mean ± SEM.

Increasing energy expenditure is a therapeutic target for preventing obesity or T2DM. Activation of sympathetic nerves can increase lipolysis and browning in white adipose tissue (WAT) or increase thermogenesis in BAT, and be able to increase energy expenditure of these tissues[148].

We hypothesized that increased energy expenditure under room temperature after *APPL2*-ASO treatment might be due to WAT browning or BAT activation. To test this hypothesis, morphology of sWAT and eWAT from HFD fed mice was observed by hematoxylin and eosin (H&E) staining. Result showed that HFD feeding significantly increased white adipocyte size, BAT from HFD also had larger lipid droplets. However, APPL2 knockdown has not obvious effect on the size of white adipocytes or BAT morphology (**Figure** 5.3) with both diet feeding.

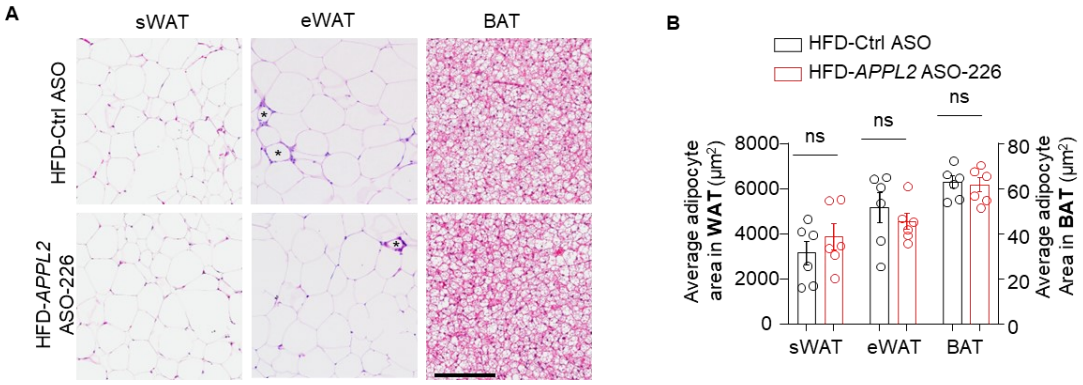


**Figure 5.3. *APPL2*-ASO-226 has not obvious effect on adipocyte size under room temperature.**

C57BL/6J mice were fed with STC or HFD and treated with ASO as description. **(A)** Representative images of H&E-stained sWAT, eWAT and BAT in HFD mice. Scale bar: 200 μm. **(B)** Adipocyte size was quantified by ImageJ. Student t-test. Data are presented as mean ± SEM.

### 5.2.2 Cold exposure reinforces the effect of hepatic APPL2 knockdown on promoting energy expenditure.

Based on the improved energy expenditure after *APPL2*-ASO treatment, I expect cold stress may reinforces this improvement by increasing thermogenesis. Metabolic cage was used to study the energy expenditure change after APPL2 knockdown under cold

stress, by monitoring $VO_2$, $VCO_2$, energy expenditure and RER at 30℃ for 36 hours, 22℃ for 24 hours, and 4℃ for 24 hours. Results showed that levels of $O_2$ consumption, $CO_2$ release and energy expenditure in HFD-*APPL2*-ASO-226 group were comparable at 30℃. When ambient temperature changed to 22℃, both sequences of *APPL2*-ASOs group significantly enhanced the energy expenditure. More importantly, the gap between two groups was significantly enlarged at 4℃ (**Figure** 5.4.a; **Figure** 5.4.b). The result indicated that the effect of APPL2 knockdown on energy expenditure was nullified under thermoneutrality of mice but enhanced under cold exposure.

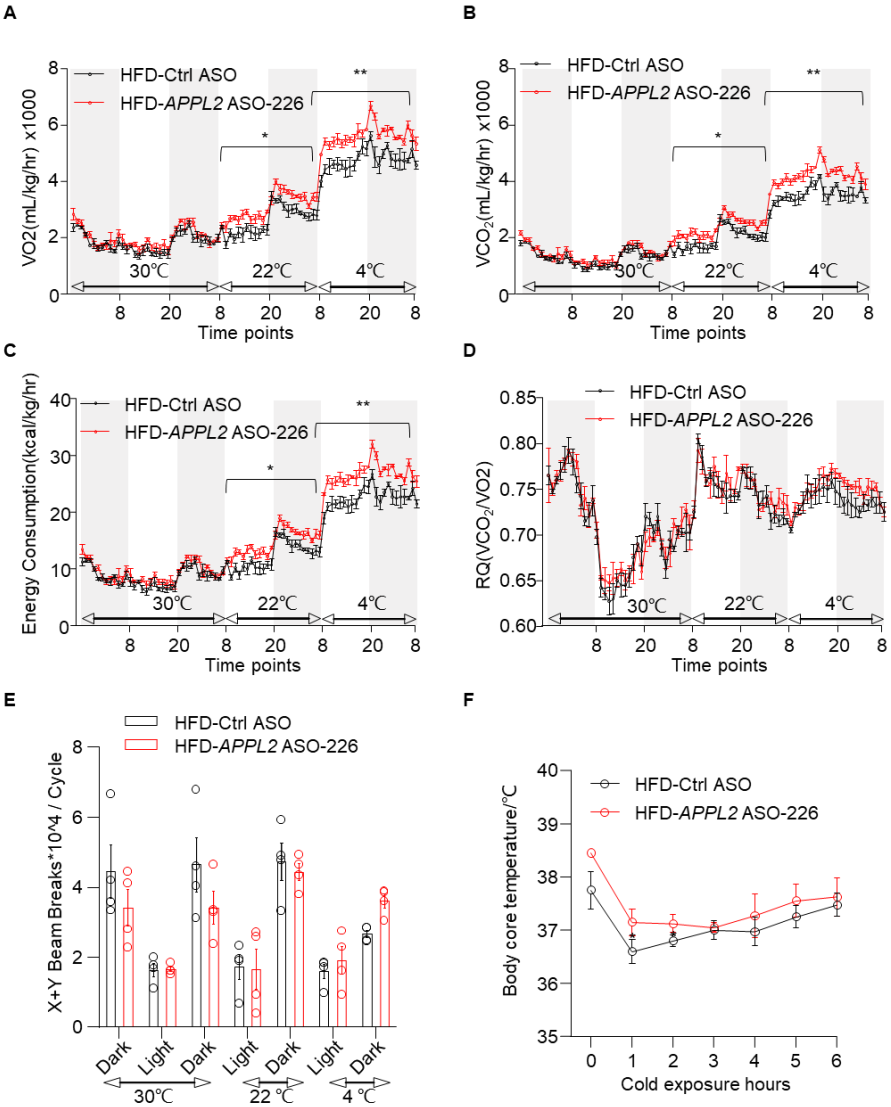

**Figure 5.4.a *APPL2*-ASO-226 improves energy expenditure in DIO mice under cold stress.**

**(A-E)** After 6 weeks of HFD, energy metabolism of mice was evaluated by monitoring $VO_2$, $VCO_2$, energy expenditure, RER and activity at 30℃ for 36 hours, 22℃ for 24 hours, and 4℃ for 24 hours, using Promethion metabolic cage system. **(F)** Mice core body temperature was monitoring during 6h under acute cold exposure (4℃). Student t test (*p<0.05 and **p<0.01). Data is presented as mean ± SEM.

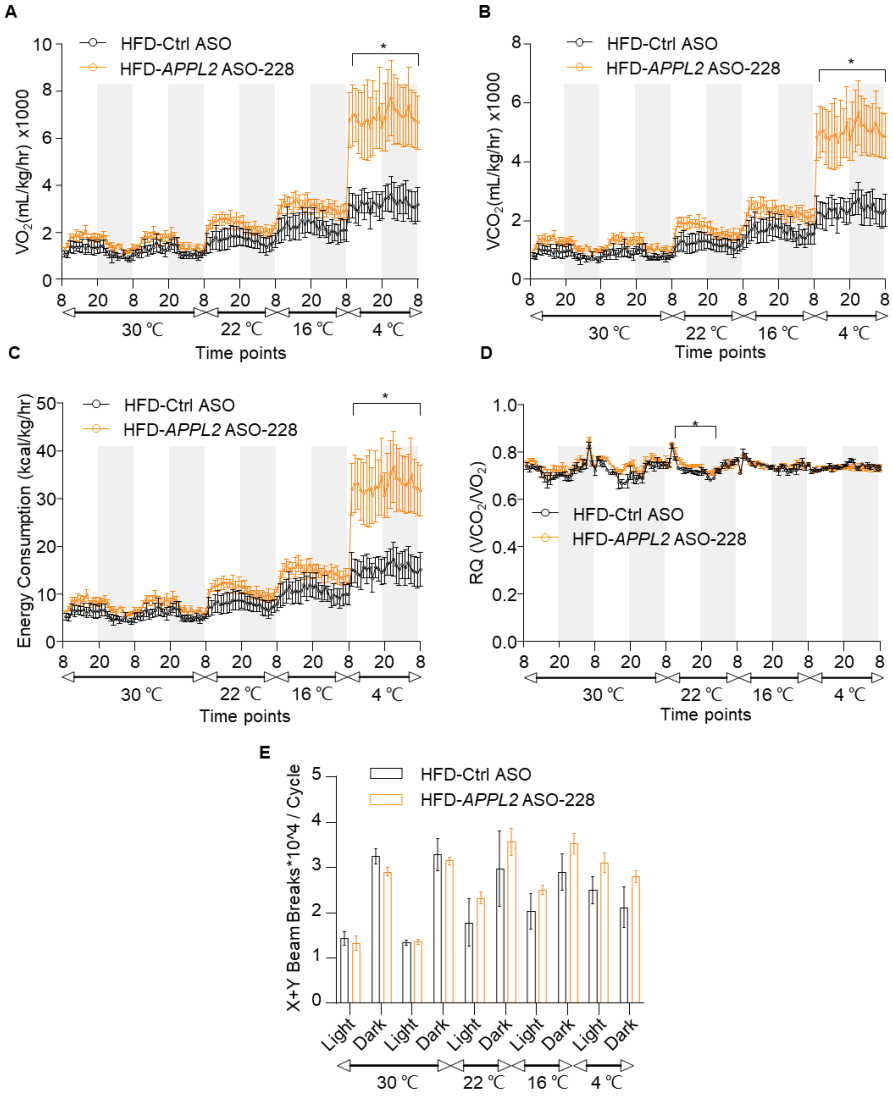


**Figure 5.4.b *APPL2*-ASO-228 improves energy expenditure in DIO mice under cold stress.**

**(A-C)** After 8 weeks of HFD, energy metabolism of mice was evaluated by monitoring $VO_2$, $VCO_2$, energy expenditure, RER and activity 30℃ for 36 hours, 22℃ for 24 hours, and 4℃ for 24 hours,

using Promethion metabolic cage system. Student t test (*p<0.05). Data is presented as mean ± SEM.

### 5.2.3 Silencing hepatic APPL2 relieves adipocyte hypertrophy and liver steatosis in DIO mice under cold stress.

Cold exposure reinforces the effect of hepatic APPL2 knockdown on promoting energy expenditure. We hypothesized that the potentiation effect maybe caused by cold-induced adaptive thermogenesis. To investigate this, the following experiment was designed.

8 weeks old C57BL/6J mice were fed with HFD for 2 weeks, then subcutaneously injected with *APPL2*-ASO-226 or Ctrl-ASO (10 mg/kg) weekly for. After 9 weeks of HFD feeding, mice were located at 30 ℃ for 14 days to keep thermoneutral, then return to 22℃ for 4 days, finally transported to 4 ℃ for 10 days to increase thermogenesis. Mice were sacrificed at 23 weeks old under 4℃-cold exposure.

Mice body weight decreased in HFD-*APPL2*-ASO-226 group from 15 weeks old, but not significantly changed until the last fed week (**Figure** 5.5. A). Tissues weight of eWAT, PAT and total white adipose tissue were decreased in HFD-*APPL2*-ASO-226 group (**Figure** 5.5. B).

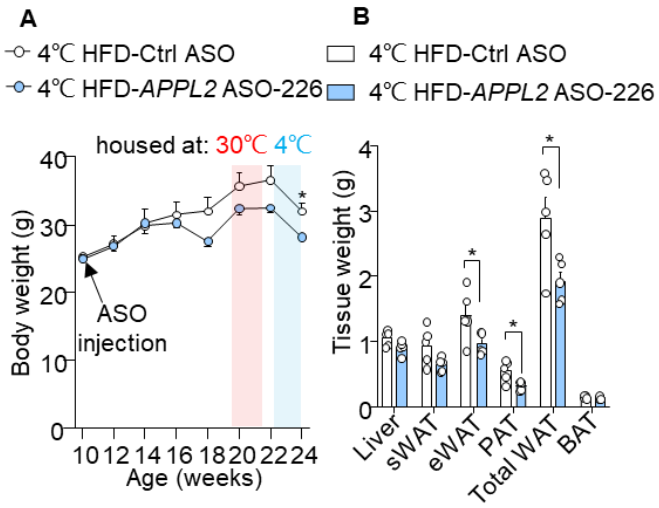


**Figure 5.5. *APPL2*-ASO-226 decreases fat mass in DIO mice under cold stress.**

Bodyweight **(A)** and tissue weight **(B)** for mice treated with *APPL2*-ASO-226 under different temperatures were monitored. Student t-test. Data are presented as mean ± SEM. PAT: Pericardial adipose tissue; total WAT sum of weights of sWAT, eWAT and PAT. HFD-Ctrl-ASO (n=5) and HFD-*APPL2*-ASO-226 (n=5). Student t test (*p<0.05). Data is presented as mean ± SEM.

High-fat-diet-induced obesity is commonly due to enlargement in adipocyte size (adipocyte hypertrophy) and insulin resistance[149]. To investigate whether the reduced fat mass is due to adipocyte atrophy, I firstly evaluate the adipocyte morphology after APPL2 knockdown under cold exposure. Mice were sacrificed at 4℃, fat pads were collected, fixed, and subjected to H&E staining. Result showed that APPL2 knockdown reduced adipocytes size (**Figure** 5.6. A, B) in sWAT, eWAT and BAT with cold stress. The result was consistent with the decreasing of total fat mass in Figure 5.5. Uncoupling protein 1 (UCP1)[150], is a unique mitochondrial membranous protein, highly expressed in brown adipocytes and beiging adipocytes. The induction of UCP1 by cold stimulation increases non-shivering thermogenesis, leading to increased energy

expenditure and prevention of obesity[151-152]. To investigate if the increasing energy expenditure after *APPL2*-ASO treatment is due to change of UCP1-dependent thermogenesis, immunohistochemical staining of UCP1 was performed in sWAT and BAT from mice under cold stress. Result showed that UCP1 expression was significantly increased after *APPL2*-ASO-226 treatment, respectively in sWAT and BAT, but the changes were not much obvious (**Figure** 5.6. C,D). Meanwhile, mRNA expression related to thermogenesis in sWAT or BAT also did not changed (**Figure** 5.6. E)

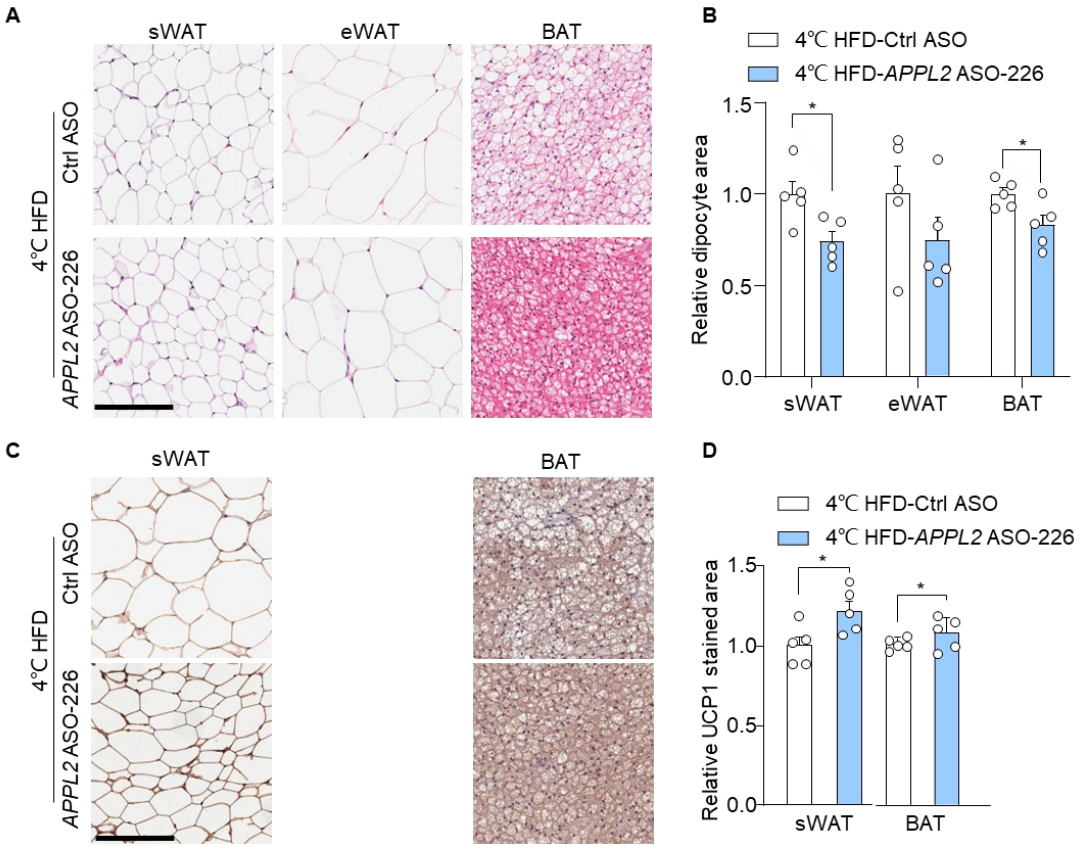

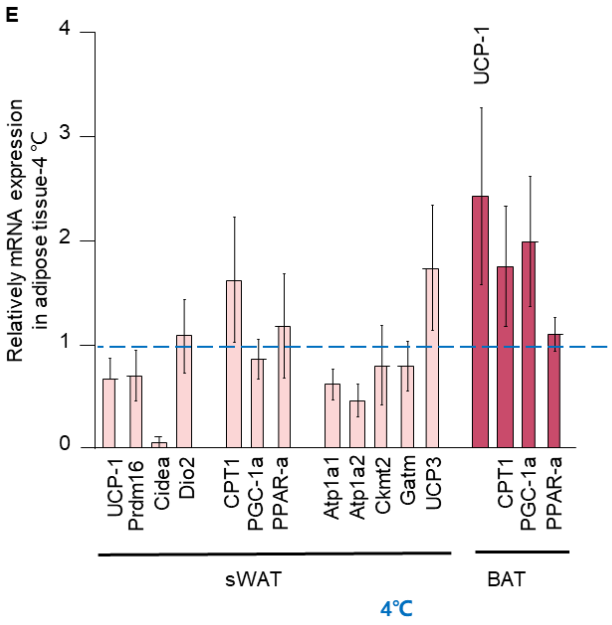


**Figure 5.6. *APPL2*-ASO-226 treatment decreases adipocyte cell size in DIO mice under cold stress.**

**(A)** Representative images of H&E-stained sWAT, eWAT and BAT in STC or HFD mice. **(B)** Adipocyte size was quantified by ImageJ and Adiposoft plugin. **(C)** Representative images of UCP1 IHC staining of sWAT and BAT. **(D)** Relative UCP1 stained area was quantified by ImageJ. **(E)** mRNA expression in sWAT and BAT related to thermogenesis. Scale bar: 200 μm. Student t test (*p<0.05). Data is presented as mean ± SEM.

Study revealed that obese mammal has lower hepatic lipid content with cold exposure[153]. H&E staining result showed that APPL2 knockdown remarkably alleviated HFD-induced hepatic steatosis (**Figure** 5.7). Since accumulation of excess nonesterified saturated FFAs or their metabolic products mediate lipotoxicity[42], the effect of APPL2-ASO on reduced hepatic steatosis might be due to alleviated lipoapoptosis or hepatic lipotoxicity induced from hypertrophy of adipose tissue[42].

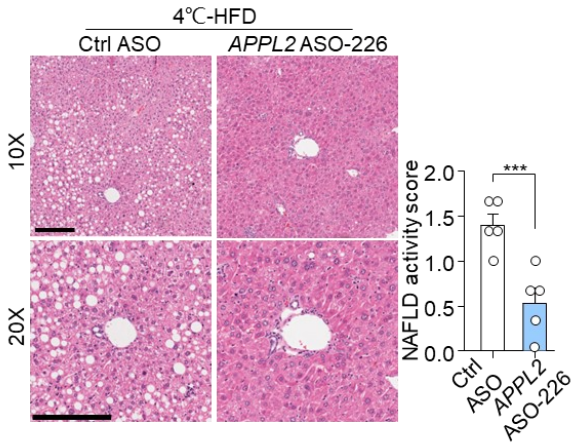


**Figure 5.7. *APPL2*-ASO-226 treatment decreases hepatic lipid content in DIO mice under cold stress.**

Representative images of H&E-stained liver. Scale bar: 200 μm. The NAS (NAFLD activity score) is calculated by the sum of scores of steatoses (0-3), lobular inflammation (0-3) and hepatocyte ballooning (0-2), which quantified by ImageJ. Student t test (***p<0.001). Data is presented as mean ± SEM.

### 5.2.4 Thermoneutrality nullifies the effect of APPL2 knockdown on glucose metabolism.

To investigate if the regulatory effect of APPL2 on glucose metabolism is associated with thermogenesis, glucose (1.0 g/kg, B.W.) and insulin (1.0 IU/kg B.W.) tolerance tests were programmed under 30℃ and 22℃ respectively. After locating under thermoneutral zone for two weeks to keep thermoneutrality, glucose and insulin response of mice from two groups were comparable (**Figure** 5.8. A, B). Then, the effect of APPL2 knockdown on alleviating glucose intolerance and improving insulin sensitivity, nullified at 30℃, was recovered at 22℃ (**Figure** 5.8. C, D). The result suggested that effect of APPL2 knockdown on glucose metabolism was nullified in

mice housed at thermoneutrality.

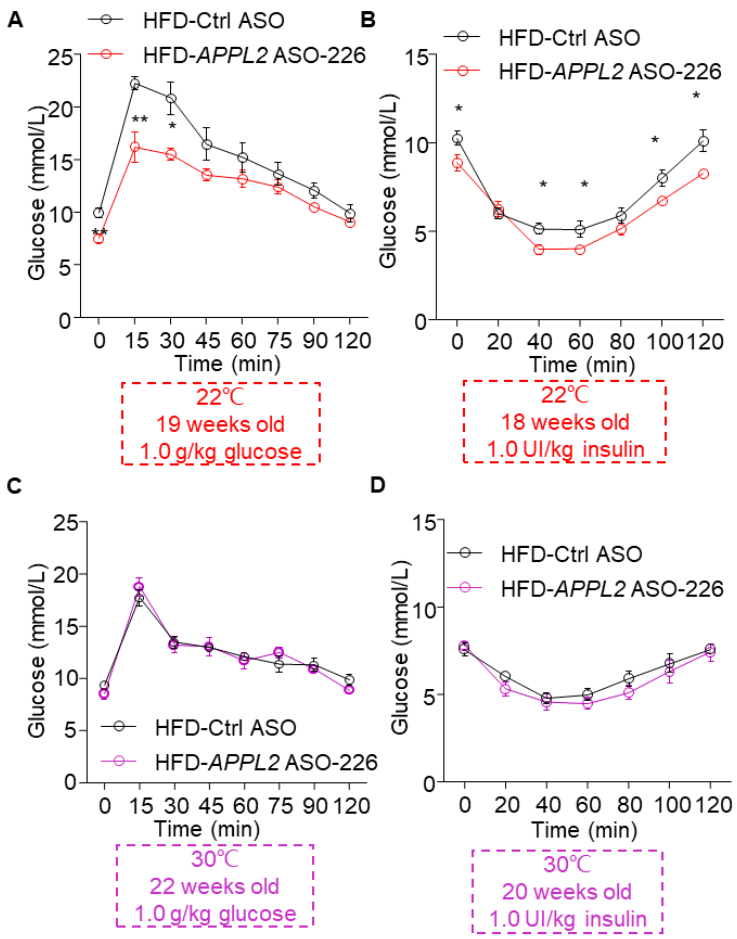


**Figure 5.8. Effect of *APPL2*-ASO-226 on glucose metabolism is nullified at thermoneutrality.**

C57BL/6J mice were fed with HFD and treated with ASO as description. After 9 weeks of HFD feeding, mice were in 30 ℃ for 14 days. **(C, D)** Upon the thermoneutral condition, the mice were fasted for 6 hours, followed by intraperitoneal injection of glucose (1.0 g/kg) or insulin (1.0 IU/kg), and measurement of glucose level as indicated. **(A, B)** Then mice were transported to 22℃ for 3 days, glucose tolerance (1.0 g/kg) and insulin sensitivity (1.0 IU/kg) were tested. Two-way repeated measures ANOVA was used to compare glucose level between two groups. (*p<0.05, **p<0.01). Data is presented as mean ± SEM.

## 5.3 Summary

RNA-Seq result proved that fatty acids metabolism and lipase activity were the

enriched two pathways associated to lipid metabolism, but not many pathways associated to glucose metabolism was enriched, since our most obvious phenotype should be glucose metabolism after APPL2 knockdown. The truth is when lipid droplets of BAT did not provide FFA to produce energy, glucose uptake increased in the brown adipocyte, which improves glycemic control[154]. In addition, lipoprotein lipase activity of triglyceride clearance and fatty acids delivery to the adipocyte was also enriched in RNA-Seq result.

Combining with the above improvement of lipid metabolism in liver and adipose tissue, one of reasonable speculations was hepatic APPL2 knockdown altered fatty acids metabolism in liver or secreted some hepatokines, which affected function of adipose tissue, especially BAT, under cold-induced thermogenesis, thereby increased glucose uptake of BAT.

# Chapter 6 Treatment with GalNAc-*APPL2*-ASO alleviates hyperlipidemia in obese animal models

## 6.1 Introduction

Insulin resistance only contributes to glucose dysmetabolism but also dyslipidemia in obese condition. Clinical trials have shown that insulin resistance is associated with elevated triglyceride levels and high non-HDL-C[155]. Insulin can promote lipogenesis in the liver[156].Under health conditions, insulin targets ApoB, the principal protein component of VLDL, for intracellular degradation and thereby decreases VLDL secretion acutely. under pathological condition insulin resistance motors metabolic-syndrome-associated VLDL secretion by failing to degrade ApoB[41]. The potential benefits of successful treatment of dyslipidemia are seen in patients with insulin resistance[157]. We analyzed the data in genome-wide association study (GWAS) and found that a single nucleotide polymorphism (SNP) in the APPL2 gene was associated with cholesterol levels in humans, which include plasma total cholesterol and LDL-cholesterol levels (**Figure** 7.1.A). The most significant variant was a genome-wide locus: rs1196760. rsID has conversed at 4 of 20 intronic regions in chromosome 12:105,606,068 (**Figure** 7.1. B). Protein and mRNA of APPL2 are highly similar in human and mouse (**Figure** 7.1. C). We therefore hypothesize that APPL2 may have a potential role in cholesterol metabolism.

(A)

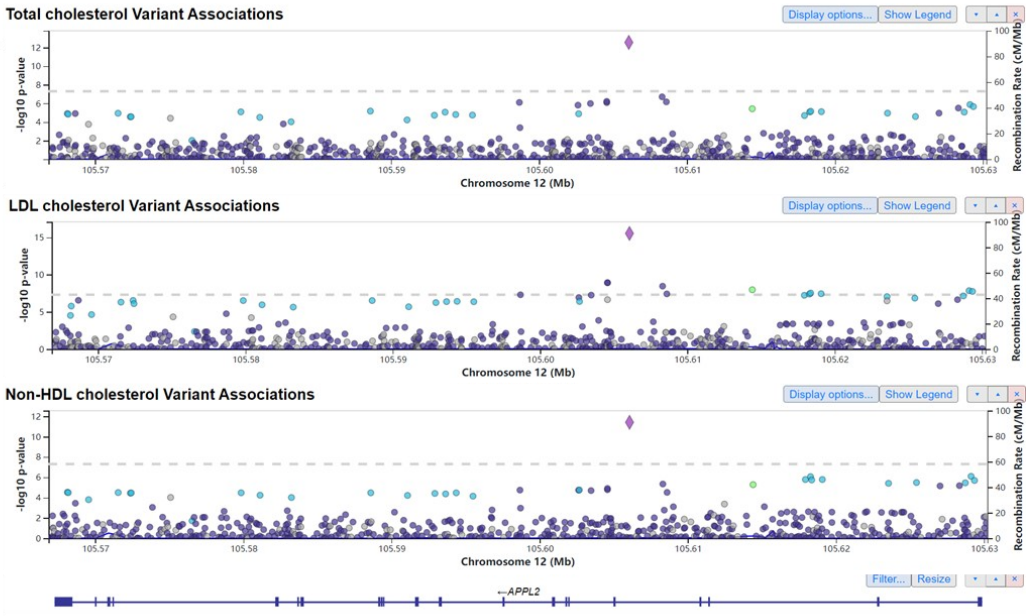


(B)

| Lead Variant(CHR:POS:REF:ALT) | dbSNP | Phenotype | Group | P-Value | Beta | Odds Ratio | View LD Proxies |
|---|---|---|---|---|---|---|---|
| 12:105546172:G:A | rs1663564 | LDL cholesterol | LIPIDS | 7.319e-17 | -0.0203 | | Show Variants |
| 12:105606068:G:C | rs1196760 | Total cholesterol | LIPIDS | 2.807e-13 | -0.0186 | | Show Variants |
| 12:105606068:G:C | rs1196760 | Non-HDL cholesterol | LIPIDS | 3.914e-12 | -0.0205 | | Show Variants |

(C)

| Human APPL2 vs Mouse APPL2 | Amino acid sequence | mRNA sequence |
|---|---|---|
| Identity | 92.5 % | 87.7% |
| Similarity | 96.1 % | N/A |

**Figure 6.1. Single nucleotide polymorphisms (SNPs) in the APPL2 gene are associated with cholesterol levels in humans.**

**(A)** Region-plot of APPL2 was associated with cholesterol levels in humans. **(B)** Associated SNPs was rs1196760. (C)Percentage of sequence identity and similarity in protein and mRNA in human and mouse APPL2 using the data from NCBI. Data were derived from https://hugeamp.org/.

In Chapter 3, we proved that *APPL2*-ASO-226 alleviated high-fat-diet-induced insulin resistance and improved glucose metabolism. However, *APPL2*-ASO-226 had not much therapeutic effect on dyslipidemia. In this chapter, *APPL2*-ASO-228 was used to treat DIO mice to investigate of the effect of hepatic APPL2 knockdown on lipid metabolism.

## 6.2 Result

### 6.2.1 Silencing hepatic APPL2 alleviates hypercholesterolemia and hepatic steatosis.

Liver plays a central role on lipid metabolism. It serves for lipoprotein transportation to circulation. Lipoproteins are assembled with non-polar lipids, such as triglycerides and cholesterol esters which are main types of lipids in circulation[158]. Imbalanced lipid transportation leads to the accumulation of excess lipids. Genetic variants of APPL2, has been associated with NAFLD, with a more severe hepatic steatosis grade[77].

I firstly evaluated the effect of APPL2 knockdown on lipid metabolism. Results showed that *APPL2*-ASO-228 significantly reduced serum total cholesterol (**Figure** 6.1. A) but did not influence TG (**Figure** 6.1. B) However, hepatic silencing APPL2 by *APPL2*-ASO-226 unaltered lipid profile in mice serum (Table 3.3). In detail, the average total cholesterol level was dramatically decreased in the HFD-*APPL2*-ASO-228 group around 80% than Ctrl-ASO group. As known, blood cholesterol is subdivided into very-VLDL, LDL, and HDL. Associated with atherogenesis, elevated levels of LDL-C are a major risk factor for cardiovascular disease[159] while HDL-C was known to have a protective effect on arteria coronaria[160]. *APPL2*-ASO-228 treatment significantly lowered LDL-C in the HFD-fed mice model, indicating a potential effect of alleviating hypercholesterolemia. Meanwhile, the treatment presented no change in HDL-C (**Figure** 6.1. C). Size exclusion chromatography was used to separate lipoproteins of serum to fractions (CM/VLDL, IDL/LDL, and HDL) via different densities. Result revealed that cholesterol in the first into two fractions were significantly decreased in hepatic APPL2 inactivation mice.

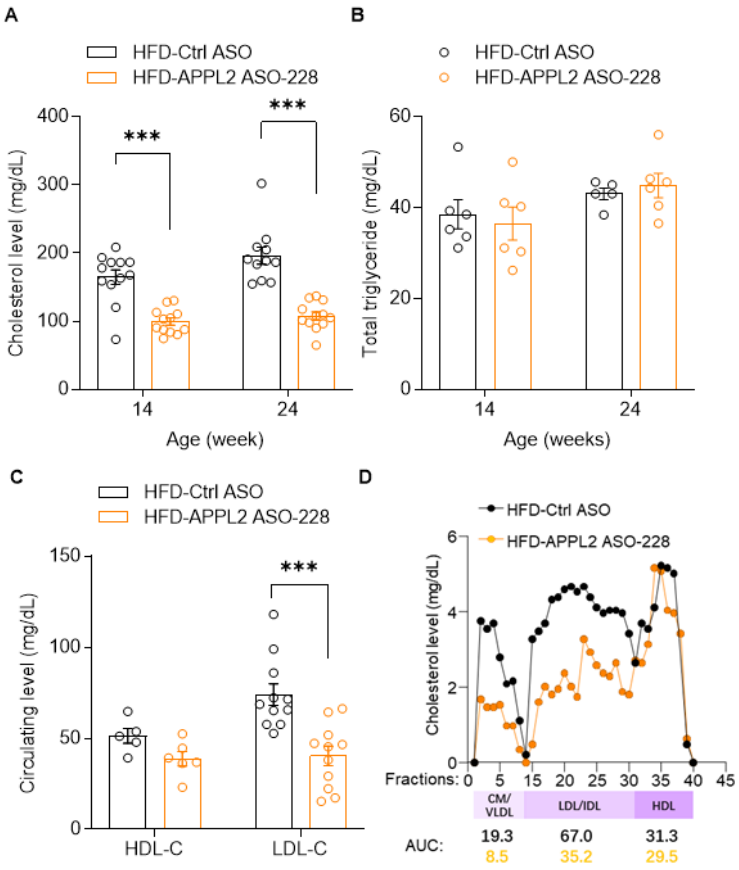


**Figure 6.2. *APPL2*-ASO-228 treatment reduces cholesterol level in serum.**

Concentration of TG **(A)**, TC **(B)**, HDL-C **(C)** and LDL-C **(C)** in serum. Different densities of lipoproteins in the serum samples were separated by SEC. Cholesterol content in each fraction was measured by kit **(D,** n=1**)**. HFD-Ctrl-ASO (n=11) and HFD-*APPL2*-ASO-228 (n=11) unless annotation. Student t-test (***p<0.001). Data are presented as mean ± SEM.

To examine whether the reduction of liver weight by *APPL2*-ASO-228 is due to decrease of lipid accumulation, hepatic lipid was determined by histological and biochemical methods. Hepatic triglyceride decreased slightly in the HFD-*APPL2*-ASO-228 group but not showing significance (**Figure** 6.3) . Hepatic cholesterol levels were similar between the two groups (**Figure** 6.3).

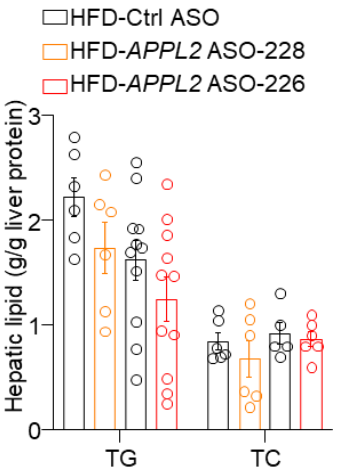


**Figure 6.3. *APPL2*-ASO-228 slightly reduced hepatic lipid content for DIO mice.**

Hepatic triglyceride and cholesterol contents were normalized with protein concentration. Student t-test. Data are presented as mean ± SEM.

Triglycerides accumulation in the liver leads to hepatic steatosis[161]. To score hepatic steatosis, liver sections from two groups were stained with H&E staining. Like the result revealed by the biochemical method, the H&E staining result showed that the steatosis area in the group treated with *APPL2*-ASO-228 decreased but not significantly (**Figure** 6.4).

The above results suggested that liver-specific knockdown of APPL2 hardly alleviated HFD-induced hepatic steatosis but significantly reduced circulating cholesterol levels.

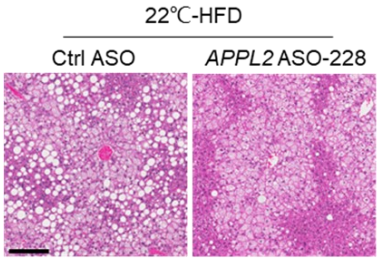


**Figure 6.4. *APPL2*-ASO-228 slightly alleviates hepatic steatosis for DIO mice.**

Representative microphotographs of liver sections stained with H&E of HFD-Ctrl-ASO and HFD-*APPL2*-ASO-228**,** Scale bar=200μm.

### 6.2.2 Silencing hepatic APPL2 decreases TG-VLDL secretion.

To evaluate the effect of hepatic APPL2 on TG-VLDL secretion, the ASO-treated mice for different periods were fasted overnight and intravenously injected with tyloxapol, a lipoprotein lipase inhibitor that prevents TG-VLDL catabolism[162]. After VLDL is secreted into circulation, lipoprotein lipase (LPL) is activated to hydrolyze TG. After 3 hours of tyloxapol injection, circulating TG dramatically increased in both groups. Treatment with *APPL2*-ASO-228 diminished tyloxapol-induced upregulation of TG-VLDL secretion(**Figure** 6.5. left panels). Total cholesterol in the *APPL2*-ASO-228 group thoroughly maintained a lower level compared to the control group (**Figure** 6.5. right panels). Reduction of TG-VLDL secretion and cholesterol were at different HFD feeding stages.

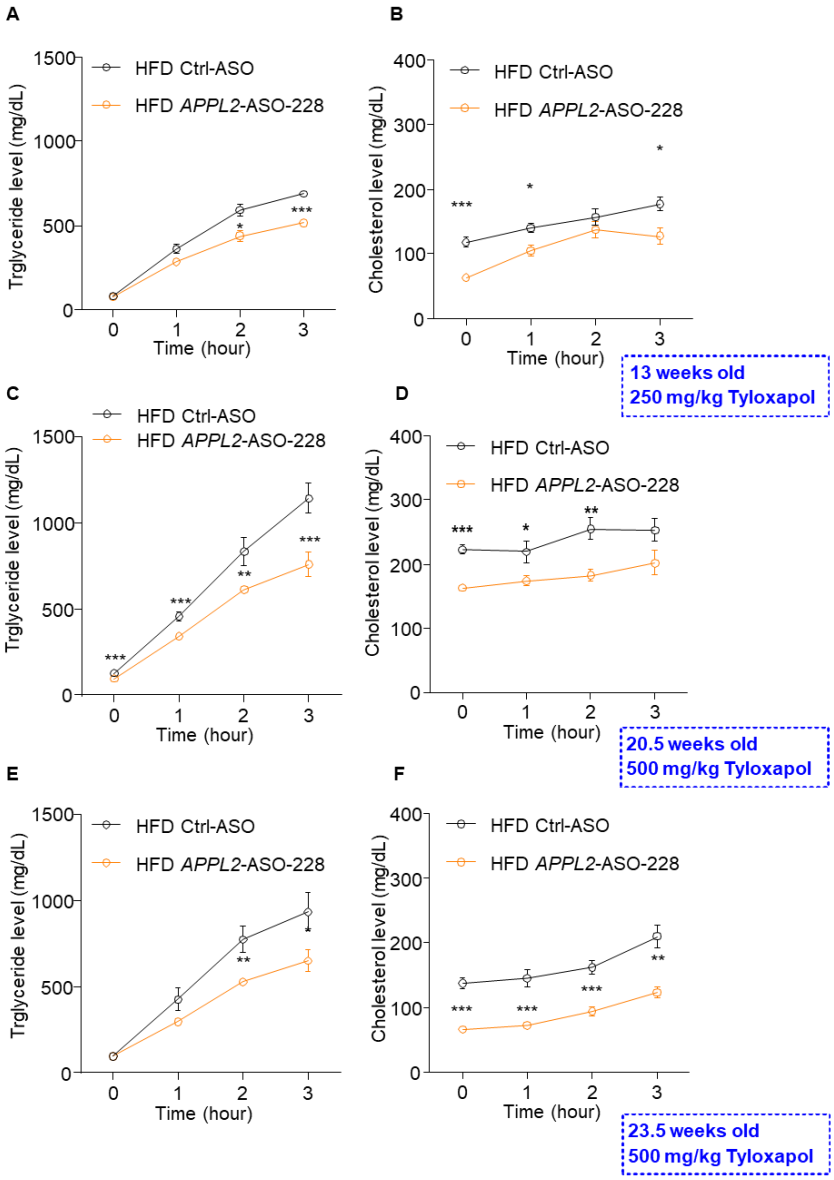


**Figure 6.5. *APPL2*-ASO-228 visibly reduces TG-VLDL secretion for DIO mice.**

Mice were fasted for 16 hours, followed by an intravenous injection of Tyloxapol (500 mg/kg b.w.) and measurement of triglyceride (left) and cholesterol (right) levels as indicated. Two-way repeated-measures ANOVA was used to compare triglyceride **(A,C,E)** or cholesterol **(B,D,F)** levels between two groups. (*p<0.05, **p<0.01 and ***p<0.001). Data are presented as mean ± SEM.

Apolipoprotein B100 (ApoB100) is exclusively synthesized in the liver and is responsible for hepatic assembly and secretion of VLDL. Immunoblot results indicated that ApoB100 secretion was markedly increased from 0 hour to 2 hours (**Figure** 6.6. A). Results showed that *APPL2*-ASO-228 did not obviously reduce the ApoB

expression in liver (**Figure** 6.6. B).

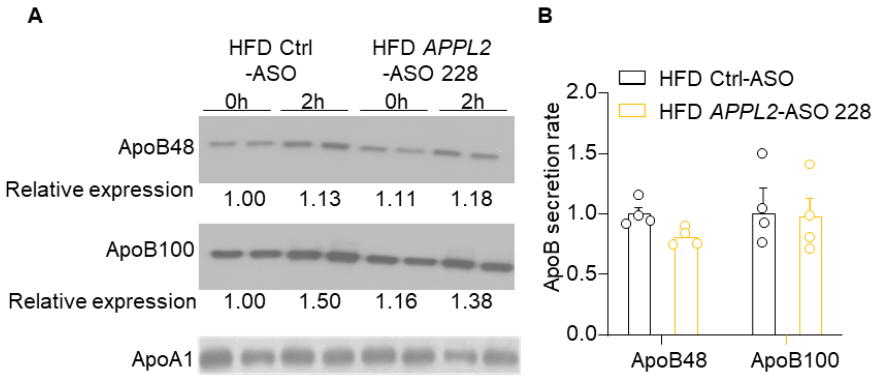


**Figure 6.6. *APPL2*-ASO-228 does not obviously reduces ApoB secretion for DIO-mice.**

Immunoblotting analysis of ApoB100, ApoB48, and ApoA-1 in the serum. **(B)** The bar chart is the densitometric quantification of ApoB48 and ApoB100 normalized with ApoA-1. Y-axis is the secretion rate of ApoB calculated as the ratio of expression at 2 hours to that of basal. Data are presented as mean ± SEM.

To further understand the altered lipid metabolism in the mice with *APPL2*-ASO-228, lipid clearance tests were performed. The mice were fasted overnight, followed by oral gavage of corn oil and lipid measurement. Similar excursions of TG and TC were found in the two groups after corn oil oral gavage (**Figure** 6.7). These findings suggested that hepatic APPL2 only regulates TG-VLDL secretion but not lipid clearance.

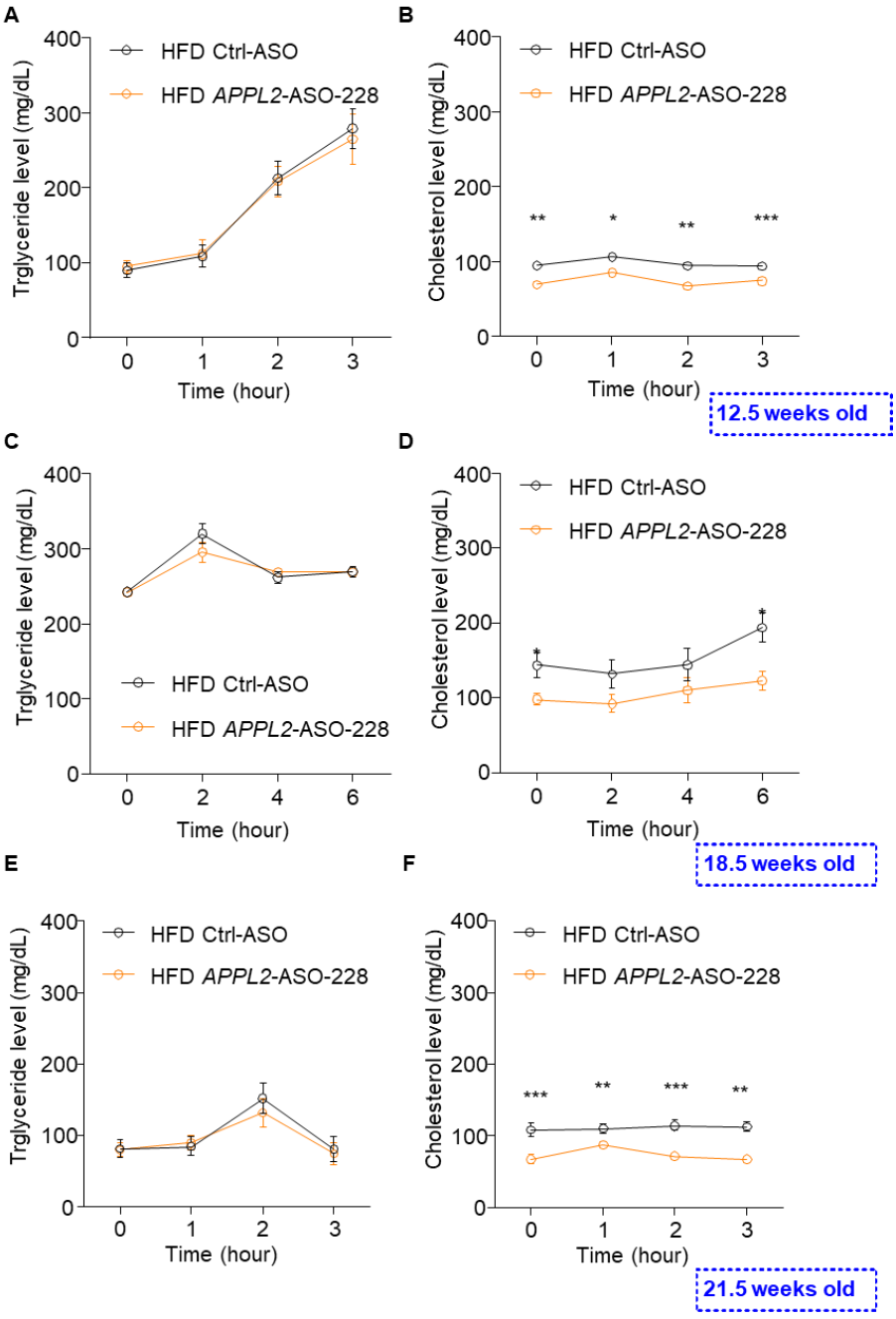


**Figure 6.7. *APPL2*-ASO-228 do not affect lipid clearance for DIO-mice.**

16-hour fasted mice were subjected to corn oil gavage (10 μL/g b.w.) and measurement of triglyceride **(left)** and cholesterol **(right)** levels as indicated. Two-way repeated-measures ANOVA was used to compare triglyceride **(A,C,E)** or cholesterol **(B,D,F)** levels between two groups. (*p<0.05, **p<0.01 and ***p<0.001). Data are presented as mean ± SEM.

### 6.2.3 Silencing hepatic APPL2 reduces low-density lipoprotein accumulation in hepatocytes.

Circulating cholesterol is closely associated to cholesterol synthesis, uptake, and excretion. The relationship is necessary to maintain whole-body cholesterol balance. Firstly, cholesterol in feces was determined. Fresh feces were collected from anus of mice each day during one week before sacrifice. Feces from each mouse were dried at cryodrying machine then homogenized into powder. Lipid in dried feces was extracted by chloroform and methanol mixture, in which cholesterol was measured and normalized by dry feces weight. The result showed that cholesterol contents of feces were comparable between HFD-Ctrl-ASO and HFD-*APPL2*-ASO-228 groups (**Figure** 6.8. A).

Secondly, hepatic genes expression associated to cholesterol metabolism were analyzed. HMG-CoA reductase (*Hmgcr*) and Squalene monooxygenase (*Sm*) are rate-limiting enzymes in cholesterol synthesis[163]. Sterol regulatory element-binding protein (*SREBP-2*) promotes cholesterol genic transcription[164]. LDLR is the major regulator of circulating LDL-C levels, through uptake of LDL particles from the circulation[165]. LDL-C binds to LDL receptor (LDLR) on the surface of hepatocyte and is absorbed from circulation. Proprotein convertase subtilisin/kexin type-9 (*Pcsk9*) binds to LDLR and targets it for degradation in hepatocytes[37]. QPCR analysis result showed that only *Pcsk9* mRNA level, but not other genes associated to cholesterol metabolism is reduced. Sm mRNA also reduced but without significant difference (**Figure** 6.8. B). LAMP proteins are highly abundant components of the lysosome membrane. Cholesterol is delivered to lysosomes by LDLR from the extracellular space. In lysosomes, cholesterol esters are hydrolyzed[166]. Immunoblotting result demonstrated that LDLR expression was slightly increased in liver (**Figure** 6.8. C, D).

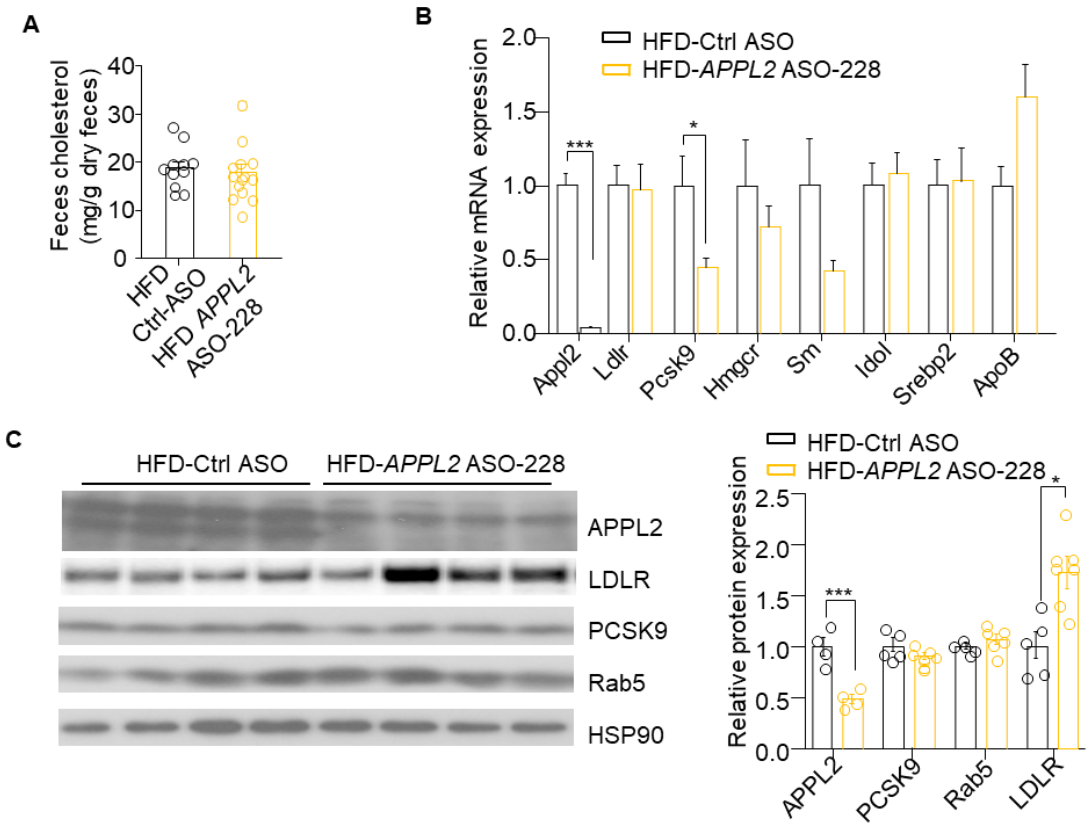


**Figure 6.8. *APPL2*-ASO-228 slightly increases LDL receptor (LDLR) expression.**

**(A)** Cholesterol contents were measured in dry feces. **(B)** mRNA of genes associated to cholesterol synthesis and degradation were analyzed in liver. **(C)** Immunoblotting showed hepatic proteins expression associated to cholesterol metabolism with quantification. n=5 for each group. Student t-test (*p<0.05 and ***p<0.001). Data are presented as mean ± SEM.

Taken together, mRNA of Pcsk9 decreased, LDL receptor protein level increased, and less LDL was accumulated in HFD-*APPL2*-ASO 228 group. Reasonably, with APPL2 knockdown, low Pcsk9 level contributed to less intracellular degradation of LDL receptor. Then, active LDLR recycled to hepatocyte membrane to uptake LDL-C and reduce LDL-C in circulation. This assumption will be validated in the future work.

## 6.3 Summary

*APPL2*-ASO-228 demonstrated obvious benefits on lipid metabolism and reduced LDL-C levels in serum. Several medicines were developed to regulate cholesterol levels, such as statin and PCSK9 inhibitors. But those drugs have some side effects, like increasing T2D incidence in patients. Therefore, this APPL2-ASO-228 therapy displayed potential benefits in simultaneously improving glucose and lipid homeostasis. Further studies are needed to explore the mechanisms of this lipid-lowering effect.

# Chapter 7 General Discussion

## 7.1 APPL2 knockdown decreases hepatic glucose production.

Silencing hepatic APPL2 can reduce hepatic glucose production (Figure 4.12). It has been revealed that APPL1 overexpression suppresses glucose production by enhancing insulin induced Akt phosphorylation[65]. Although APPL1 and APPL2 show some similarity in primary sequence, APPL1 associates with Akt2, instead of APPL2[58]. Therefore, APPL2 might affect hepatic gluconeogenesis by other pathways.

HGP was inhibited in IGFBP2-overexpressed mice (ob/ob). The inhibitory effect was enhanced with insulin treatment. It was demonstrated that IGFBP2 treatment markedly increases insulin sensitivity, primarily by suppressing hepatic glucose output by lowers expression of the rate-limiting gluconeogenic enzymes *Pck1* and *G6Pc*[132]. My study verified that APPL2 knockdown can upregulate IGFBP2 in mice liver and serum. *In vitro* experiment confirmed that elevated IGFBP2 protein expression also caused more secretion of IGFBP2 in conditional medium (Figure 4.8-4.9). Therefore, the result might explain the suppressed hepatic glucose production in hepatocyte with hepatic APPL2 knockdown, and the improved pyruvate tolerance in *APPL2*-ASO treated mice. However, QPCR result displayed that the *G6Pc* and *Pck1* in mice liver were comparable in Ctrl and *APPL2*-ASO treated mice (data not shown). These two glucagon-activated genes can be significantly down-regulated in gluconeogenesis but suppressed by insulin[167-168]. The comparability of gene expression of *G6pc* and *Pck1* in HFD-Ctrl-ASO and HFD-*APPL2*-ASO-226 group might from the worsen hyperinsulinemia in HFD-Ctrl-ASO mice.

The RNA-Seq results are helpful to explain the reduced HGP and improved pyruvate tolerance in *APPL2*-ASO group (Figure 4.5. B). Several signaling pathways associated

amino acid were discovered in KEEG signaling pathway enrichment, including 'valine, leucine and isoleucine degradation', 'glycine, serine and threonine metabolism' and 'pyruvate metabolism'. Mice with hepatic knockdown of APPL2 had higher total level of circulating amino acids, consistent with the fact that total amino acids concentration is in general lower in diabetic patients[169]. The higher amino acid concentration is probably due to the less utilization of amino acid for glucose production in APPL2 knockdown group[135]. Histidine, Valine, Leucine, serine showed increased concentration in my amino acids assay result. Compared with health control, diabetic individuals have the most significant changes on circulating glycine, serine[170] and threonine[169]. In animal model, lower concentration of serine in plasma was consistent to HGP from serine as precusor[135].

The liver is a major plase of amino acid metabolism, including synthesis, utilization, and disposal. Hepatic gluconeogenesis is frequently deregulated in T2DM, so if APPL2 as a suppressor of hepatic amino acid driven gluconeogenesis can be identified, it will be new avenues for the treatment of T2DM.

## 7.2 Elevated IGFBP2 induced by hepatic silencing APPL2 protects against insulin resistance.

IGFs (Insulin-like Growth Factors) are a family of proteins that play important roles in growth and development, as well as in regulating metabolism and cell proliferation. IGFBP family includes six binding proteins, which can bind to IGFs and regulate their actions[171]. As a member of the IGFBP family, IGFBP2 (Insulin-like Growth Factor

Binding Protein 2) was reported in many studies in which shown that IGFBPs play a pivotal role in metabolic signaling and metabolic disease[172].

Changes in IGFBP2 levels have been observed in various conditions associated with altered metabolism, such as obesity, insulin resistance, and T2DM. For example, in obese individuals, IGFBP2 levels are often decreased, which may be due to insulin resistance and impaired glucose metabolism[173-174]. Strong inverse association was found between circulating IGFBP2 concentrations and T2DM risk[175-176]. Several studies investigated the effect of IGFBP2 on glucose uptake in adipocyte. Mice over-expressed IGFBP2 improved insulin sensitivity by impair 3T3-L1 differentiation[177] and reversed diabetes by suppressing hepatic glucose production[132]. *In vitro* experiments showed that IGFBP2 significantly increased activation and induced GLUT4 translocation to enhance glucose uptake in 3T3-L1 adipocytes, through phosphorylation of PI3K, Akt, AMP-activated protein kinase (AMPK) [178] or activation of PI3K/Akt, AMPK/ TBC1D1, and PI3K/PKC/GLUT4 signaling pathways[179].

Most of previous studies focused on upregulation of circulating IGFBP2 by injection of IGFBP2 protein[180-181] or by overexpression of virus transfection[132]. However, the former one was not for diabetes prevention and the latter one cannot be applied on clinical therapy. Results in my study suggested a new way to supply IGFBP2 on animal model. It was demonstrated that down-regulating APPL2 in liver can upregulate hepatic and circulating IGFBP2 *in vivo* and *in vitro* (Figure 4.8-4.9), but rare studies explored the relationship between these two proteins in hepatic metabolic function. APPLs proteins were reported as activators of transcription[66], so it is potential to explore pathways by which APPL2 control *Igfbp2* gene expression accordingly.

## 7.3 APPL2 knockdown regulates fatty acid metabolism.

Fatty acid metabolism plays an important role in imbalanced glucose metabolism and diabetes development. Regulation of FA metabolism reduces the incidence of T2D. Both enlarged fat mass and adipose tissue dysfunction induce insulin resistance and glucose metabolism disorder by overstored fat in tissues like liver[182]. High fat diet increases circulating lipoprotein. Uptake and storage of triglycerides accumulates in hepatocytes via increased LPL activity, leading to hepatic insulin resistance. Increased de novo lipogenesis stimulated by insulin contributes to hepatic lipid accumulation. Insulin resistant also decreases hepatic mitochondrial function and inhibit FA oxidation, contributing to increased TG-VLDL production and secretion. Bile acid metabolism affects liver lipid metabolism in diabetic status[183].

In my result of Chapter 6, *APPL2*-ASO significantly reduced TC and LDL-C (Figure 6.2) without altering circulating FFA and TG. Hepatic steatosis degree and hepatic lipid contents decreased but not obviously. *APPL2*-ASO-228 remarkably decreased VLDL secretion (Figure 6.5) although lipid clearance ability not changed. With APPL2 knockdown, the major and obvious improvement on glucose metabolism instead of lipid metabolism. Given by RNA-Seq analysis, the association between glucose and lipid metabolism and improving of lipid metabolism by hepatic silencing APPL2 were more credible and explicable. In GO analysis, the biological process mainly included 'fatty acid metabolic process' and 'fatty acid oxidation'. Especially, 'fatty acid metabolic process' was upregulated in liver of HFD-*APPL2*-ASO-226 group according to GSEA result. Within them, the expression levels of several genes associated to lipid

metabolism were noticeably changed, such as *Cyp2c23*[184], *Nucb2*[185], *Scd1*[186], *Acacb*[187], *Lpl*[188] and *Cav1*[189]. The proteins encoded by these genes regulate the synthesis, catabolism, and oxidation of fatty acids in hepatocytes and thereby affect insulin sensitivity, consistent with the fact that disordered lipid metabolism unlocks insulin resistance in diabetic patients[190-191]. An increased hepatic lipid provision increases TG-VLDL secretion, glucose production, leading to impaired insulin resistance. Negatively associated with VLDL-TG secretion, Adiponectin inhibits ApoB100 secretion from hepatocytes, stimulating hepatic fatty acid oxidation, suppressing lipogenesis, and reduces hepatic TG content[192]. IGFBP2 can also downregulate hepatic fatty acid synthesis[193].

## 7.4 Cold exposure heighten the effect of silencing hepatic APPL2 on protection against adipocyte hypertrophy and diet-induced liver steatosis.

The effect of improving energy metabolism (Figure 5.4) by inactivating hepatic APPL2 under room temperature was verified to be enhanced under cold exposure (Figure 5.5), which gave a clue that *APPL2*-ASO treatment might affect adaptive thermogenesis and adipose tissue browning. When mice were in a cold environment, *APPL2*-ASO treatment showed decrease of fat mass and adipocyte atrophy of. Higher UCP1 expression in sWAT and BAT of *APPL2*-ASO groups (Figure 5.7) indicates the increase of thermogenesis. Previous research has shown that cold exposure restored BAT function, thereby improved glucose tolerance and decreased fat mass and liver steatosis[194]. The mice implanted with human beige adipocytes had lower levels of

fasting blood glucose, increased glucose tolerance and reduced hepatic steatosis[195]. Hepatic APPL2 knockdown showed less effect on alleviating hepatic steatosis under room temperature in my result. That might be because ASO has a weak protective effect on highly induced fatty liver, which can be significantly improved only under cold-induced conditions. Brown adipocytes and skeletal muscle cells originate from the same stem cells (Myf5+) and can be transformed into white or beige adipocytes[126]. Beige adipocyte differentiation into brown adipocytes is induced by molecular factors, like PRDM16, and environmental factors, like chronic cold exposure. The GLUT1 and GLUT4 can both participate in glucose uptake in human BAT, via insulin mediation or independently, with higher expression and activated translocation in BAT with cold stimulation[196]. Therefore, it can be supposed that APPL2 knockdown in the liver can induce higher secretion of certain hepatokines, indirectly causing increasing glucose uptake in brown or browning adipocytes.

## 7.5 Phenotypes distinguishment between two sequences of APPL2-ASOs

Although the treatment of APPL2-ASO-228 (5mg/kg dose) also has the effect on enhancing glucose tolerance and insulin sensitivity, it is not as obvious as APPL2-ASO-226 (10mg/kg dose). Some reports indicated that the effect of ASO is dose- and sequence-dependent, which may be an important reason for this phenotypic difference in my project. Due to the company's confidentiality, we cannot obtain the specific sequence of each ASO, it is deducible that two ASOs sequences can target to different domains of APPL2 protein and cause this distinguishment. In addition, different treatments (APPL2-ASO-228; 5mg/kg dose VS APPL2-ASO-226, 10mg/kg dose)

could lead to different knockdown efficiency, although it is necessary to test the protein expression levels from two ASOs treatmens in one immunoblot in the future.

## 7.6 Conclusion

APPL2 was verified to be associated with insulin resistance and secretion. In muscle cell, APPL2 prevents translocation of GLUT4 to the cell membrane; negatively regulates adiponectin- or insulin-stimulated glucose uptake and fatty acid oxidation. Meanwhile, However, APPL2 improves glucose stimulated insulin secretion.

My study demonstrates that selectively silencing hepatic APPL2 can improve glucose metabolism, alleviate hypercholesterolemia, and enhance energy expenditure in HFD-induced mice. GalNAc-*APPL2*-ASOs with different sequences can both be used to liver-specifically inactivate APPL2, verifying by markedly declined mRNA and protein level of APPL2 in mice liver and isolated primary hepatocyte. Evaluation of food intake, body weight and liver injury markers after GalNAc-*APPL2*-ASO treatment supported its tolerability and safety. Specifically speaking, the treatment improved glucose tolerance in diet-induced obese and insulin resistant mice, accompany with an increase of insulin sensitivity and a suppression of gluconeogenesis. One sequence of *APPL2*-ASO presented apparent improvement on lipid metabolism, decreasing circulating non-HDL cholesterol, and inhibiting TG-VLDL secretion. RNA-Seq analysis result also illustrated complementally that hepatic knockdown of APPL2 mainly regulated pathways like fatty acids metabolism, cholesterol metabolism, and amino acid metabolism.

We showed that selectively silencing hepatic APPL2 alleviated insulin resistance and hypercholesterolemia, improve energy metabolism in diet-induced obese mouse model,

indicating APPL2 as a novel therapeutic target for metabolic diseases, and providing theoretical support for clinical application GalNAc-*APPL2*-ASO with high specificity.

## 7.7 Limitation and Future work

Firstly, the effect of APPL2 knockdown by ASOs on glucose and lipid metabolism was revealed in animal studies. However, phenotypes between ASOs treatment and genetic modification existed inconsistency[197-198]. For example, a reduction in FMO3 with FMO3-ASOs decreased levels of plasma cholesterol, insulin, and glucose. but the generated FMO3-KO mice did not change obviously on the above phenotypes, compared with the WT ones[199]. To eliminate the possible off-target effect from APPL2 knockdown by ASOs, the previous alterations on mice phenotype should be validated by other hepatic APPL2 deletion models. Our lab has generated muscle-specific APPL2 KO mice by crossing APPL2$^{floxed}$ mice[69] with transgenic mice expressing Cre recombinase under the control of muscle creatine kinase promoter. Therefore, we can cross APPL2 floxed mice with albumin-Cre transgenic mice[200] to generate hepatocyte-specific APPL2 knockout mice and validate the altered phenotype in current results.

Secondly, according to the circulating amino acids analysis, valine and serine concentrations significantly increased in the serum of DIO-mice treated with *APPL2*-ASO-226. In addition, RNA-Seq results also enriched the associated amino acids metabolism pathways. Despite the decreased level of glucose production that has been verified in primary hepatocytes, pyruvate was the only used gluconeogenesis precursor in the current result. The study reported that hepatic gluconeogenesis is a major

pathway for serine consumption in some contexts and can be regulated by insulin[201]. Therefore, glucose-exhausted primary hepatocytes will be used to study if decreasing APPL2 expression results in lower glucose production with utilization of valine and serine.

Thirdly, as previously speculated, improved whole-body glucose metabolism might be contributed by higher uptake and activated GLUT4 translocation in adipocyte and muscle cells from hepatokines alteration of hepatic APPL2 knockdown mice. As hepatokine with a similar structure to insulin, IGFBP2 induces GLUT4 translocation and glucose uptake in 3T3-L1 adipocytes or supresses gluconeogenesis. Therefore, increasing IGFBP2 secretion in circulation by *APPL2*-ASOs might be the contributor. IGFBP2 was increased in primary hepatocytes isolated from mice treated with *APPL2*-ASO-226. IGFBP2 with a certain concentration of in collected conditioned medium can be used to culture differentiated 3T3-L1 adipocytes. 2-deoxy-2-[(7-nitro-2,1,3-benzoxadiazol-4-yl) amino]-D-glucose (2-DG) is a fluorescent deoxyglucose analog that can be taken up by cells through GLUTs. It cannot be fully utilized in glycolysis and thus accumulates into cells. Fluorescence of 2-DG is proportional to glucose uptake by the cells and can be used to measure glucose uptake using a fluorescence microplate reader and flow cytometry. To verify the effect of promoting glucose uptake is from IGFBP2, IGFBP2 antibody can be used to block the IGFBP2 protein by binding in the above conditioned medium. Alteration of GLUT4 expression in membrane of adipocytes can be further assessed by immunoblotting and translocation of GLUT4 can also be investigated by immunofluorescence staining. Similar approach can be used to verify the effect of supression of gluconeogenesis is from IGFBP2. As an interacting partner and downstream effector of APPL2, TBC1D1 locates on IGF-1 storage vesicles

and mediate IGF-1 secretion[202]. Therefore, we can also detect if the phosphorylation of TBC1D1 in liver and colocalization of TBC1D1 in substructures of hepatocytes are changed by APPL2 inactivation.

At last, APPL2 knockdown distinctly alleviated lipid accumulation under cold, and alteration of fatty acids metabolism of the tissue was also verified by RNA-Seq result. Although total free fatty acids did not change by hepatic APPL2 inactivation in my current result, individual fatty acids and associated metabolites should be determined in both circulation and liver lysate by targeted metabolomics. Since RIP-APPL2 knockout can affect insulin secretion, we will also investigate APPL2 expression in pancreas by using IHC.

# References

(1) Kleinert, M.; Clemmensen, C.; Hofmann, S. M.; Moore, M. C.; Renner, S.; Woods, S. C.; Huypens, P.; Beckers, J.; de Angelis, M. H.; Schürmann, A.; et al. Animal models of obesity and diabetes mellitus. *Nat Rev Endocrinol* **2018**, *14* (3), 140-162.

(2) Saeedi, P.; Petersohn, I.; Salpea, P.; Malanda, B.; Karuranga, S.; Unwin, N.; Colagiuri, S.; Guariguata, L.; Motala, A. A.; Ogurtsova, K.; et al. Global and regional diabetes prevalence estimates for 2019 and projections for 2030 and 2045: Results from the International Diabetes Federation Diabetes Atlas, 9(th) edition. *Diabetes Res Clin Pract* **2019**, *157*, 107843.

(3) Tomic, D.; Shaw, J. E.; Magliano, D. J. The burden and risks of emerging complications of diabetes mellitus. *Nat Rev Endocrinol* **2022**, *18* (9), 525-539.

(4) Röder, P. V.; Wu, B.; Liu, Y.; Han, W. Pancreatic regulation of glucose homeostasis. *Exp Mol Med* **2016**, *48* (3), e219.

(5) Huang, J.; Imamura, T.; Olefsky, J. M. Insulin can regulate GLUT4 internalization by signaling to Rab5 and the motor protein dynein. *Proc Natl Acad Sci U S A* **2001**, *98* (23), 13084-13089.

(6) Czech, M. P. Insulin action and resistance in obesity and type 2 diabetes. *Nat Med* **2017**, *23* (7), 804-814.

(7) Zhang, Y.; Shen, T.; Wang, S. Progression from prediabetes to type 2 diabetes mellitus induced by overnutrition. *Hormones (Athens)* **2022**, *21* (4), 591-597.

(8) Kahn, S. E.; Hull, R. L.; Utzschneider, K. M. Mechanisms linking obesity to insulin resistance and type 2 diabetes. *Nature* **2006**, *444* (7121), 840-846.

(9) Lai, M.; Chandrasekera, P. C.; Barnard, N. D. You are what you eat, or are you? The challenges of translating high-fat-fed rodents to human obesity and diabetes. *Nutr Diabetes* **2014**, *4* (9), e135.

(10) Parhofer, K. G. Interaction between Glucose and Lipid Metabolism: More than Diabetic Dyslipidemia. *Diabetes Metab J* **2015**, *39* (5), 353-362.

(11) Bechmann, L. P.; Hannivoort, R. A.; Gerken, G.; Hotamisligil, G. S.; Trauner, M.; Canbay, A. The interaction of hepatic lipid and glucose metabolism in liver diseases. *J Hepatol* **2012**, *56* (4), 952-964.

(12) Adeva-Andany, M. M.; Pérez-Felpete, N.; Fernández-Fernández, C.; Donapetry-García, C.; Pazos-García, C. Liver glucose metabolism in humans. *Biosci Rep* **2016**, *36*

(6).

(13) DeFronzo, R. A. Pathogenesis of type 2 diabetes mellitus. *Med Clin North Am* **2004**, *88* (4), 787-835, ix.

(14) Hellerstein, M. K.; Neese, R. A.; Linfoot, P.; Christiansen, M.; Turner, S.; Letscher, A. Hepatic gluconeogenic fluxes and glycogen turnover during fasting in humans. A stable isotope study. *J Clin Invest* **1997**, *100* (5), 1305-1319.

(15) Jang, C.; Hui, S.; Lu, W.; Cowan, A. J.; Morscher, R. J.; Lee, G.; Liu, W.; Tesz, G. J.; Birnbaum, M. J.; Rabinowitz, J. D. The Small Intestine Converts Dietary Fructose into Glucose and Organic Acids. *Cell Metab* **2018**, *27* (2), 351-361.e353.

(16) Takeda, J.; Kayano, T.; Fukomoto, H.; Bell, G. I. Organization of the human GLUT2 (pancreatic beta-cell and hepatocyte) glucose transporter gene. *Diabetes* **1993**, *42* (5), 773-777.

(17) Woerle, H. J.; Meyer, C.; Dostou, J. M.; Gosmanov, N. R.; Islam, N.; Popa, E.; Wittlin, S. D.; Welle, S. L.; Gerich, J. E. Pathways for glucose disposal after meal ingestion in humans. *Am J Physiol Endocrinol Metab* **2003**, *284* (4), E716-725.

(18) Solinas, G.; Borén, J.; Dulloo, A. G. De novo lipogenesis in metabolic homeostasis: More friend than foe? *Mol Metab* **2015**, *4* (5), 367-377.

(19) Roden, M.; Bernroider, E. Hepatic glucose metabolism in humans--its role in health and disease. *Best Pract Res Clin Endocrinol Metab* **2003**, *17* (3), 365-383.

(20) Lemaigre, F. P.; Rousseau, G. G. Transcriptional control of genes that regulate glycolysis and gluconeogenesis in adult liver. *Biochem J* **1994**, *303 ( Pt 1)* (Pt 1), 1-14.

(21) Guo, X.; Li, H.; Xu, H.; Woo, S.; Dong, H.; Lu, F.; Lange, A. J.; Wu, C. Glycolysis in the control of blood glucose homeostasis. *Acta Pharmaceutica Sinica B* **2012**, *2* (4), 358-367.

(22) Wu, C.; Okar, D. A.; Newgard, C. B.; Lange, A. J. Increasing fructose 2,6-bisphosphate overcomes hepatic insulin resistance of type 2 diabetes. *Am J Physiol Endocrinol Metab* **2002**, *282* (1), E38-45.

(23) Petersen, M. C.; Vatner, D. F.; Shulman, G. I. Regulation of hepatic glucose metabolism in health and disease. *Nat Rev Endocrinol* **2017**, *13* (10), 572-587.

(24) Lewis, G. F.; Carpentier, A. C.; Pereira, S.; Hahn, M.; Giacca, A. Direct and indirect control of hepatic glucose production by insulin. *Cell Metab* **2021**, *33* (4), 709-720.

(25) Treadway, J. L.; Mendys, P.; Hoover, D. J. Glycogen phosphorylase inhibitors for treatment of type 2 diabetes mellitus. *Expert Opin Investig Drugs* **2001**, *10* (3), 439-454.

(26) Basu, R.; Chandramouli, V.; Dicke, B.; Landau, B.; Rizza, R. Obesity and type 2

diabetes impair insulin-induced suppression of glycogenolysis as well as gluconeogenesis. *Diabetes* **2005**, *54* (7), 1942-1948.

(27) Hatting, M.; Tavares, C. D. J.; Sharabi, K.; Rines, A. K.; Puigserver, P. Insulin regulation of gluconeogenesis. *Ann N Y Acad Sci* **2018**, *1411* (1), 21-35.

(28) Sekizkardes, H.; Chung, S. T.; Chacko, S.; Haymond, M. W.; Startzell, M.; Walter, M.; Walter, P. J.; Lightbourne, M.; Brown, R. J. Free fatty acid processing diverges in human pathologic insulin resistance conditions. *J Clin Invest* **2020**, *130* (7), 3592-3602.

(29) Gross, D. N.; van den Heuvel, A. P.; Birnbaum, M. J. The role of FoxO in the regulation of metabolism. *Oncogene* **2008**, *27* (16), 2320-2336.

(30) Herzig, S.; Long, F.; Jhala, U. S.; Hedrick, S.; Quinn, R.; Bauer, A.; Rudolph, D.; Schutz, G.; Yoon, C.; Puigserver, P.; et al. CREB regulates hepatic gluconeogenesis through the coactivator PGC-1. *Nature* **2001**, *413* (6852), 179-183.

(31) Kurukulasuriya, R.; Link, J. T.; Madar, D. J.; Pei, Z.; Richards, S. J.; Rohde, J. J.; Souers, A. J.; Szczepankiewicz, B. G. Potential drug targets and progress towards pharmacologic inhibition of hepatic glucose production. *Curr Med Chem* **2003**, *10* (2), 123-153.

(32) Rachek, L. I. Free fatty acids and skeletal muscle insulin resistance. *Prog Mol Biol Transl Sci* **2014**, *121*, 267-292.

(33) Jones, J. G. Hepatic glucose and lipid metabolism. *Diabetologia* **2016**, *59* (6), 1098-1103.

(34) Bergen, W. G.; Mersmann, H. J. Comparative aspects of lipid metabolism: impact on contemporary research and use of animal models. *J Nutr* **2005**, *135* (11), 2499-2502.

(35) Alves-Bezerra, M.; Cohen, D. E. Triglyceride Metabolism in the Liver. *Compr Physiol* **2017**, *8* (1), 1-8.

(36) Kwiterovich, P. O., Jr. The metabolic pathways of high-density lipoprotein, low-density lipoprotein, and triglycerides: a current review. *Am J Cardiol* **2000**, *86* (12a), 5l-10l.

(37) Lagace, T. A. PCSK9 and LDLR degradation: regulatory mechanisms in circulation and in cells. *Curr Opin Lipidol* **2014**, *25* (5), 387-393.

(38) Tailleux, A.; Duriez, P.; Fruchart, J. C.; Clavey, V. Apolipoprotein A-II, HDL metabolism and atherosclerosis. *Atherosclerosis* **2002**, *164* (1), 1-13.

(39) Shin, S. Regulation of Adipose Tissue Biology by Long-Chain Fatty Acids: Metabolic Effects and Molecular Mechanisms. *J Obes Metab Syndr* **2022**, *31* (2), 147-160.

(40) Vidal-Puig, A. Adipose tissue expandability, lipotoxicity and the metabolic syndrome. *Endocrinol Nutr* **2013**, *60 Suppl 1*, 39-43.

(41) Biddinger, S. B.; Hernandez-Ono, A.; Rask-Madsen, C.; Haas, J. T.; Alemán, J. O.; Suzuki, R.; Scapa, E. F.; Agarwal, C.; Carey, M. C.; Stephanopoulos, G.; et al. Hepatic insulin resistance is sufficient to produce dyslipidemia and susceptibility to atherosclerosis. *Cell Metab* **2008**, *7* (2), 125-134.

(42) Cazanave, S. C.; Gores, G. J. Mechanisms and clinical implications of hepatocyte lipoapoptosis. *Clin Lipidol* **2010**, *5* (1), 71-85.

(43) Kusminski, C. M.; Shetty, S.; Orci, L.; Unger, R. H.; Scherer, P. E. Diabetes and apoptosis: lipotoxicity. *Apoptosis* **2009**, *14* (12), 1484-1495.

(44) Rada, P.; González-Rodríguez, Á.; García-Monzón, C.; Valverde Á, M. Understanding lipotoxicity in NAFLD pathogenesis: is CD36 a key driver? *Cell Death Dis* **2020**, *11* (9), 802.

(45) Najjar, S. M.; Yang, Y.; Fernström, M. A.; Lee, S. J.; Deangelis, A. M.; Rjaily, G. A.; Al-Share, Q. Y.; Dai, T.; Miller, T. A.; Ratnam, S.; et al. Insulin acutely decreases hepatic fatty acid synthase activity. *Cell Metab* **2005**, *2* (1), 43-53.

(46) Flynn, D. C. Adaptor proteins. *Oncogene* **2001**, *20* (44), 6270-6272.

(47) Ryu, J.; Galan, A. K.; Xin, X.; Dong, F.; Abdul-Ghani, M. A.; Zhou, L.; Wang, C.; Li, C.; Holmes, B. M.; Sloane, L. B.; et al. APPL1 potentiates insulin sensitivity by facilitating the binding of IRS1/2 to the insulin receptor. *Cell Rep* **2014**, *7* (4), 1227-1238.

(48) Mitsuuchi, Y.; Johnson, S. W.; Sonoda, G.; Tanno, S.; Golemis, E. A.; Testa, J. R. Identification of a chromosome 3p14.3-21.1 gene, APPL, encoding an adaptor molecule that interacts with the oncoprotein-serine/threonine kinase AKT2. *Oncogene* **1999**, *18* (35), 4891-4898.

(49) Liu, J.; Yao, F.; Wu, R.; Morgan, M.; Thorburn, A.; Finley, R. L., Jr.; Chen, Y. Q. Mediation of the DCC apoptotic signal by DIP13 alpha. *J Biol Chem* **2002**, *277* (29), 26281-26285.

(50) Li, J.; Mao, X.; Dong, L. Q.; Liu, F.; Tong, L. Crystal structures of the BAR-PH and PTB domains of human APPL1. *Structure* **2007**, *15* (5), 525-533.

(51) Zhu, G.; Chen, J.; Liu, J.; Brunzelle, J. S.; Huang, B.; Wakeham, N.; Terzyan, S.; Li, X.; Rao, Z.; Li, G.; et al. Structure of the APPL1 BAR-PH domain and characterization of its interaction with Rab5. *Embo j* **2007**, *26* (14), 3484-3493.

(52) Habermann, B. The BAR-domain family of proteins: a case of bending and binding? *EMBO Rep* **2004**, *5* (3), 250-255.

(53) Peter, B. J.; Kent, H. M.; Mills, I. G.; Vallis, Y.; Butler, P. J.; Evans, P. R.; McMahon, H. T. BAR domains as sensors of membrane curvature: the amphiphysin BAR structure. *Science* **2004**, *303* (5657), 495-499.

(54) Lemmon, M. A. Pleckstrin homology domains: not just for phosphoinositides.

*Biochem Soc Trans* **2004**, *32* (Pt 5), 707-711.

(55) Uhlik, M. T.; Temple, B.; Bencharit, S.; Kimple, A. J.; Siderovski, D. P.; Johnson, G. L. Structural and evolutionary division of phosphotyrosine binding (PTB) domains. *J Mol Biol* **2005**, *345* (1), 1-20.

(56) Miaczynska, M.; Christoforidis, S.; Giner, A.; Shevchenko, A.; Uttenweiler-Joseph, S.; Habermann, B.; Wilm, M.; Parton, R. G.; Zerial, M. APPL proteins link Rab5 to nuclear signal transduction via an endosomal compartment. *Cell* **2004**, *116* (3), 445-456.

(57) Chial, H. J.; Wu, R.; Ustach, C. V.; McPhail, L. C.; Mobley, W. C.; Chen, Y. Q. Membrane targeting by APPL1 and APPL2: dynamic scaffolds that oligomerize and bind phosphoinositides. *Traffic* **2008**, *9* (2), 215-229.

(58) Nechamen, C. A.; Thomas, R. M.; Dias, J. A. APPL1, APPL2, Akt2 and FOXO1a interact with FSHR in a potential signaling complex. *Mol Cell Endocrinol* **2007**, *260-262*, 93-99.

(59) Varsano, T.; Dong, M. Q.; Niesman, I.; Gacula, H.; Lou, X.; Ma, T.; Testa, J. R.; Yates, J. R., 3rd; Farquhar, M. G. GIPC is recruited by APPL to peripheral TrkA endosomes and regulates TrkA trafficking and signaling. *Mol Cell Biol* **2006**, *26* (23), 8942-8952.

(60) Chial, H. J.; Lenart, P.; Chen, Y. Q. APPL proteins FRET at the BAR: direct observation of APPL1 and APPL2 BAR domain-mediated interactions on cell membranes using FRET microscopy. *PLoS One* **2010**, *5* (8), e12471.

(61) Cheng, K. K.; Lam, K. S.; Wang, B.; Xu, A. Signaling mechanisms underlying the insulin-sensitizing effects of adiponectin. *Best Pract Res Clin Endocrinol Metab* **2014**, *28* (1), 3-13.

(62) Mao, X.; Kikani, C. K.; Riojas, R. A.; Langlais, P.; Wang, L.; Ramos, F. J.; Fang, Q.; Christ-Roberts, C. Y.; Hong, J. Y.; Kim, R. Y.; et al. APPL1 binds to adiponectin receptors and mediates adiponectin signalling and function. *Nat Cell Biol* **2006**, *8* (5), 516-523.

(63) Wang, C.; Xin, X.; Xiang, R.; Ramos, F. J.; Liu, M.; Lee, H. J.; Chen, H.; Mao, X.; Kikani, C. K.; Liu, F.; et al. Yin-Yang regulation of adiponectin signaling by APPL isoforms in muscle cells. *J Biol Chem* **2009**, *284* (46), 31608-31615.

(64) Cheng, K. K.; Lam, K. S.; Wang, Y.; Huang, Y.; Carling, D.; Wu, D.; Wong, C.; Xu, A. Adiponectin-induced endothelial nitric oxide synthase activation and nitric oxide production are mediated by APPL1 in endothelial cells. *Diabetes* **2007**, *56* (5), 1387-1394.

(65) Cheng, K. K.; Iglesias, M. A.; Lam, K. S.; Wang, Y.; Sweeney, G.; Zhu, W.; Vanhoutte, P. M.; Kraegen, E. W.; Xu, A. APPL1 potentiates insulin-mediated inhibition of hepatic glucose production and alleviates diabetes via Akt activation in mice. *Cell Metab* **2009**, *9* (5), 417-427.

(66) Rashid, S.; Pilecka, I.; Torun, A.; Olchowik, M.; Bielinska, B.; Miaczynska, M. Endosomal adaptor proteins APPL1 and APPL2 are novel activators of beta-catenin/TCF-mediated transcription. *J Biol Chem* **2009**, *284* (27), 18115-18128.

(67) Ryu, J.; Hadley, J. T.; Li, Z.; Dong, F.; Xu, H.; Xin, X.; Zhang, Y.; Chen, C.; Li, S.; Guo, X.; et al. Adiponectin Alleviates Diet-Induced Inflammation in the Liver by Suppressing MCP-1 Expression and Macrophage Infiltration. *Diabetes* **2021**, *70* (6), 1303-1316.

(68) Cleasby, M. E.; Lau, Q.; Polkinghorne, E.; Patel, S. A.; Leslie, S. J.; Turner, N.; Cooney, G. J.; Xu, A.; Kraegen, E. W. The adaptor protein APPL1 increases glycogen accumulation in rat skeletal muscle through activation of the PI3-kinase signalling pathway. *J Endocrinol* **2011**, *210* (1), 81-92.

(69) Cheng, K. K.; Zhu, W.; Chen, B.; Wang, Y.; Wu, D.; Sweeney, G.; Wang, B.; Lam, K. S.; Xu, A. The adaptor protein APPL2 inhibits insulin-stimulated glucose uptake by interacting with TBC1D1 in skeletal muscle. *Diabetes* **2014**, *63* (11), 3748-3758.

(70) Cheng, K. K.; Lam, K. S.; Wu, D.; Wang, Y.; Sweeney, G.; Hoo, R. L.; Zhang, J.; Xu, A. APPL1 potentiates insulin secretion in pancreatic β cells by enhancing protein kinase Akt-dependent expression of SNARE proteins in mice. *Proc Natl Acad Sci U S A* **2012**, *109* (23), 8919-8924.

(71) Wang, C.; Li, X.; Mu, K.; Li, L.; Wang, S.; Zhu, Y.; Zhang, M.; Ryu, J.; Xie, Z.; Shi, D.; et al. Deficiency of APPL1 in mice impairs glucose-stimulated insulin secretion through inhibition of pancreatic beta cell mitochondrial function. *Diabetologia* **2013**, *56* (9), 1999-2009.

(72) Wang, B.; Lin, H.; Li, X.; Lu, W.; Kim, J. B.; Xu, A.; Cheng, K. K. Y. The adaptor protein APPL2 controls glucose-stimulated insulin secretion via F-actin remodeling in pancreatic β-cells. *Proc Natl Acad Sci U S A* **2020**, *117* (45), 28307-28315.

(73) Wang, B.; Li, A.; Li, X.; Ho, P. W.; Wu, D.; Wang, X.; Liu, Z.; Wu, K. K.; Yau, S. S.; Xu, A.; et al. Activation of hypothalamic RIP-Cre neurons promotes beiging of WAT via sympathetic nervous system. *EMBO Rep* **2018**, *19* (4).

(74) Canciglieri, P. H.; Kuga, G. K.; Muñoz, V. R.; Gaspar, R. C.; da Rocha, A. L.; Breda, L.; Anaruma, C. P.; Minuzzi, L. G.; da Silva, A. S. R.; Cintra, D. E.; et al. The reversal effect of physical exercise on aging-related increases in APPL2 content in skeletal muscle. *Life Sci* **2018**, *210*, 209-213.

(75) Ma, X. W.; Ding, S.; Ma, X. D.; Gu, N.; Guo, X. H. Genetic variability in adapter proteins with APPL1/2 is associated with the risk of coronary artery disease in type 2 diabetes mellitus in Chinese Han population. *Chin Med J (Engl)* **2011**, *124* (22), 3618-3621.

(76) Jiang, S.; Fang, Q.; Yu, W.; Zhang, R.; Hu, C.; Dong, K.; Bao, Y.; Wang, C.; Xiang, K.; Jia, W. Genetic variations in APPL2 are associated with overweight and obesity in a Chinese population with normal glucose tolerance. *BMC Med Genet* **2012**, *13*, 22.

(77) Barbieri, M.; Esposito, A.; Angellotti, E.; Rizzo, M. R.; Marfella, R.; Paolisso, G. Association of genetic variation in adaptor protein APPL1/APPL2 loci with non-alcoholic fatty liver disease. *PLoS One* **2013**, *8* (8), e71391.

(78) Klaus, V. S.; Schriever, S. C.; Monroy Kuhn, J. M.; Peter, A.; Irmler, M.; Tokarz, J.; Prehn, C.; Kastenmüller, G.; Beckers, J.; Adamski, J.; et al. Correlation guided Network Integration (CoNI) reveals novel genes affecting hepatic metabolism. *Mol Metab* **2021**, *53*, 101295.

(79) Faghihi, M. A.; Wahlestedt, C. Regulatory roles of natural antisense transcripts. *Nat Rev Mol Cell Biol* **2009**, *10* (9), 637-643.

(80) Bennett, C. F.; Condon, T. P.; Grimm, S.; Chan, H.; Chiang, M. Y. Inhibition of endothelial cell adhesion molecule expression with antisense oligonucleotides. *J Immunol* **1994**, *152* (7), 3530-3540.

(81) Mansoor, M.; Melendez, A. J. Advances in antisense oligonucleotide development for target identification, validation, and as novel therapeutics. *Gene Regul Syst Bio* **2008**, *2*, 275-295.

(82) Geary, R. S.; Norris, D.; Yu, R.; Bennett, C. F. Pharmacokinetics, biodistribution and cell uptake of antisense oligonucleotides. *Adv Drug Deliv Rev* **2015**, *87*, 46-51.

(83) Tillman, L. G.; Geary, R. S.; Hardee, G. E. Oral delivery of antisense oligonucleotides in man. *J Pharm Sci* **2008**, *97* (1), 225-236.

(84) Geary, R. S. Antisense oligonucleotide pharmacokinetics and metabolism. *Expert Opin Drug Metab Toxicol* **2009**, *5* (4), 381-391.

(85) Yu, R. Z.; Grundy, J. S.; Geary, R. S. Clinical pharmacokinetics of second generation antisense oligonucleotides. *Expert Opin Drug Metab Toxicol* **2013**, *9* (2), 169-182.

(86) Mustonen, E. K.; Palomäki, T.; Pasanen, M. Oligonucleotide-based pharmaceuticals: Non-clinical and clinical safety signals and non-clinical testing strategies. *Regul Toxicol Pharmacol* **2017**, *90*, 328-341.

(87) Alves, R. J. Statin Use and Hypercholesterolemia: Are the Current Guidelines' Recommendations Being Followed? *Arq Bras Cardiol* **2021**, *116* (4), 742-743.

(88) Zhang, L.; McCabe, T.; Condra, J. H.; Ni, Y. G.; Peterson, L. B.; Wang, W.; Strack, A. M.; Wang, F.; Pandit, S.; Hammond, H.; et al. An anti-PCSK9 antibody reduces LDL-cholesterol on top of a statin and suppresses hepatocyte SREBP-regulated genes. *Int J Biol Sci* **2012**, *8* (3), 310-327.

(89) Crooke, S. T.; Baker, B. F.; Crooke, R. M.; Liang, X. H. Antisense technology: an overview and prospectus. *Nat Rev Drug Discov* **2021**, *20* (6), 427-453.

(90) Roberts, T. C.; Langer, R.; Wood, M. J. A. Advances in oligonucleotide drug delivery. *Nat Rev Drug Discov* **2020**, *19* (10), 673-694.

(91) Dhuri, K.; Bechtold, C.; Quijano, E.; Pham, H.; Gupta, A.; Vikram, A.; Bahal, R. Antisense Oligonucleotides: An Emerging Area in Drug Discovery and Development. *J Clin Med* **2020**, *9* (6).

(92) Yang, L.; Ma, F.; Liu, F.; Chen, J.; Zhao, X.; Xu, Q. Efficient Delivery of Antisense Oligonucleotides Using Bioreducible Lipid Nanoparticles In Vitro and In Vivo. *Mol Ther Nucleic Acids* **2020**, *19*, 1357-1367.

(93) Cerrato, C. P.; Kivijärvi, T.; Tozzi, R.; Lehto, T.; Gestin, M.; Langel, Ü. Intracellular delivery of therapeutic antisense oligonucleotides targeting mRNA coding mitochondrial proteins by cell-penetrating peptides. *J Mater Chem B* **2020**, *8* (47), 10825-10836.

(94) Debacker, A. J.; Voutila, J.; Catley, M.; Blakey, D.; Habib, N. Delivery of Oligonucleotides to the Liver with GalNAc: From Research to Registered Therapeutic Drug. *Mol Ther* **2020**, *28* (8), 1759-1771.

(95) Janas, M. M.; Harbison, C. E.; Perry, V. K.; Carito, B.; Sutherland, J. E.; Vaishnaw, A. K.; Keirstead, N. D.; Warner, G. The Nonclinical Safety Profile of GalNAc-conjugated RNAi Therapeutics in Subacute Studies. *Toxicol Pathol* **2018**, *46* (7), 735-745.

(96) Tanowitz, M.; Hettrick, L.; Revenko, A.; Kinberger, G. A.; Prakash, T. P.; Seth, P. P. Asialoglycoprotein receptor 1 mediates productive uptake of N-acetylgalactosamine-conjugated and unconjugated phosphorothioate antisense oligonucleotides into liver hepatocytes. *Nucleic Acids Res* **2017**, *45* (21), 12388-12400.

(97) Huang, X.; Leroux, J. C.; Castagner, B. Well-Defined Multivalent Ligands for Hepatocytes Targeting via Asialoglycoprotein Receptor. *Bioconjug Chem* **2017**, *28* (2), 283-295.

(98) Baenziger, J. U.; Fiete, D. Galactose and N-acetylgalactosamine-specific endocytosis of glycopeptides by isolated rat hepatocytes. *Cell* **1980**, *22* (2 Pt 2), 611-620.

(99) Schoch, K. M.; Miller, T. M. Antisense Oligonucleotides: Translation from Mouse Models to Human Neurodegenerative Diseases. *Neuron* **2017**, *94* (6), 1056-1070.

(100) Yoshida, T.; Naito, Y.; Yasuhara, H.; Sasaki, K.; Kawaji, H.; Kawai, J.; Naito, M.; Okuda, H.; Obika, S.; Inoue, T. Evaluation of off-target effects of gapmer antisense oligonucleotides using human cells. *Genes Cells* **2019**, *24* (12), 827-835.

(101) Vickers, T. A.; Crooke, S. T. Antisense oligonucleotides capable of promoting specific target mRNA reduction via competing RNase H1-dependent and independent mechanisms. *PLoS One* **2014**, *9* (10), e108625.

(102) Williams, B. R. Role of the double-stranded RNA-activated protein kinase (PKR) in cell regulation. *Biochem Soc Trans* **1997**, *25* (2), 509-513.

(103) Ormazabal, V.; Nair, S.; Elfeky, O.; Aguayo, C.; Salomon, C.; Zuñiga, F. A.

Association between insulin resistance and the development of cardiovascular disease. *Cardiovasc Diabetol* **2018**, *17* (1), 122.

(104) Cimminiello, C.; Zambon, A.; Polo Friz, H. Hypercholesterolemia and cardiovascular risk: advantages and limitations of current treatment options. *G Ital Cardiol (Rome)* **2016**, *17* (4 Suppl 1), 6s-13.

(105) Newman, J. D.; Schwartzbard, A. Z.; Weintraub, H. S.; Goldberg, I. J.; Berger, J. S. Primary Prevention of Cardiovascular Disease in Diabetes Mellitus. *J Am Coll Cardiol* **2017**, *70* (7), 883-893.

(106) Giannini, E. G.; Testa, R.; Savarino, V. Liver enzyme alteration: a guide for clinicians. *Cmaj* **2005**, *172* (3), 367-379.

(107) Wang, C. Y.; Liao, J. K. A mouse model of diet-induced obesity and insulin resistance. *Methods Mol Biol* **2012**, *821*, 421-433.

(108) Ramzan, A. A.; Bitler, B. G.; Hicks, D.; Barner, K.; Qamar, L.; Behbakht, K.; Powell, T.; Jansson, T.; Wilson, H. Adiponectin receptor agonist AdipoRon induces apoptotic cell death and suppresses proliferation in human ovarian cancer cells. *Mol Cell Biochem* **2019**, *461* (1-2), 37-46.

(109) Wang, Z.; Gerstein, M.; Snyder, M. RNA-Seq: a revolutionary tool for transcriptomics. *Nat Rev Genet* **2009**, *10* (1), 57-63.

(110) Kukurba, K. R.; Montgomery, S. B. RNA Sequencing and Analysis. *Cold Spring Harb Protoc* **2015**, *2015* (11), 951-969.

(111) Young, M. D.; Wakefield, M. J.; Smyth, G. K.; Oshlack, A. Gene ontology analysis for RNA-seq: accounting for selection bias. *Genome Biol* **2010**, *11* (2), R14.

(112) Ge, Q.; Feng, F.; Liu, L.; Chen, L.; Lv, P.; Ma, S.; Chen, K.; Yao, Q. RNA-Seq analysis of the pathogenesis of STZ-induced male diabetic mouse liver. *J Diabetes Complications* **2020**, *34* (2), 107444.

(113) Khatri, P.; Sirota, M.; Butte, A. J. Ten years of pathway analysis: current approaches and outstanding challenges. *PLoS Comput Biol* **2012**, *8* (2), e1002375.

(114) Zhang, Y.; Zhou, J.; Liu, J.; Li, S.; Zhou, S.; Zhang, C.; Wang, Y.; Shi, J.; Liu, J.; Wu, Q. RNA-Seq analysis of the protection by Dendrobium nobile alkaloids against carbon tetrachloride hepatotoxicity in mice. *Biomed Pharmacother* **2021**, *137*, 111307.

(115) Esteghamat, F.; Broughton, J. S.; Smith, E.; Cardone, R.; Tyagi, T.; Guerra, M.; Szabó, A.; Ugwu, N.; Mani, M. V.; Azari, B.; et al. CELA2A mutations predispose to early-onset atherosclerosis and metabolic syndrome and affect plasma insulin and platelet activation. *Nat Genet* **2019**, *51* (8), 1233-1243.

(116) Yau, S. W.; Henry, B. A.; Russo, V. C.; McConell, G. K.; Clarke, I. J.; Werther, G. A.; Sabin, M. A. Leptin enhances insulin sensitivity by direct and sympathetic nervous system regulation of muscle IGFBP-2 expression: evidence from nonrodent

models. *Endocrinology* **2014**, *155* (6), 2133-2143.

(117) Du, Y.; Duan, Y.; Zhao, J.; Liu, C.; Zhang, Z.; Zhang, J.; Meng, Z.; Wang, X.; Lau, W. B.; Xie, D.; et al. Dysfunctional APPL1-Mediated Epigenetic Regulation in Diabetic Vascular Injury. *Arterioscler Thromb Vasc Biol* **2023**.

(118) Yee, J. K.; Wahjudi, P. N.; Vega, J.; Lim, S.; Martin, A.; Patterson, M. E.; Cohen, J. N.; Mao, C. S.; Lee, W. N. Stearoyl-CoA desaturase enzyme 1 inhibition reduces glucose utilization for de novo fatty acid synthesis and cell proliferation in 3T3-L1 adipocytes. *Metabolomics* **2013**, *9* (4), 809-816.

(119) Razani, B.; Combs, T. P.; Wang, X. B.; Frank, P. G.; Park, D. S.; Russell, R. G.; Li, M.; Tang, B.; Jelicks, L. A.; Scherer, P. E.; et al. Caveolin-1-deficient mice are lean, resistant to diet-induced obesity, and show hypertriglyceridemia with adipocyte abnormalities. *J Biol Chem* **2002**, *277* (10), 8635-8647.

(120) Evangelakos, I.; Kuhl, A.; Baguhl, M.; Schlein, C.; John, C.; Rohde, J. K.; Heine, M.; Heeren, J.; Worthmann, A. Cold-Induced Lipoprotein Clearance in Cyp7b1-Deficient Mice. *Front Cell Dev Biol* **2022**, *10*, 836741.

(121) Worthmann, A.; John, C.; Rühlemann, M. C.; Baguhl, M.; Heinsen, F. A.; Schaltenberg, N.; Heine, M.; Schlein, C.; Evangelakos, I.; Mineo, C.; et al. Cold-induced conversion of cholesterol to bile acids in mice shapes the gut microbiome and promotes adaptive thermogenesis. *Nat Med* **2017**, *23* (7), 839-849.

(122) Maliszewska, K.; Kretowski, A. Brown Adipose Tissue and Its Role in Insulin and Glucose Homeostasis. *Int J Mol Sci* **2021**, *22* (4).

(123) Shore, A. M.; Karamitri, A.; Kemp, P.; Speakman, J. R.; Graham, N. S.; Lomax, M. A. Cold-induced changes in gene expression in brown adipose tissue, white adipose tissue and liver. *PLoS One* **2013**, *8* (7), e68933.

(124) Jensen-Cody, S. O.; Potthoff, M. J. Hepatokines and metabolism: Deciphering communication from the liver. *Mol Metab* **2021**, *44*, 101138.

(125) Iroz, A.; Couty, J. P.; Postic, C. Hepatokines: unlocking the multi-organ network in metabolic diseases. *Diabetologia* **2015**, *58* (8), 1699-1703.

(126) Townsend, K. L.; Tseng, Y. H. Brown fat fuel utilization and thermogenesis. *Trends Endocrinol Metab* **2014**, *25* (4), 168-177.

(127) Richter, E. A.; Hargreaves, M. Exercise, GLUT4, and skeletal muscle glucose uptake. *Physiol Rev* **2013**, *93* (3), 993-1017.

(128) Haddad, D.; Al Madhoun, A.; Nizam, R.; Al-Mulla, F. Role of Caveolin-1 in Diabetes and Its Complications. *Oxid Med Cell Longev* **2020**, *2020*, 9761539.

(129) Pulinilkunnil, T.; Rodrigues, B. Cardiac lipoprotein lipase: metabolic basis for diabetic heart disease. *Cardiovasc Res* **2006**, *69* (2), 329-340.

(130) Camporez, J. P.; Asrih, M.; Zhang, D.; Kahn, M.; Samuel, V. T.; Jurczak, M. J.; Jornayvaz, F. R. Hepatic insulin resistance and increased hepatic glucose production in mice lacking Fgf21. *J Endocrinol* **2015**, *226* (3), 207-217.

(131) Murphy, L. J. The role of the insulin-like growth factors and their binding proteins in glucose homeostasis. *Exp Diabesity Res* **2003**, *4* (4), 213-224.

(132) Hedbacker, K.; Birsoy, K.; Wysocki, R. W.; Asilmaz, E.; Ahima, R. S.; Farooqi, I. S.; Friedman, J. M. Antidiabetic effects of IGFBP2, a leptin-regulated gene. *Cell Metab* **2010**, *11* (1), 11-22.

(133) Kammel, A.; Saussenthaler, S.; Jähnert, M.; Jonas, W.; Stirm, L.; Hoeflich, A.; Staiger, H.; Fritsche, A.; Häring, H. U.; Joost, H. G.; et al. Early hypermethylation of hepatic Igfbp2 results in its reduced expression preceding fatty liver in mice. *Hum Mol Genet* **2016**, *25* (12), 2588-2599.

(134) Gray, L. R.; Tompkins, S. C.; Taylor, E. B. Regulation of pyruvate metabolism and human disease. *Cell Mol Life Sci* **2014**, *71* (14), 2577-2604.

(135) Just, P. A.; Charawi, S.; Denis, R. G. P.; Savall, M.; Traore, M.; Foretz, M.; Bastu, S.; Magassa, S.; Senni, N.; Sohier, P.; et al. Lkb1 suppresses amino acid-driven gluconeogenesis in the liver. *Nat Commun* **2020**, *11* (1), 6127.

(136) Mutel, E.; Gautier-Stein, A.; Abdul-Wahed, A.; Amigó-Correig, M.; Zitoun, C.; Stefanutti, A.; Houberdon, I.; Tourette, J. A.; Mithieux, G.; Rajas, F. Control of blood glucose in the absence of hepatic glucose production during prolonged fasting in mice: induction of renal and intestinal gluconeogenesis by glucagon. *Diabetes* **2011**, *60* (12), 3121-3131.

(137) Qian, K.; Zhong, S.; Xie, K.; Yu, D.; Yang, R.; Gong, D. W. Hepatic ALT isoenzymes are elevated in gluconeogenic conditions including diabetes and suppressed by insulin at the protein level. *Diabetes Metab Res Rev* **2015**, *31* (6), 562-571.

(138) Cohen, P.; Spiegelman, B. M. Cell biology of fat storage. *Mol Biol Cell* **2016**, *27* (16), 2523-2527.

(139) Cannon, B.; Nedergaard, J. Brown adipose tissue: function and physiological significance. *Physiol Rev* **2004**, *84* (1), 277-359.

(140) Chondronikola, M.; Volpi, E.; Børsheim, E.; Porter, C.; Annamalai, P.; Enerbäck, S.; Lidell, M. E.; Saraf, M. K.; Labbe, S. M.; Hurren, N. M.; et al. Brown adipose tissue improves whole-body glucose homeostasis and insulin sensitivity in humans. *Diabetes* **2014**, *63* (12), 4089-4099.

(141) White, J. D.; Dewal, R. S.; Stanford, K. I. The beneficial effects of brown adipose tissue transplantation. *Mol Aspects Med* **2019**, *68*, 74-81.

(142) Rosen, E. D.; Spiegelman, B. M. What we talk about when we talk about fat. *Cell* **2014**, *156* (1-2), 20-44.

(143) Mössenböck, K.; Vegiopoulos, A.; Rose, A. J.; Sijmonsma, T. P.; Herzig, S.; Schafmeier, T. Browning of white adipose tissue uncouples glucose uptake from insulin signaling. *PLoS One* **2014**, *9* (10), e110428.

(144) Wang, T. Y.; Liu, C.; Wang, A.; Sun, Q. Intermittent cold exposure improves glucose homeostasis associated with brown and white adipose tissues in mice. *Life Sci* **2015**, *139*, 153-159.

(145) Brychta, R. J.; Chen, K. Y. Cold-induced thermogenesis in humans. *Eur J Clin Nutr* **2017**, *71* (3), 345-352.

(146) Škop, V.; Guo, J.; Liu, N.; Xiao, C.; Hall, K. D.; Gavrilova, O.; Reitman, M. L. Mouse Thermoregulation: Introducing the Concept of the Thermoneutral Point. *Cell Rep* **2020**, *31* (2), 107501.

(147) Menéndez, J. A.; Atrens, D. M. Insulin increases energy expenditure and respiratory quotient in the rat. *Pharmacol Biochem Behav* **1989**, *34* (4), 765-768.

(148) Blaszkiewicz, M.; Townsend, K. L. Adipose Tissue and Energy Expenditure: Central and Peripheral Neural Activation Pathways. *Curr Obes Rep* **2016**, *5* (2), 241-250.

(149) Poret, J. M.; Souza-Smith, F.; Marcell, S. J.; Gaudet, D. A.; Tzeng, T. H.; Braymer, H. D.; Harrison-Bernard, L. M.; Primeaux, S. D. High fat diet consumption differentially affects adipose tissue inflammation and adipocyte size in obesity-prone and obesity-resistant rats. *Int J Obes (Lond)* **2018**, *42* (3), 535-541.

(150) Ricquier, D. Uncoupling protein 1 of brown adipocytes, the only uncoupler: a historical perspective. *Front Endocrinol (Lausanne)* **2011**, *2*, 85.

(151) Chang, S. H.; Song, N. J.; Choi, J. H.; Yun, U. J.; Park, K. W. Mechanisms underlying UCP1 dependent and independent adipocyte thermogenesis. *Obes Rev* **2019**, *20* (2), 241-251.

(152) Watanabe, M.; Yamamoto, T.; Mori, C.; Okada, N.; Yamazaki, N.; Kajimoto, K.; Kataoka, M.; Shinohara, Y. Cold-induced changes in gene expression in brown adipose tissue: implications for the activation of thermogenesis. *Biol Pharm Bull* **2008**, *31* (5), 775-784.

(153) Sellers, E. A.; You, R. W. Prevention of dietary fatty livers by exposure to a cold environment. *Science* **1949**, *110* (2870), 713.

(154) Hankir, M. K.; Klingenspor, M. Brown adipocyte glucose metabolism: a heated subject. *EMBO Rep* **2018**, *19* (9).

(155) Lin, D.; Qi, Y.; Huang, C.; Wu, M.; Wang, C.; Li, F.; Yang, C.; Yan, L.; Ren, M.; Sun, K. Associations of lipid parameters with insulin resistance and diabetes: A population-based study. *Clin Nutr* **2018**, *37* (4), 1423-1429.

(156) Grundy, S. M. Hypertriglyceridemia, atherogenic dyslipidemia, and the

metabolic syndrome. *Am J Cardiol* **1998**, *81* (4a), 18b-25b.

(157) Howard, B. V. Insulin resistance and lipid metabolism. *Am J Cardiol* **1999**, *84* (1a), 28j-32j.

(158) Feingold, K. R. Introduction to Lipids and Lipoproteins. In *Endotext*, Feingold, K. R., Anawalt, B., Boyce, A., Chrousos, G., de Herder, W. W., Dhatariya, K., Dungan, K., Hershman, J. M., Hofland, J., Kalra, S., et al. Eds.; MDText.com, Inc.



(159) Jiang, X. C.; Paultre, F.; Pearson, T. A.; Reed, R. G.; Francis, C. K.; Lin, M.; Berglund, L.; Tall, A. R. Plasma sphingomyelin level as a risk factor for coronary artery disease. *Arterioscler Thromb Vasc Biol* **2000**, *20* (12), 2614-2618.

(160) Mahdy Ali, K.; Wonnerth, A.; Huber, K.; Wojta, J. Cardiovascular disease risk reduction by raising HDL cholesterol--current therapies and future opportunities. *Br J Pharmacol* **2012**, *167* (6), 1177-1194.

(161) Liu, Q.; Bengmark, S.; Qu, S. The role of hepatic fat accumulation in pathogenesis of non-alcoholic fatty liver disease (NAFLD). *Lipids Health Dis* **2010**, *9*, 42.

(162) Toth, P. P. Triglyceride-rich lipoproteins as a causal factor for cardiovascular disease. *Vasc Health Risk Manag* **2016**, *12*, 171-183.

(163) Gill, S.; Stevenson, J.; Kristiana, I.; Brown, A. J. Cholesterol-dependent degradation of squalene monooxygenase, a control point in cholesterol synthesis beyond HMG-CoA reductase. *Cell Metab* **2011**, *13* (3), 260-273.

(164) Zhang, L.; Reue, K.; Fong, L. G.; Young, S. G.; Tontonoz, P. Feedback regulation of cholesterol uptake by the LXR-IDOL-LDLR axis. *Arterioscler Thromb Vasc Biol* **2012**, *32* (11), 2541-2546.

(165) Starr, A. E.; Lemieux, V.; Noad, J.; Moore, J. I.; Dewpura, T.; Raymond, A.; Chrétien, M.; Figeys, D.; Mayne, J. β-Estradiol results in a proprotein convertase subtilisin/kexin type 9-dependent increase in low-density lipoprotein receptor levels in human hepatic HuH7 cells. *Febs j* **2015**, *282* (14), 2682-2696.

(166) Meng, Y.; Heybrock, S.; Neculai, D.; Saftig, P. Cholesterol Handling in Lysosomes and Beyond. *Trends Cell Biol* **2020**, *30* (6), 452-466.

(167) Zhang, Y.; Li, R.; Chen, W.; Li, Y.; Chen, G. Retinoids induced Pck1 expression and attenuated insulin-mediated suppression of its expression via activation of retinoic acid receptor in primary rat hepatocytes. *Mol Cell Biochem* **2011**, *355* (1-2), 1-8.

(168) Honma, K.; Kamikubo, M.; Mochizuki, K.; Goda, T. Insulin-induced inhibition of gluconeogenesis genes, including glutamic pyruvic transaminase 2, is associated with reduced histone acetylation in a human liver cell line. *Metabolism* **2017**, *71*, 118-124.

(169) Bertea, M.; Rütti, M. F.; Othman, A.; Marti-Jaun, J.; Hersberger, M.; von Eckardstein, A.; Hornemann, T. Deoxysphingoid bases as plasma markers in diabetes mellitus. *Lipids Health Dis* **2010**, *9*, 84.

(170) Drábková, P.; Šanderová, J.; Kovařík, J.; kanďár, R. An Assay of Selected Serum Amino Acids in Patients with Type 2 Diabetes Mellitus. *Adv Clin Exp Med* **2015**, *24* (3), 447-451.

(171) Cohen, P.; Rosenfeld, R. G. Physiologic and clinical relevance of the insulin-like growth factor binding proteins. *Curr Opin Pediatr* **1994**, *6* (4), 462-467.

(172) Kang, H. S.; Cho, H. C.; Lee, J. H.; Oh, G. T.; Koo, S. H.; Park, B. H.; Lee, I. K.; Choi, H. S.; Song, D. K.; Im, S. S. Metformin stimulates IGFBP-2 gene expression through PPARalpha in diabetic states. *Sci Rep* **2016**, *6*, 23665.

(173) Faramia, J.; Hao, Z.; Mumphrey, M. B.; Townsend, R. L.; Miard, S.; Carreau, A. M.; Nadeau, M.; Frisch, F.; Baraboi, E. D.; Grenier-Larouche, T.; et al. IGFBP-2 partly mediates the early metabolic improvements caused by bariatric surgery. *Cell Rep Med* **2021**, *2* (4), 100248.

(174) Ko, J. M.; Park, H. K.; Yang, S.; Kim, E. Y.; Chung, S. C.; Hwang, I. T. Association between insulin-like growth factor binding protein-2 levels and cardiovascular risk factors in Korean children. *Endocr J* **2012**, *59* (4), 335-343.

(175) Wittenbecher, C.; Ouni, M.; Kuxhaus, O.; Jähnert, M.; Gottmann, P.; Teichmann, A.; Meidtner, K.; Kriebel, J.; Grallert, H.; Pischon, T.; et al. Insulin-Like Growth Factor Binding Protein 2 (IGFBP-2) and the Risk of Developing Type 2 Diabetes. *Diabetes* **2019**, *68* (1), 188-197.

(176) Rajpathak, S. N.; He, M.; Sun, Q.; Kaplan, R. C.; Muzumdar, R.; Rohan, T. E.; Gunter, M. J.; Pollak, M.; Kim, M.; Pessin, J. E.; et al. Insulin-like growth factor axis and risk of type 2 diabetes in women. *Diabetes* **2012**, *61* (9), 2248-2254.

(177) Wheatcroft, S. B.; Kearney, M. T.; Shah, A. M.; Ezzat, V. A.; Miell, J. R.; Modo, M.; Williams, S. C.; Cawthorn, W. P.; Medina-Gomez, G.; Vidal-Puig, A.; et al. IGF-binding protein-2 protects against the development of obesity and insulin resistance. *Diabetes* **2007**, *56* (2), 285-294.

(178) Assefa, B.; Mahmoud, A. M.; Pfeiffer, A. F. H.; Birkenfeld, A. L.; Spranger, J.; Arafat, A. M. Insulin-Like Growth Factor (IGF) Binding Protein-2, Independently of IGF-1, Induces GLUT-4 Translocation and Glucose Uptake in 3T3-L1 Adipocytes. *Oxid Med Cell Longev* **2017**, *2017*, 3035184.

(179) Wilhelm, F.; Kässner, F.; Schmid, G.; Kratzsch, J.; Laner, A.; Wabitsch, M.; Körner, A.; Kiess, W.; Garten, A. Phosphatidylinositol 3-kinase (PI3K) signalling regulates insulin-like-growth factor binding protein-2 (IGFBP-2) production in human adipocytes. *Growth Horm IGF Res* **2015**, *25* (3), 115-120.

(180) Monget, P.; Mazerbourg, S.; Delpuech, T.; Maurel, M. C.; Manière, S.; Zapf, J.; Lalmanach, G.; Oxvig, C.; Overgaard, M. T. Pregnancy-associated plasma protein-A is

involved in insulin-like growth factor binding protein-2 (IGFBP-2) proteolytic degradation in bovine and porcine preovulatory follicles: identification of cleavage site and characterization of IGFBP-2 degradation. *Biol Reprod* **2003**, *68* (1), 77-86.

(181) Png, K. J.; Halberg, N.; Yoshida, M.; Tavazoie, S. F. A microRNA regulon that mediates endothelial recruitment and metastasis by cancer cells. *Nature* **2011**, *481* (7380), 190-194.

(182) Bergman, R. N.; Ader, M. Free fatty acids and pathogenesis of type 2 diabetes mellitus. *Trends Endocrinol Metab* **2000**, *11* (9), 351-356.

(183) Stinkens, R.; Goossens, G. H.; Jocken, J. W.; Blaak, E. E. Targeting fatty acid metabolism to improve glucose metabolism. *Obes Rev* **2015**, *16* (9), 715-757.

(184) Li, Z.; Zhao, X.; Jian, L.; Wang, B.; Luo, H. Rumen microbial-driven metabolite from grazing lambs potentially regulates body fatty acid metabolism by lipid-related genes in liver. *J Anim Sci Biotechnol* **2023**, *14* (1), 39.

(185) Schalla, M. A.; Unniappan, S.; Lambrecht, N. W. G.; Mori, M.; Taché, Y.; Stengel, A. NUCB2/nesfatin-1 - Inhibitory effects on food intake, body weight and metabolism. *Peptides* **2020**, *128*, 170308.

(186) Silbernagel, G.; Kovarova, M.; Cegan, A.; Machann, J.; Schick, F.; Lehmann, R.; Häring, H. U.; Stefan, N.; Schleicher, E.; Fritsche, A.; et al. High hepatic SCD1 activity is associated with low liver fat content in healthy subjects under a lipogenic diet. *J Clin Endocrinol Metab* **2012**, *97* (12), E2288-2292.

(187) Im, S. S.; Hammond, L. E.; Yousef, L.; Nugas-Selby, C.; Shin, D. J.; Seo, Y. K.; Fong, L. G.; Young, S. G.; Osborne, T. F. Sterol regulatory element binding protein 1a regulates hepatic fatty acid partitioning by activating acetyl coenzyme A carboxylase 2. *Mol Cell Biol* **2009**, *29* (17), 4864-4872.

(188) Olivecrona, G. Role of lipoprotein lipase in lipid metabolism. *Curr Opin Lipidol* **2016**, *27* (3), 233-241.

(189) Fernández-Rojo, M. A.; Gongora, M.; Fitzsimmons, R. L.; Martel, N.; Martin, S. D.; Nixon, S. J.; Brooks, A. J.; Ikonomopoulou, M. P.; Martin, S.; Lo, H. P.; et al. Caveolin-1 is necessary for hepatic oxidative lipid metabolism: evidence for crosstalk between caveolin-1 and bile acid signaling. *Cell Rep* **2013**, *4* (2), 238-247.

(190) Lewis, G. F.; Carpentier, A.; Adeli, K.; Giacca, A. Disordered fat storage and mobilization in the pathogenesis of insulin resistance and type 2 diabetes. *Endocr Rev* **2002**, *23* (2), 201-229.

(191) Savage, D. B.; Petersen, K. F.; Shulman, G. I. Disordered lipid metabolism and the pathogenesis of insulin resistance. *Physiol Rev* **2007**, *87* (2), 507-520.

(192) Magkos, F.; Fabbrini, E.; Patterson, B. W.; Eagon, J. C.; Klein, S. Portal vein and systemic adiponectin concentrations are closely linked with hepatic glucose and lipoprotein kinetics in extremely obese subjects. *Metabolism* **2011**, *60* (11), 1641-1648.

(193) Yang, J.; Zhou, W.; Wu, Y.; Xu, L.; Wang, Y.; Xu, Z.; Yang, Y. Circulating IGFBP-2 levels are inversely associated with the incidence of nonalcoholic fatty liver disease: A cohort study. *J Int Med Res* **2020**, *48* (8), 300060520935219.

(194) Poekes, L.; Legry, V.; Schakman, O.; Detrembleur, C.; Bol, A.; Horsmans, Y.; Farrell, G. C.; Leclercq, I. A. Defective adaptive thermogenesis contributes to metabolic syndrome and liver steatosis in obese mice. *Clin Sci (Lond)* **2017**, *131* (4), 285-296.

(195) Kajimura, S. Adipose tissue in 2016: Advances in the understanding of adipose tissue biology. *Nat Rev Endocrinol* **2017**, *13* (2), 69-70.

(196) Czech, M. P. Mechanisms of insulin resistance related to white, beige, and brown adipocytes. *Mol Metab* **2020**, *34*, 27-42.

(197) Rossi, A.; Kontarakis, Z.; Gerri, C.; Nolte, H.; Hölper, S.; Krüger, M.; Stainier, D. Y. Genetic compensation induced by deleterious mutations but not gene knockdowns. *Nature* **2015**, *524* (7564), 230-233.

(198) Kok, F. O.; Shin, M.; Ni, C. W.; Gupta, A.; Grosse, A. S.; van Impel, A.; Kirchmaier, B. C.; Peterson-Maduro, J.; Kourkoulis, G.; Male, I.; et al. Reverse genetic screening reveals poor correlation between morpholino-induced and mutant phenotypes in zebrafish. *Dev Cell* **2015**, *32* (1), 97-108.

(199) Shih, D. M.; Zhu, W.; Schugar, R. C.; Meng, Y.; Jia, X.; Miikeda, A.; Wang, Z.; Zieger, M.; Lee, R.; Graham, M.; et al. Genetic Deficiency of Flavin-Containing Monooxygenase 3 ( Fmo3) Protects Against Thrombosis but Has Only a Minor Effect on Plasma Lipid Levels-Brief Report. *Arterioscler Thromb Vasc Biol* **2019**, *39* (6), 1045-1054.

(200) Lin, H.; Wang, L.; Liu, Z.; Long, K.; Kong, M.; Ye, D.; Chen, X.; Wang, K.; Wu, K. K.; Fan, M.; et al. Hepatic MDM2 Causes Metabolic Associated Fatty Liver Disease by Blocking Triglyceride-VLDL Secretion via ApoB Degradation. *Adv Sci (Weinh)* **2022**, *9* (20), e2200742.

(201) Handzlik, M. K.; Gengatharan, J. M.; Frizzi, K. E.; McGregor, G. H.; Martino, C.; Rahman, G.; Gonzalez, A.; Moreno, A. M.; Green, C. R.; Guernsey, L. S.; et al. Insulin-regulated serine and lipid metabolism drive peripheral neuropathy. *Nature* **2023**, *614* (7946), 118-124.

(202) Chen, L.; Chen, Q.; Xie, B.; Quan, C.; Sheng, Y.; Zhu, S.; Rong, P.; Zhou, S.; Sakamoto, K.; MacKintosh, C.; et al. Disruption of the AMPK-TBC1D1 nexus increases lipogenic gene expression and causes obesity in mice via promoting IGF1 secretion. *Proc Natl Acad Sci U S A* **2016**, *113* (26), 7219-7224.